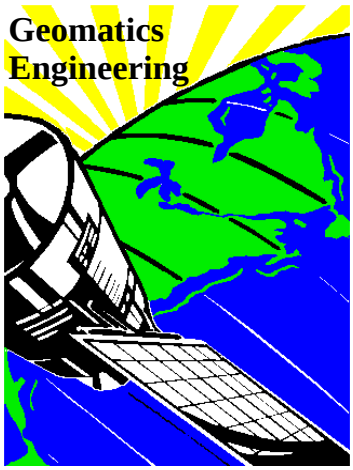

UCGE Reports
Number 20044

Department of Geomatics Engineering

Investigations of C/A Code and Carrier Measurements and Techniques for Rapid Static GPS Surveys

MSc Thesis

Caroline Erickson

June 1992

(www.ensu.ucalgary.ca/GradTheses.html)

THE UNIVERSITY OF CALGARY

INVESTIGATIONS OF C/A CODE AND CARRIER MEASUREMENTS AND TECHNIQUES FOR RAPID STATIC GPS SURVEYS

by

CAROLINE ERICKSON

A THESIS

SUBMITTED TO THE FACULTY OF GRADUATE STUDIES

IN PARTIAL FULFILLMENT OF THE REQUIREMENTS FOR THE

DEGREE OF MASTER OF SCIENCE

DEPARTMENT OF SURVEYING ENGINEERING

CALGARY, ALBERTA

JUNE, 1992

ABSTRACT

Code and carrier measurements and techniques for rapid static GPS surveys are investigated. Developments are based on using only single frequency carrier phase data with high accuracy C/A code measurements. Theory of GPS observables, least squares solutions and preanalysis as applied to GPS is reviewed. Solutions using code measurements, carrier measurements and code-carrier measurements combined with up to five minutes of data for 720 m and 4.1 km baselines are analyzed. The ambiguity function method, the fast ambiguity resolution approach and the least squares ambiguity search technique are each investigated as means for ambiguity resolution in rapid static surveys. Although each of these methods is shown to be negatively affected by code or carrier multipath, they are shown to be successful within certain constraints. The investigations made in this thesis are important to the objective of achieving centimetre accuracies in minutes using rapid static GPS surveying techniques.

ACKNOWLEDGEMENTS

I wish to express my appreciation to my supervisor, Professor Gérard Lachapelle, for his inspiration and guidance throughout the course of my graduate studies.

Special thanks are extended to Professor M. Elizabeth Cannon and Mr. Gang Lu for the valued time and knowledge they shared in discussing topics related to this thesis. Professor Cannon is acknowledged for providing preprocessing software used in these investigations. Mr. Bryan Townsend is thanked for his assistance in software development and Mr. Dingsheng Chen, Mr. Lu and Mr. Townsend are all thanked for their assistance in data collection. The many other graduate students and Faculty members who have made the course of my graduate studies both fruitful and enjoyable through discussions and fellowship, are sincerely appreciated.

The Geodetic Survey of Canada is gratefully acknowledged for providing me with the opportunity to pursue graduate studies through educational leave and financial support. I extend my gratitude to my colleagues at Geodetic Survey for their helpfulness throughout my leave of absence. NovAtel Communications Corporation is acknowledged for providing the NovAtel GPSCard™ data used in this thesis.

Finally, thanks go to my husband Dave for his support, encouragement and patience.

TABLE OF CONTENTS

Page

LIST OF TABLES

Table

LIST OF FIGURES

Figure **Page**

NOTATION

i) Symbols

^	denotes estimated quantity
A	first design matrix (n × u)
ACP	active control point
AF(x,y,z)	ambiguity function evaluated at point (x,y,z)
α	significance level (Type I error probability)
$1 - \alpha$	confidence level
β	Type II error probability
$1 - \beta$	power of the test
c	speed of light, or
c	zero vector, with a 1 in one row (n × 1)
calc	calculated double difference
C_l	covariance matrix of the observations (n × n)
C_x	covariance matrix of the parameters (u × u)
C_v	covariance matrix of the residuals (n × n)
df	degrees of freedom
d_{ion}	error due to the ionosphere
$d\rho$	orbital errors
dt	satellite clock error
dT	receiver clock error
d_{trop}	error due to the troposphere
$e^{i\theta}$	phasor or complex vector $e^{i\theta} = \cos\theta + i \sin\theta$

ξ_F	Fisher distribution
$\xi_{\chi 2}$	Chi squared distribution
ξ_t	Student t distribution
δ	difference between code and carrier double differences, or
δ	correction vector to approximate values of the unknowns
$\bar{\delta}_{o,i}$	datum independent measure of external reliability for the ith observation
l_i	minimal detectable error of the i'th observation
X	vector of external reliabilities (u × 1)
ε_p	code measurement noise
$\varepsilon_{p_{rx}}$	receiver component of code measurement noise
$\varepsilon_{p_{mult}}$	multipath component of code measurement noise
ε_Φ	carrier measurement noise
$\varepsilon_{\Phi_{rx}}$	receiver component of carrier measurement noise
$\varepsilon_{\Phi_{mult}}$	multipath component of carrier measurement noise
$e^{i\theta}$	phasor or complex number $e^{i\theta} = \cos\theta + i \sin\theta$
h	height
φ	latitude
Φ	carrier phase observation
λ	carrier wavelength, or
λ	longitude
λ_o	non-centrality parameter
l	vector of observations (n × 1)
L1	GPS carrier with frequency of 1575.42 MHz
L2	GPS carrier with frequency of 1227.60 MHz

n	number of observations
N	carrier phase ambiguity, or
N	normal equations matrix
NA	potential integer ambiguity
nepoch	number of epochs
nsat	number of satellites
obs	observed double difference
p	pseudorange observation
ρ	range between satellite and receiver
r	redundancy
r_i	redundancy number for the i'th observation
σ	standard deviation
σ^2	variance
$\hat{\sigma}_o^2$	estimated a posteriori variance factor
σ_{sp}	achievable single point positioning accuracy
σ_Δ	achievable double difference positioning accuracy
$\sigma_{o_{sp}}$	single point measurement accuracy
σ_{o_Δ}	double difference measurement accuracy
σ_{ij}	covariance between i and j
t	time, or
t	critical value from Student t probability distribution
u	right hand side of normal equations, or
u	number of parameters
v	residual vector (n × 1)
w	misclosure vector (n × 1)

x_r, y_r, z_r	receiver cartesian coordinates
x^s, y^s, z^s	satellite cartesian coordinates

ii) Defined Operators

A^T	matrix transpose
C^{-1}	matrix inverse
$\overline{\Delta}$	between satellite single difference
Δ	between receiver single difference
$\overline{\Delta}$	double difference
nint(•)	nearest integer of
$\frac{\partial f}{\partial x}$	partial derivative of the function f with respect to x
Π	product of
Σ	summation of
tr(•)	trace of, i.e. sum of matrix diagonal components

iii) Acronyms

AF	ambiguity function
AFM	ambiguity function method
C/A code	coarse acquisition code
DD	double difference
DoD	United States Department of Defense
DOP	dilution of precision
EDM	electronic distance measurement
FARA	fast ambiguity resolution approach
GDOP	geometrical dilution of precision

GPS	Global Positioning System
HDOP	horizontal dilution of precision
LSAST	least squares ambiguity search technique
MDE	minimal detectable error
P code	precise acquisition code
PDOP	positional dilution of precision
PPS	precise positioning service
RDOP	relative dilution of precision
RGDOP	relative geometrical dilution of precision
RHDOP	relative horizontal dilution of precision
RMS	root mean square
RPDOP	relative positional dilution of precision
RVDOP	relative vertical dilution of precision
S/A	selective availability
SPS	standard positioning service
SV	space vehicle (used to reference specific GPS satellites)
TDOP	time dilution of precision
VDOP	vertical dilution of precision

CHAPTER 1

INTRODUCTION

1.1 BACKGROUND AND OBJECTIVE

The Global Positioning System (GPS), a satellite-based radio-navigation system established by the U.S. Department of Defense, has become a well accepted tool in static surveying, replacing conventional surveying techniques for many applications. Static GPS carrier phase relative positioning has yielded accuracies ranging from a few parts per million to a few parts per 100 million (Delikaraoglou et al., 1985; Lichten and Bertiger, 1989), depending on the observation and processing methodology used. To achieve a few parts per million accuracy, site observation periods of at least one hour are typically recommended for short baselines (< 10 km), with longer observation periods necessary for longer baselines. The objective of rapid static surveys is to achieve comparable accuracies with short observation periods (typically < five minutes), and thereby dramatically increase GPS surveying efficiency.

Efforts towards higher GPS surveying efficiency first led to the development of semi-kinematic and pseudo-kinematic survey techniques, but neither have the logistical and efficiency advantages of rapid static survey techniques. In semi-kinematic surveys

(Remondi, 1985), one GPS receiver is left stationary at a "monitor" site, as a second "rover" receiver is moved successively to sites to be positioned. High accuracy is achieved by determining the integer ambiguities at the initial rover site, and then maintaining lock on at least four satellites (i.e. retaining constant carrier phase integer ambiguities) while moving between sites to be positioned (Cannon, 1990). The requirement of maintaining satellite phase lock is very restrictive since the rover antenna must be transported from site to site, with an unobstructed line of sight between the antenna and satellites. In pseudo-kinematic surveys (Remondi, 1990), the benefit of different satellite geometry in ambiguity resolution is exploited by occupying the rover site for two to three minutes twice, at least one hour apart, after the satellite geometry has changed significantly. The requirement to visit each station at least twice and timing site visits to ensure sufficient geometry change between satellites poses logistical constraints and reduces efficiency.

Rapid static surveys, which require simultaneous occupation of monitor and remote sites for periods of several minutes, provide high accuracies and efficiencies without the cumbersome constraints inherent to semi-kinematic and pseudo-kinematic techniques. They are based on the ability to resolve carrier phase ambiguities in minutes.

To investigate rapid static surveys, it is important to review related developments. Advances in rapid static surveys have paralleled advances in precise kinematic surveys, where one desires the position of a moving "remote" receiver with respect to a stationary "monitor" receiver. Ideally, kinematic surveys should be carried out in real–time using "on the fly" ambiguity resolution techniques and computationally efficient processing algorithms. Comparatively, rapid static surveys are less demanding since both monitor and remote receivers are stationary, and real-time computations are not vital. Since both

rely on ambiguity resolution, developments in kinematic surveys may be used in a rapid static environment.

Over the past few years several techniques for rapid ambiguity resolution have been developed. These include "extra-widelaning" (Wübbena, 1989; Abidin and Wells, 1990), "multiple observable processing techniques" (Allison, 1991), "sequential phase ambiguity resolution" (Talbot, 1991), "short-time application with ambiguity preselection" (Euler et al., 1990), the "fast ambiguity resolution approach" (Frei and Beutler, 1990), the "least squares ambiguity search technique" (Hatch, 1991a; Hatch, 1991b) and the "ambiguity function method" (Counselman and Gourevitch, 1981; Remondi, 1984). Although each of these techniques has some unique element, each also has elements shared with other ambiguity resolution techniques. Furthermore, a combination of techniques may be used as proposed in Abidin (1991).

The first two techniques listed above rely on the combined use of P code and carrier phase observations. In "extra wide-laning", narrow-lane and wide-lane carrier phase observations and narrow-lane P code observations are constructed and used together to resolve ambiguities (Abidin and Wells, 1990). For "multiple observable techniques" Allison (1991) considers the case of 3-observable processing, where carrier phase observations are available on L1 and L2, but P code observations are only available on L2 (as is the case with the Trimble Geodetic Surveyor IIP™ receiver). He combines wide-lane carrier phase observations with L2 P code observations to aid ambiguity resolution and shows the method to be 25 times less susceptible to ionospheric delay than an L1 only process. The main limitation of extra wide-laning and multiple observable techniques is their dependence on P code observations, because P code is scheduled to be unavailable for civilian use in 1993 when the full satellite constellation is operational (McNeff, 1991).

In "sequential phase ambiguity resolution" each carrier phase observation is tested and constrained to an integer ambiguity independently (Talbot, 1991). As each ambiguity is successively constrained, the computed solution is improved making it easier to resolve the remaining ambiguities. Talbot (1991) describes a real–time rapid static system, which lets an observer know in the field when ambiguities are resolved. He reported resolution of ambiguities in 17 minutes for six satellite single frequency data. The disadvantage of this technique is its time requirements exceeds the short periods desired for rapid static surveys. Although not addressed in this thesis, the combination of sequential techniques with other rapid ambiguity resolution techniques could prove to be fruitful.

"Short-time application with ambiguity preselection", the "fast ambiguity resolution approach" and the "least squares ambiguity search technique" are similar in that each uses potential ambiguity sets to compute several least squares solutions with fixed integer ambiguities, and the ambiguities which yield the solution with the smallest variance factor and pass requisite statistical testing are deemed "correct". "Short-time application with ambiguity preselection" (Euler et al., 1990) requires use of dual frequency data (P code or squaring), and adds the additional constraints of ambiguities being integers on L2 as well as L1. The "fast ambiguity resolution approach" (FARA) uses ambiguity covariance information from an adjustment with floating carrier phase ambiguities to reduce the number of ambiguity sets to be considered, along with several statistical tests (Frei and Beutler, 1990). The "least squares ambiguity search technique" (LSAST) uses four "primary" satellites to define a point and redundant "secondary" satellites to test the validity of the point and corresponding ambiguities (Hatch, 1991a).

The final rapid ambiguity resolution technique listed above is the "ambiguity function method" (AFM). Developed for conventional static GPS surveys (Counselman and Gourevitch, 1981), it has recently been applied to pseudo-kinematic and kinematic

surveys (Remondi, 1990; Mader, 1990). The ambiguity function method is unique compared to the other techniques mentioned because it is unaffected by cycle slips.

This thesis focuses on a subset of rapid static GPS surveys, considering the case where only single frequency data with high accuracy C/A code measurements are available. Of the ambiguity resolution techniques described, only the last three, namely FARA, LSAST and AFM, can be used with single frequency observations. (Sequential phase ambiguity resolution is not included here since reports indicate it takes much longer than the periods being considered for these investigations (Talbot, 1991).) In 1991, a new technology which allows for high accuracy C/A code measurements was unveiled and implemented in the single frequency NovAtel Model 1001 GPSCard™ (Fenton et al., 1991). The unprecedented C/A code accuracy of 10 cm shown with this receiver (Erickson et al., 1991) opens new possibilities for rapid ambiguity resolution using single frequency data, which are investigated in this thesis.

The objective of this thesis is to investigate rapid static survey measurements and techniques using single frequency carrier phase data and high accuracy C/A code data. Code, carrier and code-carrier measurements combined, over observation periods of up to five minutes and baselines up to four km, are studied through preanalysis and post-processing of data, providing insight into the measurements which affect the ambiguity resolution techniques and rapid static survey results. Three ambiguity resolution techniques are tested and compared: the ambiguity function method, the fast ambiguity resolution approach and the least squares ambiguity search technique. Some modifications of these techniques are explored. Investigations are limited to short baselines, where most observational errors are reduced or eliminated through double differencing. The investigations made in this thesis are a subset of those needed towards the objective of developing efficient, effective rapid static surveying techniques.

1.2 THESIS OUTLINE

In Chapter 2 background theory which is fundamental to developments in the subsequent chapters is provided. GPS observables are described, observation equations are formulated and errors are summarized. Double differencing, which is used in all the rapid static techniques examined in this thesis, is explained along with its associated equations. The formulation of least squares solutions for pseudorange observations, and carrier phase observations with fixed and floating ambiguities is given. Methods of preanalysis for GPS baseline solutions using dilution of precision (DOP), relative dilution of precision (RDOP) and statistical reliability are discussed.

In Chapter 3 the field tests conducted and data sets used in the subsequent chapters are described. The elevations and DOPs given for each data set, make useful references in the discussion of results given in Chapters 4, 5 and 6.

In Chapter 4 coordinate estimation accuracies achievable based on double differencing using code only, carrier only and combined code and carrier observations are investigated. RDOP preanalysis is carried out for each solution type to show what should be achievable under ideal conditions, and reliability preanalysis is carried out for each to analyze their statistical reliability characteristics. Results from actual data for code solutions are compared to "truth" to give a measure of achievable code accuracies. These are compared to RDOP preanalysis results, and discrepancies found are investigated through analysis of code multipath. Results from actual data for carrier and code-carrier combined solutions are also analyzed, demonstrating the benefits of a fixed over float solution, the inadequacy of code-carrier combined solutions, the benefits of accurate code solutions over carrier float solutions for short observation periods, and the need for

special techniques for rapid ambiguity resolution to ensure ambiguities are resolved to the correct integers.

In Chapter 5 one method of rapid ambiguity resolution, the ambiguity function method, is investigated. The theory behind the ambiguity function method is given followed by a description of search techniques which may be used. The reliability of AFM results is discussed with consideration of the observation conditions under which it is applied, the adequacy of the search technique, and criteria to decide the acceptability of the AFM results. AFM is then put to the test using actual data along with the accompanying search techniques.

In Chapter 6 two least squares ambiguity resolution techniques for rapid static GPS, namely the fast ambiguity resolution approach (FARA) and the least squares ambiguity search technique (LSAST), are investigated. For each of these methods, the underlying theory is reviewed and results are presented. The relation between AFM and LSAST is discussed, followed by a comparison of these techniques with FARA.

Conclusions formed throughout this thesis and recommendations for further investigations are presented in Chapter 7

CHAPTER 2

BACKGROUND THEORY

2.1 GPS OBSERVABLES

The Global Positioning System (GPS) consists of a constellation of radio-navigation satellites, a ground control unit which manages satellite operation, and users with specialized receivers who use the satellite data to satisfy a broad range of positioning requirements. The system was established by the United States Department of Defense (DoD) to fulfill defence positioning needs and as a by-product, to serve the civilian navigational community. The satellite constellation, to be fully operational in 1993 (McNeff, 1991) will consist of 21 satellites and three active spares at an altitude of 20,000 km, positioned in a manner which ensures the visibility of four or more satellites almost anywhere in the world at anytime. The launch of prototype satellites as early as 1978 and the current constellation of some 17 satellites has resulted in a well developed GPS industry of receiver manufacturers, software developers and application oriented users, of which surveyors are a small portion.

2.1.1 GPS Signals

The signals transmitted by the satellites and received at a GPS user's receiver form the GPS observables, which are manipulated to attain position estimates. Much of the power of GPS lies in the wealth of information provided in these signals. They are transmitted autonomously from all GPS satellites on two carrier frequencies; an L1 frequency of 1575.42 MHz and an L2 frequency of 1227.60 MHz. A pseudo-random noise C/A code of 1.023 MHz is modulated on the L1 carrier and a pseudo-random noise P code of 10.23 MHz is modulated on both the L1 and L2 carriers. A satellite message, which among other information contains the satellite's ephemeris, is also modulated on both frequencies. A summary of the signal components is given in Table 2.1.

Table 2.1
GPS Signal Components

Carrier	Freq.	Wavelength	Modulation	Freq.	Chip Length
L1	1575.42 MHz	19 cm	C/A code	1.023 MHz	293 m
			P code	10.23 MHz	29.3 m
			Message	50 Hz	
L2	1227.60 MHz	24 cm	P code	10.23 MHz	29.3 m
			Message	50 Hz	

GPS receivers are classified as either being single frequency, meaning they receive L1 signals only, or dual frequency, meaning they receive both L1 and L2 signals. Most provide access to C/A code data by correlating the incoming signal from a satellite with a replica of the code generated in the receiver. Dual frequency receivers may provide access to C/A code data, P code data or both. When only C/A code data is used in dual frequency receivers, the L2 carrier is squared to remove the unknown P code modulation, resulting in an effective L2 wavelength of 12 cm. The dual frequency receivers which provide access to P code data do so through code correlation, allowing for a full L2

wavelength of 24 cm. Access to P code data is expected to be denied to civilian users by the U.S. DoD after the full constellation is operational (McNeff, 1991).

The type of data that a receiver collects has a direct impact on achievable accuracies, and usually a corresponding impact on price. The least expensive receivers on the market are ones which provide real time position solutions based only on C/A code data with SPS (standard positioning service) accuracies of 100 m horizontal and 156 m vertical. P code receivers which are similar in operation but boast accuracies of 25 m horizontal and 30 m vertical as per the PPS (precise positioning service) requirements are limited to U.S. and NATO military users. Receivers which base their solutions on carrier phase observations rather than pseudorange observations are inherently more accurate due to the much finer resolution of the 19 cm and 24 cm carrier wavelengths as compared to the 293 m and 29 m code chip lengths. The most sophisticated receivers on the market are dual frequency P code receivers. These receivers are used to support some of the most exacting relative positioning needs, such as crustal motion studies with accuracies ranging from a part per million to a few parts per billion. Between the two extremes one finds a wide range of receiver equipment which meets a comparably wide range of user accuracy requirements.

2.1.2 Observation Equations

A code observation (also called pseudorange) is the difference between the signal transmission time at the satellite and reception time at the receiver. It is scaled to units of length using the speed of light. The equation to solve for an unknown position using code observations is given as:

$$p = \rho + c(dt - dT) + d_{ion} + d_{trop} + d\rho + \varepsilon_p, \qquad (2.1)$$

where p is the observed pseudorange, ρ is the unknown satellite-receiver range, c is the speed of light, dt is the satellite clock error, dT is the receiver clock error, d_{ion} is the error due to the ionosphere, d_{trop} is the error due to the troposphere, d_ρ is the orbital error and ε_p is the code measurement noise (Wells et al., 1986). The code measurement noise ε_p is a function of the code receiver noise, ε_{prx} and multipath ε_{mult}, i.e.,

$$\varepsilon_p = f \{ \varepsilon_{prx}, \varepsilon_{pmult} \} \tag{2.2}$$

(Lachapelle, 1991). The satellite-receiver range, ρ, when expanded has the form

$$\rho = \sqrt{(x^s - x_r)^2 + (y^s - y_r)^2 + (z^s - z_r)^2} \quad , \tag{2.3}$$

where x^s, y^s and z^s are satellite coordinates computed using broadcast ephemeris data and x_r, y_r and z_r are the unknown receiver coordinates. Since there are four unknowns in total (x_r, y_r, z_r and dT), a minimum of four satellites are needed to solve for a solution at a single epoch (meaning four different equations of the form of (2.1)).

A carrier phase observation is more complex to define than a pseudorange observation. At the epoch t_o when a satellite is "locked on", the carrier phase observation is a measure of the misalignment between an incoming signal and that generated by the receiver oscillator. Assuming continuous lock, at subsequent epochs this measurement is a sum of the initial phase misalignment at epoch t_o and the number of integer cycles from epoch t_o to the current epoch t. Accordingly, from Wells et al. (1986) the measured carrier phase, $\Phi_{measured}$, can be written as

$$\Phi_{measured} = \text{fraction}(\Phi) + \text{integer}(\Phi; t_o, t). \tag{2.4}$$

From herein Φ will be used to represent the measured carrier phase as per equation (2.4). Carrier phase measurements are scaled by their wavelength to convert them from cycles to units of length.

For a carrier phase measurement to represent a satellite-receiver range, one needs to add an ambiguity term which accounts for the unknown number of integer cycles between the satellite and receiver at epoch t_o. Then the equation to solve for an unknown position using carrier phase observation is given as

$$\Phi = \rho + c(dt - dT) + \lambda \bullet N - d_{ion} + d_{trop} + d\rho + \varepsilon_\Phi, \qquad (2.5)$$

where λ is the carrier wavelength, N is the unknown integer cycle ambiguity, ε_Φ is the carrier phase measurement noise, and all other terms are as defined above. The carrier measurement noise ε_Φ resembles the code measurement noise of equation (2.2) since it is also a function of the receiver noise, $\varepsilon_{\Phi rx}$ and multipath, ε_{mult}, i.e.

$$\varepsilon_\Phi = f \{ \varepsilon_{\Phi rx}, \varepsilon_{\Phi mult} \}. \qquad (2.6)$$

Note the similarities between the pseudorange observation equation (2.1) and the carrier observation equation (2.5). The only differences between the two are the addition of an ambiguity term, λN, for carrier phase observations and the reversal of signs for the ionospheric correction term d_{ion}. Carrier phase observations alone may not be used to solve for a position at one epoch of time because the addition of an unknown ambiguity term for each satellite observation results in an underdetermined system of equations.

2.1.3 Errors

Both pseudorange and carrier phase observations are subject to a number of errors, which are described in Table 2.2.

Table 2.2
GPS Errors

Error		Description
d_ρ	orbital	- nominal errors due to inaccuracies in broadcast ephemeris data - additional errors due to the intentional orbital degradation of selective availability (S/A)
d_{ion}	ionospheric	- delay of pseudorange measurements and equivalent advance of carrier phase measurements due to free electrons in the ionosphere (the region of the atmosphere extending from 50 to 1000 km above the earth)
d_{trop}	tropospheric	- delay in signal transmission due to wet and dry components in the region of the atmosphere extending up to 80 km above the earth
dt	satellite clock	- difference between satellite time and true GPS time
dT	receiver clock	- difference between receiver time and true GPS time
ε_{prx}	code receiver noise	- inaccuracies of code measurements due to receiver noise
$\varepsilon\Phi_{rx}$	carrier receiver noise	- inaccuracies of carrier measurements due to receiver noise
ε_{mult}	multipath	- phenomena where the measured signal includes the superimposition of one or more reflected signals, rather than the direct signal alone

These errors, their magnitudes and methods for handling them are discussed in Lachapelle (1991).

A phenomenon unique to carrier phase observations is the cycle slip. Recall from the discussion of integer cycle ambiguities with equations (2.4) and (2.5), that carrier phase observations will have the same integer ambiguity if satellite lock is maintained. Cycle slips always occur when satellite lock is lost and occasionally occur as a result of a

receiver malfunction. When a processing algorithm depends on one integer ambiguity per satellite for the full observation period it is important to implement preprocessing techniques to detect and correct for the effect of cycle slips. Such techniques are described in Wells et al. (1986) and Leick (1990).

One method for reducing or eliminating some of the errors of Table 2.2 is double differencing.

2.2 DOUBLE DIFFERENCING

Double differencing is a very common and accepted technique for processing GPS observables (code or carrier) when the coordinates of an unknown point are sought with respect to a known point. Double difference observation equations are presented followed by a discussion of residual double difference errors.

2.2.1 Observation Equations

The concept of double differencing is illustrated in Figure 2.1. Observations from two satellites to one receiver are differenced, then observations from the same two satellites to a second receiver are differenced, and the resulting differences are differenced, hence the name double differencing.

In the figure, the symbol A1 represents the observation between receiver A and satellite 1, the symbol B2 represents the observation between receiver B and satellite 2 and so on. The double difference operation defined in equation (2.7) can be represented with the operator Δ.

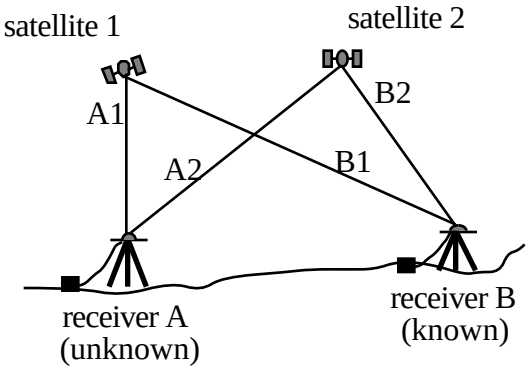

double difference
= (B2 - B1) - (A2 - A1) (2.7)

Figure 2.1
Double Differencing

To transform the undifferenced pseudorange and carrier phase observation equations of (2.1) and (2.5) to double difference equations, each term is double differenced, i.e.:

$$\Delta p = \Delta\rho + \Delta d_{ion} + \Delta d_{trop} + \Delta d\rho + \varepsilon_{\Delta p}, \quad \text{and} \tag{2.8}$$

$$\Delta\Phi = \Delta\rho + \lambda \bullet \Delta N - \Delta d_{ion} + \Delta d_{trop} + \Delta d\rho + \varepsilon_{\Delta\Phi}. \tag{2.9}$$

The variables of equation (2.8) and (2.9) are simply the double differences of the variables described following equations (2.1) and (2.5). Instead of having unknown coordinates within the satellite-receiver range, ρ, of equation (2.2), unknown coordinates fall within the double difference range, $\Delta\rho$, which is written as

$$\begin{aligned}\Delta\rho = {} & \left(\sqrt{(x^{s2} - x_{rB})^2 + (y^{s2} - y_{rB})^2 + (z^{s2} - z_{rB})^2}\right. \\ & \left. - \sqrt{(x^{s1} - x_{rB})^2 + (y^{s1} - y_{rB})^2 + (z^{s1} - z_{rB})^2}\right) \\ - & \left(\sqrt{(x^{s2} - x_{rA})^2 + (y^{s2} - y_{rA})^2 + (z^{s2} - z_{rA})^2}\right. \\ & \left. - \sqrt{(x^{s1} - x_{rA})^2 + (y^{s1} - y_{rA})^2 + (z^{s1} - z_{rA})^2}\right).\end{aligned} \tag{2.10}$$

The superscripts s1 and s2 indicate coordinates of satellites 1 and 2 respectively and the subscripts rA and rB indicate the coordinates of receivers A and B respectively (as illustrated in Figure 2.1). Note the only unknowns in equation (2.10) are the x, y and z coordinates of receiver A ($x_{rA,}$ y_{rA} and z_{rA}).

A disadvantage of double differencing is the resulting correlations (illustrated in Figure 2.2) that must be accounted for in double difference processing.

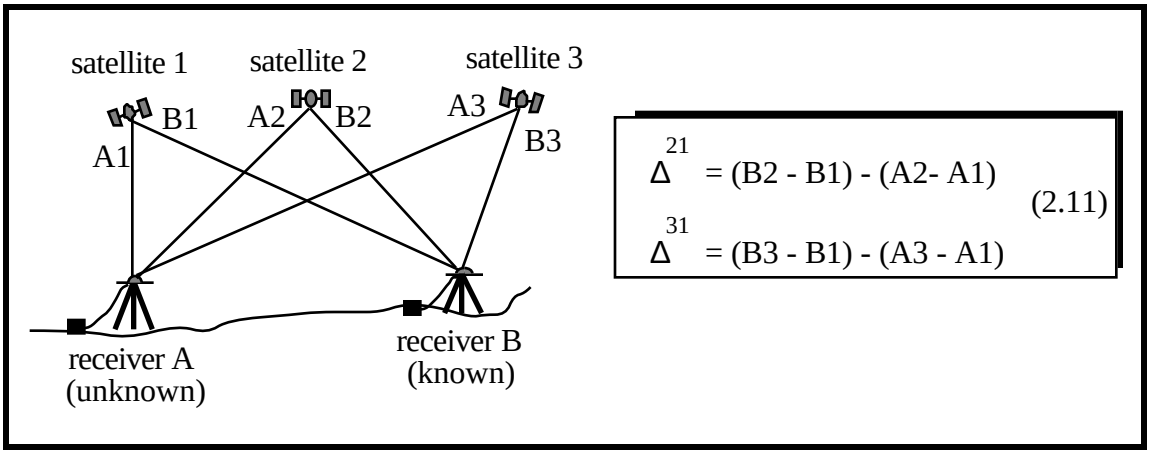

Figure 2.2
Double Difference Correlations

Figure 2.2 follows that of Figure 2.1, but three satellites are included instead of two, resulting in two double difference equations instead of one. The ranges A1 and B1 are used in both equation Δ^{21} for double differences using satellites 2 and 1, and equation Δ^{31} for double differences using satellites 3 and 1, hence their mathematical correlation. Methods for accounting for these correlations in processing are given in Remondi (1984) and Biacs et al. (1990).

2.2.2 Errors

A key benefit of double differencing is its ability to reduce or eliminate many GPS observations errors. There are no clock errors present in equations (2.8) or (2.9) because the satellite clock errors cancelled in inter-receiver differencing, and the receiver clock errors cancelled in inter-satellite differencing. Ionospheric, tropospheric and orbital errors are greatly reduced through double differencing for short baselines (< 10 km), where the errors at the two receiver sites tend to be highly correlated. As the spatial distance between receivers increases, these errors decorrelate and become significant. Receiver noise and multipath errors are receiver and site dependent, and so are not reduced through double differencing, but rather are amplified by a factor of two (Lachapelle, 1991).

Receiver measurement noise is a result of thermal noise intercepted by the antenna, noise from the receiver oscillator and other hardware components. It is a function of the tracking bandwidth, carrier to noise density ratios and code tracking mechanization parameters. Although a narrow tracking bandwidth results in more accurate measurements, the bandwidth must be wide enough to maintain carrier phase lock (Lachapelle et al., 1987). Receiver noise for code and carrier measurements is given for the NovAtel GPSCard™ and Ashtech P-XII receivers in Table 3.1 (under the row headings of 'code accuracy' and 'carrier accuracy').

Over short baselines, where most errors are dramatically reduced through double differencing, multipath errors can be a limiting factor. Georgiadou and Kleusberg (1988) have shown that the amplitude of multipath carrier phase errors theoretically cannot exceed $\lambda/4$, or 4.8 cm for an L1 wavelength. In practical applications one would not expect to see such high magnitudes of carrier multipath errors since highly reflective surfaces are avoided in choosing GPS observation sites and minimization of multipath is

considered in receiver and antenna design. For example, Henson et al. (1985) claim 0.0 to 1.5 cm as the double difference carrier phase multipath error budget of the TI-4100 receiver. C/A code multipath can theoretically reach up to 293 m and in practice has been shown to have magnitudes of up to 20 m (Lachapelle et al., 1989). However, technology implemented in the new NovAtel GPSCard™ (Van Dierendonck et al., 1992) effectively reduces code multipath to sub-metre levels (Cannon and Lachapelle, 1992a).

One of the drawbacks of multipath in a static environment is its cyclical nature. Its periodicity may range from a few minutes to over an hour for carrier phase observations (Georgiadou and Kleusberg, 1988) or code observations (Tranquilla and Carr, 1990), and so would require the corresponding averaging times to nullify its effects. Multipath can be reduced through site selection and the use of ground planes (Lachapelle et al., 1989; Tranquilla and Carr, 1990; Cannon and Lachapelle, 1992b).

2.3 LEAST SQUARES SOLUTIONS

The system of equations for undifferenced observations, (2.1), and double difference observations, (2.8) and (2.9), can be solved through a parametric least squares adjustment with math models of the form

$$\underset{(nx1)}{l} = \underset{(nxu)}{A}\ \underset{(ux1)}{x} + \underset{(nx1)}{w} \qquad (2.12)$$

Here, l is the vector of observations, A is the design matrix, x is the vector of unknown parameters and w is the vector of misclosures. Dimensions are given under each variable of equation (2.12), where n is the number of observations and u is the number of unknown parameters.

The explicit form of the unknown parameters vector and the design matrix for an epoch t using the pseudorange observations from a single receiver (as per equation (2.1)) is given in Table 2.3a. In this case the number of observations equals the number of satellites (nsat) and so the A matrix has dimensions (nsat x 4). Carrier phase observations are not used for single point positioning since orbital errors are too great to fully exploit the accuracy of pseudorange observations, let alone the more accurate carrier phase observations.

The explicit form of the unknown parameters vector and the design matrix for a single epoch using double differenced pseudorange observations (as per equation (2.8)) is given in Table 2.3b. Note the number of unknowns has been reduced from four to three due to the elimination of the clock term through double differencing. The number of observations in this case refers to the number of double difference observations. Hence the dimensions of the A matrix are reduced from (nsat x 4) in Table 2.3a to ((nsat-1) x 3) in Table 2.3b.

If the unknown double difference carrier phase ambiguities, ΔN, are determined by some independent means prior to a least squares GPS solution, equation (2.9) reduces to the same form as the pseudorange equation (2.8) and the unknown parameters vector and design matrix are identical to the pseudorange double difference case of Table 2.3b.

Table 2.3
Explicit Forms of The Parameter Vectors and Design Matrices

(a) ***For Single Point Pseudorange Solutions***

$$x = \begin{bmatrix} x_r \\ y_r \\ z_r \\ dT \end{bmatrix} \qquad A = \begin{bmatrix} \frac{\partial f_1}{\partial x_r} & \frac{\partial f_1}{\partial y_r} & \frac{\partial f_1}{\partial z_r} & 1 \\ \frac{\partial f_2}{\partial x_r} & \frac{\partial f_2}{\partial y_r} & \frac{\partial f_2}{\partial z_r} & 1 \\ \cdots & \cdots & \cdots & \cdots \end{bmatrix}$$

$$\frac{\partial f_1}{\partial x_r} = \frac{-\left(x^{s1} - x_r\right)}{\rho_r^{s1}}$$

$$\frac{\partial f_1}{\partial y_r} = \frac{-\left(y^{s1} - y_r\right)}{\rho_r^{s1}}$$

$$\frac{\partial f_1}{\partial z_r} = \frac{-\left(z^{s1} - z_r\right)}{\rho_r^{s1}}$$

(b) ***For Double Difference Pseudorange Solutions*** **OR**
Double Difference Carrier Phase Solutions with Fixed Ambiguities

$$x = \begin{bmatrix} x_{rA} \\ y_{rA} \\ z_{rA} \end{bmatrix} \qquad A = \begin{bmatrix} \frac{\partial f_1}{\partial x_{rA}} & \frac{\partial f_1}{\partial y_{rA}} & \frac{\partial f_1}{\partial z_{rA}} \\ \frac{\partial f_2}{\partial x_{rA}} & \frac{\partial f_2}{\partial y_{rA}} & \frac{\partial f_2}{\partial z_{rA}} \\ \cdots & \cdots & \cdots \end{bmatrix}$$

$$\frac{\partial f_1}{\partial x_{rA}} = \frac{-\left(x^{s2} - x_{rB}\right)}{\rho_{rB}^{s2}} + \frac{\left(x^{s1} - x_{rB}\right)}{\rho_{rB}^{s1}}$$

$$\frac{\partial f_1}{\partial y_{rA}} = \frac{-\left(y^{s2} - y_{rB}\right)}{\rho_{rB}^{s2}} + \frac{\left(y^{s1} - y_{rB}\right)}{\rho_{rB}^{s1}}$$

$$\frac{\partial f_1}{\partial z_{rA}} = \frac{-\left(z^{s2} - z_{rB}\right)}{\rho_{rB}^{s2}} + \frac{\left(z^{s1} - z_{rB}\right)}{\rho_{rB}^{s1}}$$

(c) ***For Double Difference Carrier Phase Solutions with Floating Ambiguities***

$$x = \begin{bmatrix} x_{rA} \\ y_{rA} \\ z_{rA} \\ \Delta N^{s2s1} \\ \Delta N^{s3s1} \\ \cdots \end{bmatrix} \qquad A = \begin{bmatrix} \frac{\partial f_1}{\partial x_{rA}} & \frac{\partial f_1}{\partial y_{rA}} & \frac{\partial f_1}{\partial z_{rA}} & 1 & 0 & \cdots \\ \frac{\partial f_2}{\partial x_{rA}} & \frac{\partial f_2}{\partial y_{rA}} & \frac{\partial f_2}{\partial z_{rA}} & 0 & 1 & \cdots \\ \cdots & \cdots & \cdots & \cdots & \cdots & \cdots \end{bmatrix}$$

partial derivatives for x_{rA}, y_{rA}, and z_{rA} are the same as in (b)

The ambiguities are then said to be "fixed", meaning they are held at some constant predetermined integer value.

When double difference ambiguities are not predetermined, they must be estimated as unknowns along with receiver coordinates. In this case the ambiguities are said to be "floating" since they are not restricted to integer values. The explicit form of the unknown parameters vector and the design matrix for a single epoch using double differenced carrier phase observations with floating ambiguities (as per equation (2.8)) is given in Table 2.3c. The number of double difference observations is (nsat-1). The unknowns include three receiver coordinates and (nsat-1) double difference ambiguities.

The linearized form of equation (2.12) is

$$\underset{(nx1)}{v} = \underset{(nxu)}{A}\ \underset{(ux1)}{\delta} + \underset{(nx1)}{w} \qquad (2.13)$$

where v is the vector of residuals, A the design matrix, δ the correction vector to the approximate values and w the misclosure vector. The corresponding least squares solution is

$$\delta = -\left(A^T C_l^{-1} A\right)^{-1} A^T C_l^{-1} w \qquad (2.14)$$

where C_l is the covariance matrix of the observations (Krakiwsky, 1990). Equation (2.14) can be written as

$$\delta = -N^{-1} u \qquad \text{where,} \qquad (2.15)$$

$$N = \left(A^T C_l^{-1} A\right) \qquad \text{and} \qquad (2.16)$$

$$u = A^T C_l^{-1} w. \qquad (2.17)$$

The design matrices given in Table 2.3 all correspond to a single epoch in time. Assuming GPS observations are uncorrelated between epochs, the normal equations matrix, N, corresponding to a set of consecutive epochs of observations is block diagonal, meaning summation techniques may be used in solution computations (Mikhail, 1976).

2.4 PREANALYSIS

Much can be learned about the relative accuracies achievable with the above models under a variety of observing conditions using dilution of precision (DOP) and statistical reliability. Both are suited for preanalysis since they require only a simulation of observing conditions (i.e., time, satellite constellation etc.) and do not require observations.

2.4.1 DOP and RDOP

Dilution of precision (DOP) is a scalar which represents the geometrical contribution of observations to a solution. Conventionally DOP is used to represent the geometry of single point positioning, but it can be extended to represent the geometry of double differencing for pseudorange and carrier phase observations. This extension will be referred to as RDOP (relative dilution of precision). Equations for computing and using DOPs and RDOPs follow.

DOP Computations

DOPs are computed as the square root of the trace of the covariance matrix of the parameters C_x, which is the inverse of the normal equations matrix, i.e.,

$$C_x = N^{-1} = \left(A^T C_l^{-1} A\right)^{-1} \tag{2.18}$$

where A is the design matrix given in Table 2.3a. Here C_l^{-1} is unscaled and used to represent relative weighting of the observations. For single point positioning, since observations are assumed uncorrelated and of equal weight, C_l^{-1} reduces to a diagonal matrix and equation 2.18 reduces to

$$C_x = N^{-1} = \left(A^T A\right)^{-1} . \tag{2.19}$$

Covariance matrix components for cartesian and geodetic coordinate systems are given in equations 2.20a and 2.20b respectively:

$$C_x = \begin{bmatrix} \sigma_\varphi^2 & \sigma_{\varphi\lambda} & \sigma_{\varphi h} & \sigma_{\varphi t} \\ \sigma_{\lambda\varphi} & \sigma_\lambda^2 & \sigma_{\lambda h} & \sigma_{\lambda t} \\ \sigma_{h\varphi} & \sigma_{h\lambda} & \sigma_h^2 & \sigma_{ht} \\ \sigma_{t\varphi} & \sigma_{t\lambda} & \sigma_{th} & \sigma_t^2 \end{bmatrix} \tag{2.20a}$$

$$C_x = \begin{bmatrix} \sigma_x^2 & \sigma_{xy} & \sigma_{xz} & \sigma_{xt} \\ \sigma_{yx} & \sigma_y^2 & \sigma_{yz} & \sigma_{yt} \\ \sigma_{zx} & \sigma_{zy} & \sigma_z^2 & \sigma_{zt} \\ \sigma_{tx} & \sigma_{ty} & \sigma_{tz} & \sigma_t^2 \end{bmatrix} . \tag{2.20b}$$

In the geodetic coordinate system, φ, λ and h represent the latitude, longitude and height parameters respectively, and t the clock offset. In the cartesian coordinate system,

parameters are as previously defined. From these covariance matrices the influence of the satellite geometry on the full solution or any component thereof may be calculated from the square root of the sum of the diagonal components as shown in Table 2.4.

Table 2.4
Types of DOPs

Acronym	Type	Cartesian (x, y, z)	Geodetic (ϕ, λ, h)
GDOP	geometrical	$(\sigma_x^2 + \sigma_y^2 + \sigma_z^2 + \sigma_t^2)^{1/2}$	$(\sigma_\varphi^2 + \sigma_\lambda^2 + \sigma_h^2 + \sigma_t^2)^{1/2}$
PDOP	positional	$(\sigma_x^2 + \sigma_y^2 + \sigma_z^2)^{1/2}$	$(\sigma_\varphi^2 + \sigma_\lambda^2 + \sigma_h^2)^{1/2}$
HDOP	horizontal	---	$(\sigma_\varphi^2 + \sigma_\lambda^2)^{1/2}$
VDOP	vertical	---	σ_h
TDOP	time	σ_t	σ_t

RDOP Computations

RDOPs, like DOPs are computed as the square root of the trace of the covariance matrix C_X (Lu et al., 1990). For double difference pseudorange solutions or carrier phase solutions with fixed ambiguities, the covariance matrix of the parameters is computed using the design matrix of Table 2.3b, and for carrier phase solutions with floating ambiguities, it is computed using the design matrix of Table 2.3c. In both cases the covariance matrix of the observations should be included to account for double difference correlations.

Covariance matrix components in the geodetic coordinate system corresponding to double difference pseudorange solutions or carrier phase solutions with fixed ambiguities are given as

$$C_X = \begin{bmatrix} \sigma_\varphi^2 & \sigma_{\varphi\lambda} & \sigma_{\varphi h} \\ \sigma_{\lambda\varphi} & \sigma_\lambda^2 & \sigma_{\lambda h} \\ \sigma_{h\varphi} & \sigma_{h\lambda} & \sigma_h^2 \end{bmatrix}. \qquad (2.21)$$

Covariance matrix components in the geodetic coordinate system corresponding to double difference carrier phase solutions with floating ambiguities (assuming four satellites are observed, i.e. three double differences) are given as

$$C_X = \begin{bmatrix} \sigma_\varphi^2 & \sigma_{\varphi\lambda} & \sigma_{\varphi h} & \sigma_{\varphi N1} & \sigma_{\varphi N2} & \sigma_{\varphi N3} \\ \sigma_{\lambda\varphi} & \sigma_\lambda^2 & \sigma_{\lambda h} & \sigma_{\lambda N1} & \sigma_{\lambda N2} & \sigma_{\lambda N3} \\ \sigma_{h\varphi} & \sigma_{h\lambda} & \sigma_h^2 & \sigma_{hN1} & \sigma_{hN2} & \sigma_{hN3} \\ \sigma_{N1\varphi} & \sigma_{N1\lambda} & \sigma_{N1h} & \sigma_{N1}^2 & \sigma_{N1N2} & \sigma_{N1N3} \\ \sigma_{N2\varphi} & \sigma_{N2\lambda} & \sigma_{N2h} & \sigma_{N2N1} & \sigma_{N2}^2 & \sigma_{N2N3} \\ \sigma_{N3\varphi} & \sigma_{N3\lambda} & \sigma_{N3h} & \sigma_{N3N1} & \sigma_{N3N2} & \sigma_{N3}^2 \end{bmatrix}. \qquad (2.22)$$

From these covariance matrices of the parameters, the influence of the satellite geometry on the full solution or any component thereof may be calculated from the square root of the sum of the diagonal components as shown in Table 2.5.

Table 2.5
Types of RDOPs

Acronym	Type	Code or Carrier with Fixed Ambiguities	Carrier with Floating Ambiguities
RGDOP	geometrical	$(\sigma_\varphi^2 + \sigma_\lambda^2 + \sigma_h^2)^{1/2}$	$(\sigma_\varphi^2 + \sigma_\lambda^2 + \sigma_h^2 + \sigma_{N1}^2 + \sigma_{N2}^2 + \sigma_{N3}^2)^{1/2}$
RPDOP	positional	$(\sigma_\varphi^2 + \sigma_\lambda^2 + \sigma_h^2)^{1/2}$	$(\sigma_\varphi^2 + \sigma_\lambda^2 + \sigma_h^2)^{1/2}$
RHDOP	horizontal	$(\sigma_\varphi^2 + \sigma_\lambda^2)^{1/2}$	$(\sigma_\varphi^2 + \sigma_\lambda^2)^{1/2}$
RVDOP	vertical	σ_h	σ_h

Significance of DOPs and RDOPs

The effect that satellite geometry has on single point pseudorange positioning accuracy is given in Wells et al. (1986) as

$$\sigma_{sp} = DOP \bullet \sigma_{o_{sp}}, \tag{2.23}$$

where σ_{sp} is the achievable single point positioning accuracy, DOP is a dilution of precision measure from Table 2.4 and $\sigma_{o_{sp}}$ is the measurement accuracy encompassing all the errors discussed in Section 2.1.3. The effect that satellite geometry has on double difference positioning accuracy can similarly be written as

$$\sigma_\Delta = RDOP \bullet \sigma_{o_\Delta}, \tag{2.24}$$

where σ_Δ is the achievable double difference positioning accuracy, RDOP is a dilution of precision measure from Table 2.5 and σ_{o_Δ} is measurement accuracy encompassing errors which remain after double differencing.

In practice, DOP measures are commonly used and well accepted. In contrast, RDOP values are rarely used and not as well accepted. Part of the problem with RDOPs is their ambiguous definition. Above two definitions for RDOPs are given, one assuming fixed ambiguities and the other assuming floating ambiguities. When using RDOP values it is important to specify such assumptions.

It should be noted that DOPs and RDOPs are scalar numbers and do not provide the full set of information made available in the covariance matrices. Nevertheless, both measures are significant tools that can be used to analyze the geometrical strength of GPS solutions.

2.4.2 Reliability

Reliability analysis (Baarda, 1968), which has been applied to network strength in conventional surveying applications (MacKenzie, 1985; Caspary, 1988) has been extended to GPS surveys (Van der Marel and Kö sters, 1989; Biacs and Krakiwsky, 1990; Biacs et al., 1990; Lu, 1990). By specifying the appropriate alternative hypothesis, the sensitivity to and effect of undetected errors in GPS surveys may be analyzed. In GPS baseline adjustments, errors may include code or carrier outliers, uncorrected cycle slips, satellite ephemeris errors or atmospheric modeling errors. In GPS network adjustments, errors may include station set-up errors, station misidentifications, incorrect antenna heights or coordinate difference errors (Van der Marel, 1990). Only the reliability analysis for baseline adjustments are presented in this thesis.

Reliability may be classified as internal or external. Internal reliability is the minimum size an observation error must be to be detected through statistical testing. External reliability is the influence of undetected errors on the adjustment results. An

overview of the formulation of each follows, but for detailed explanations and derivational developments one may refer to Mackenzie (1985) or Caspary (1988). Since reliability is based on redundancy numbers, redundancy numbers are discussed first.

Redundancy Numbers

Redundancy in an adjustment is equivalent to the degrees of freedom. For a parametric adjustment the redundancy, r, is given as the number of observations, n, minus the number of unknowns u, i.e.

$$r = n - u. \tag{2.25}$$

From MacKenzie (1985), redundancy may alternatively be derived as

$$r = tr\left(C_{\hat{v}}\, C_l^{-1}\right), \tag{2.26}$$

where C_v is the covariance matrix of the residuals which may be computed as

$$C_{\hat{v}} = C_l^{-1} - AC_x A^T. \tag{2.27}$$

While redundancy refers to the total redundancy of an adjustment, redundancy numbers give the contribution of a specific observation to the total redundancy. The redundancy number of the i'th observation is given as

$$r_i = tr\left(C_{\hat{v}}\, C_l^{-1}\right)_{ii}. \tag{2.28}$$

Redundancy numbers are always greater than zero and less than one, i.e.

$$0 < r_i < 1 \tag{2.29}$$

and the sum of all redundancy numbers equals the total redundancy, i.e.

$$r = \sum_{i=1}^{n} r_i. \qquad (2.30)$$

The smaller the redundancy number the more critical the i'th observation is to the adjustment solution and vice versa (Förstner, 1979).

Internal Reliability

Since internal reliability is the minimum size an error must be to be detected through statistical testing, it is referred to as the "minimal detectable error" (MDE). Computations of internal reliability are based on the assumption that all observations are normally distributed except for one which is biased by some non-stochastic error. The non-centrality parameter λ_o which corresponds to the significance level α_o and power of the test $1 - \beta_o$ to be used in statistical testing to detect outliers (Vanicek and Krakiwsky, 1982; Caspary, 1988), is used in internal reliability computations. For uncorrelated observations the MDE is computed as

$$l_i = \sigma_{l_i} \sqrt{\frac{\lambda_o}{r_i}} \ , \qquad (2.31)$$

where l_i is the MDE of the i'th observation, σ_{l_i} is the standard deviation of the i'th observation, λ_o is the non-centrality parameter and r_i is the redundancy number. The smaller the MDE, the weaker the adjustment and vice versa (Mackenzie, 1985).

External Reliability

External reliability is the influence of undetected errors on the adjustment results. It can be computed following the least squares solution equation of (2.14) by replacing the misclosure vector with an expression to represent MDEs (Caspary, 1988), i.e.

$$X = \left(A^T C_l^{-1} A\right)^{-1} A^T C_l^{-1} c \quad l_i \tag{2.32}$$

where $$c = (0, ..., 0, 1, 0, \ldots, 0)^T. \tag{2.33}$$

Here X is the vector of external reliabilities for the parameter vector x, l_i is the vector of internal reliabilities (MDEs) for each observation, and c is a zero vector with a 1 in the i'th row corresponding to the observation MDE whose effect is being tested.

The usefulness of the external reliability measure given in equation 2.32 is limited since like the unknown parameters x, the external reliabilities X are datum dependent (Mackenzie, 1985), meaning they are biased by the chosen reference base. Instead, a datum independent measure of external reliability, $\bar{\delta}_{o,i}$, can be used as given by Grün dig and Bahndorf (1984)

$$\bar{\delta}_{o,i} = \lambda_o \frac{1 - r_i}{r_i} . \tag{2.34}$$

This equation is based on the assumption of observations being uncorrelated.

Redundancy numbers, internal reliability and external reliability can all be computed in preanalysis mode to analyze the strengths and weaknesses of GPS solutions. They have been used by Van der Marel (1990), Lu et al (1990) and Biacs et al (1990) to analyze static GPS surveys. They are used to analyze rapid static surveys and the combination of code and carrier measurements in Chapter 4.

CHAPTER 3
DATA DESCRIPTION

Descriptions of data sets used to test the methods presented in the following chapters are given. The receiver types used, baselines observed and data sets collected are described.

3.1 RECEIVER TYPES

Two receiver types were used for data collection, the NovAtel Model 1001 GPSCard™ and the Ashtech P-XII receivers. The NovAtel receiver was introduced to the GPS industry in mid-1991 (Fenton et al., 1991) and The University of Calgary had access to the NovAtel GPSCard™ data for analysis prior to the expected 1992 production (Erickson et al., 1991). The Ashtech P code receivers used were recent purchases of the Department of Surveying Engineering at The University of Calgary (delivered November 1991). The technological currency of these two types of receivers has significant implications for the investigations made in this thesis. In particular, they dramatically improve initial coordinate estimation as discussed in Chapter 4.

The NovAtel GPSCard™ is a 10 channel receiver card which tracks C/A code and carrier phase observations from up to 10 satellites simultaneously. It is most noteworthy for its high accuracy C/A code measurements, shown to be accurate to the 10 cm level (Erickson et al., 1991) as opposed to the one to three m level which typifies C/A code accuracies of other receivers (Lachapelle et al., 1989). This high accuracy is achieved through the innovative code tracking loop technology employed (Fenton et al., 1991). The receiver is also resistant to much of the multipath effects which usually plague C/A code measurements (Van Dierendonck et al., 1992; Cannon and Lachapelle, 1992a). The C/A code accuracy of the NovAtel GPSCard™ is similar to P code accuracy, without the impending access denial facing the P code.

The Ashtech P-XII is a 36 channel dual frequency receiver which receives carrier phase and P code observations on L1 and L2 frequencies from up to 12 satellites simultaneously. It also collects C/A code data, making it unique as compared to other receivers which collect either P code data or C/A code data. The dual frequency P code data opens many possibilities for rapid static positioning, especially concerning the use of various widelaning and extra-widelaning techniques (Wübbena, 1989; Abidin and Wells, 1990). However, these are not investigated in this thesis, as the scope has been limited to single frequency observations. P code data on a single frequency is used on occasion to compare with the NovAtel C/A code data, and to assist in some of the developments in this thesis. Major characteristics of the NovAtel GPSCard™ and Ashtech P-XII receivers are given in Table 3.1.

Table 3.1
Characteristics of the NovAtel GPSCard™ 1001 and Ashtech P-XII Receivers

Characteristics	NovAtel GPSCard™	Ashtech P-XII
carrier frequencies	L1	L1 & L2
number of channels	10	36 (12 x 3)
code modulation	C/A on L1	C/A on L1, P on L1 & L2
C/A code accuracy	10 cm	1 - 2.5 m*
P code accuracy	--	10 - 30 cm*
Carrier accuracy	4 mm†	< 0.5 mm*

* (Cannon and Lachapelle, 1992b) † (NovAtel Communications Ltd., 1991)

3.2 BASELINE LENGTHS

Observations used in this thesis were made over baselines with lengths of 0 m, 700 m and 4 km, as the scope for this thesis was limited to the short baseline case. The zero baseline consisted of two receivers connected to one antenna through an antenna splitter. Since the same observations were received at both receivers, all errors with the exception of the receiver noise and a small amount of residual multipath cancelled out in double differencing, giving an ideal data set for initial investigations of theories and algorithms. The 700 m baselines measured were on two concrete pillars (Piers 2 and 4) of the Calgary EDM Calibration Baseline, established by the Province of Alberta. The piers were designed for positional stability and forced centering. A "known" distance between piers, from very precise electronic distance measurements (EDM), was available from the Geodetic Survey of Canada. (See Gillis and Nabe (1988) for details on EDM Calibration Baselines.) This provided a good independent interstation distance check for

the GPS observations. Precise x, y and z coordinate differences were not available and instead were derived using the program SEMIKIN (Cannon, 1990) using carrier phase observations over time spans of at least 20 minutes. The 4 km baseline was measured on points without any ground truth. Therefore it was necessary to attain precise coordinate and distance differences using SEMIKIN once again.

3.3 DESCRIPTION OF DATA SETS

The characteristics of each data set used are given in Table 3.2. Antenna choke ring ground planes were used in all data collection to reduce multipath effects.

Table 3.2
Summary of Data Sets

Date	Receiver	Baseline Length	Data Rate	S/A†
Jan. 25	Ashtech P-XII	0.0 m	2 s	active
Feb. 12	NovAtel 1001	720.1 m	1 s	active
Feb. 15	NovAtel 1001	720.1 m	1 s	active
Feb. 17	NovAtel 1001	4.1 km	1 s	active

† based on observations at ACP sites (Héroux, 1992)

The number and position of satellites used have great importance when analyzing results. For this reason elevations for each data set are shown in Figures 3.1 to 3.4. The PDOP range (positional dilution of precision) for each data set is shown in the top right hand corner of each graph. The horizontal axis shows time in seconds of GPS week, with the interval between each major tick representing five minutes and the interval between each minor tick representing one minute.

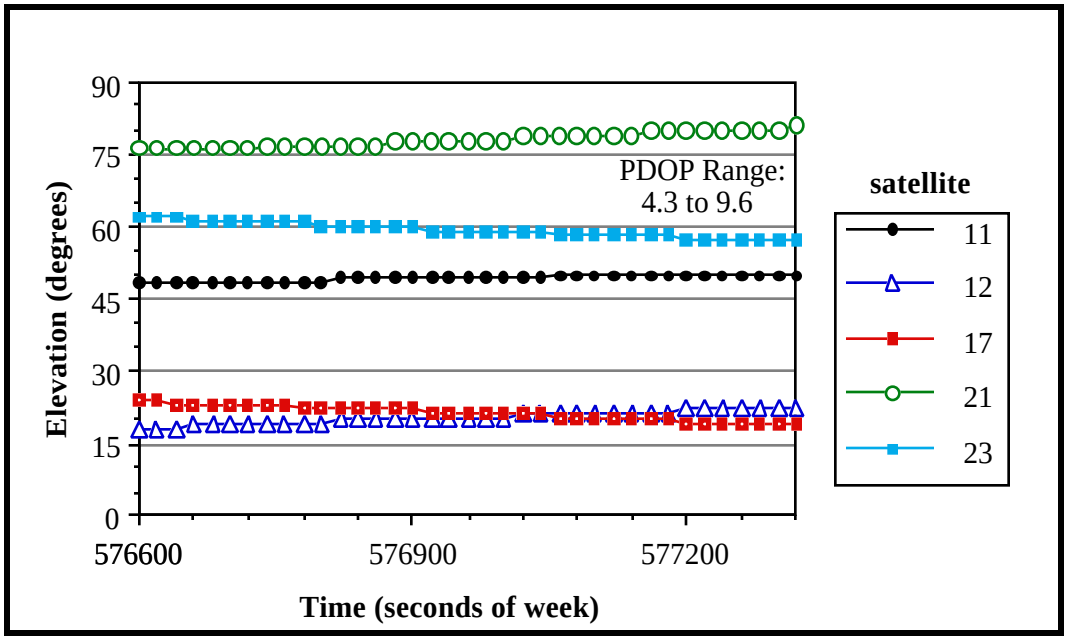

Figure 3.1
Satellite Elevations For Jan. 25th Ashtech Data - Zero Baseline

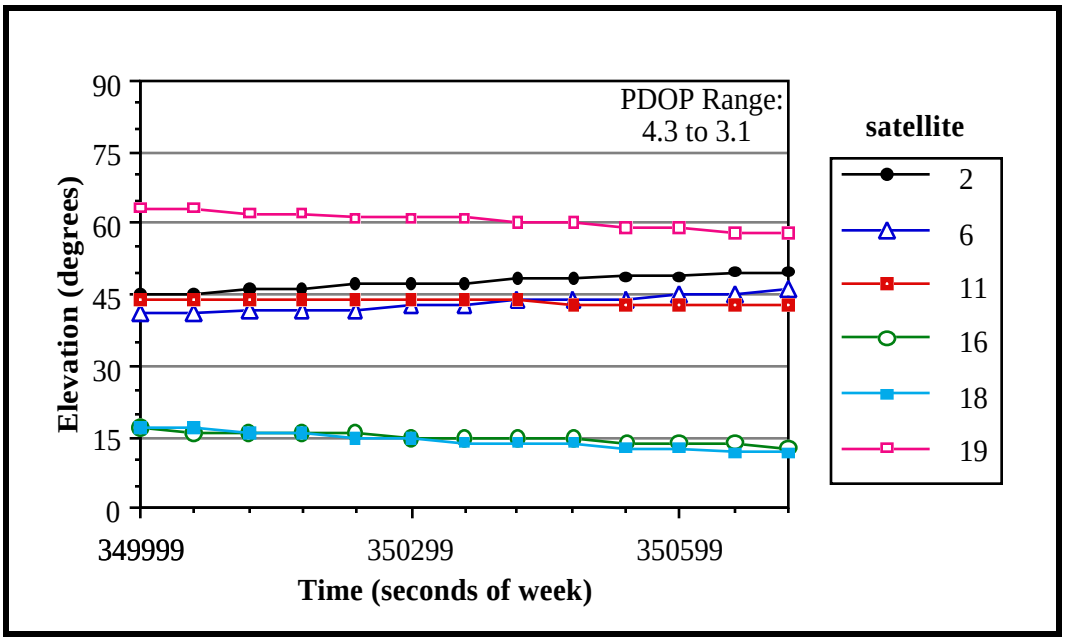

Figure 3.2
Satellite Elevations For Feb. 12th NovAtel Data - 720 m Baseline

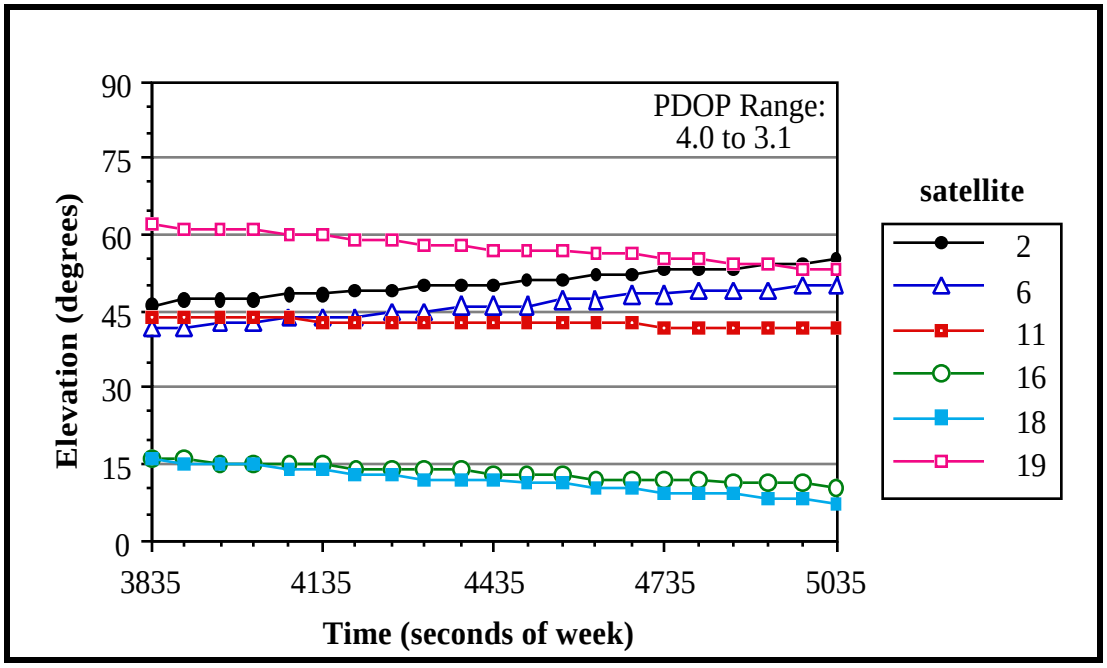

Figure 3.3
Satellite Elevations For Feb. 15th NovAtel Data - 720 m Baseline

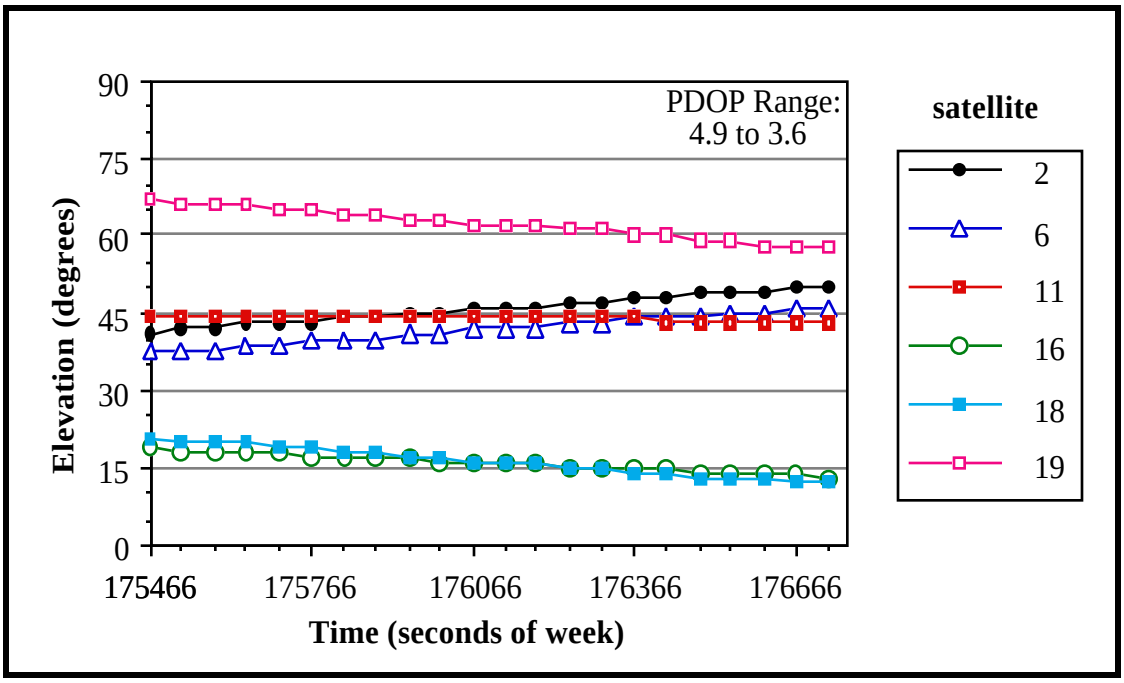

Figure 3.4
Satellite Elevations For Feb. 17th NovAtel Data - 4.1 km Baseline

CHAPTER 4

COORDINATE ESTIMATION BASED ON CODE AND CARRIER MEASUREMENTS

In surveying applications using GPS, it is important to understand the potential and limitations of code and carrier measurements. This is even more critical for rapid static surveys where few epochs of observations are used over short time periods. The potential of these measurements in an adjustment may be assessed through preanalysis and their limitations may be evaluated by comparing the ideal preanalysis with achievable results. In this chapter coordinate estimation based on least squares double difference solutions using code only, carrier only and code and carrier observations combined, are reviewed.

The first section examines the strength of solutions through preanalysis, the second section examines code double difference solutions and the third section examines carrier and code-carrier double difference solutions.

4.1 PREANALYSIS

Through preanalysis, the behavior of double difference solutions using code only, carrier only, and code and carrier observations combined may be studied. Relative

dilution of precisions (RDOPs) and reliability measures are presented for each solution type.

All results presented are from a C-language program specifically written to compute RDOP and reliability measures. The program allows for varied code and carrier data rates and observation weighting.

4.1.1 RDOP

Relative geometrical dilution of precision (RGDOP) values were computed following the equations described in Section 2.4.1 over a five minute observation on February 12th from 350100 to 350400 GPS seconds of week, and are plotted in Figures 4.1 to 4.4. Although observations were not used in RGDOP computations, the time span used falls within the same period for which six satellite NovAtel GPSCard™ data was collected (see Figure 3.2). Double difference mathematical correlations were accounted for in RGDOP computations.

In all cases accumulated rather than instantaneous RGDOPs are shown. This means RGDOPs at one minute are a product of all data up to and including the one minute mark, RGDOPs at two minutes are a product of all data up to and including the two minute mark and so on. RGDOPs are also computed and shown for different data intervals. The varied data intervals over rapid static survey observation periods of say five minutes, are insignificant in terms of satellite geometry but greatly affect the total number of observation epochs. For instance, at a 60 second interval, RDOPs are derived from six observation epochs while at a one second interval RDOPs are derived from 61 observation epochs.

The first calculations were made for carrier observations with ambiguities unknown (float solutions) and are shown in Figure 4.1. The second calculations were made for carrier observations with ambiguities known (fixed solutions) and are shown in Figure 4.2. Two vertical scales appear in each figure, one with unitless RGDOPs and the other with scaled RGDOPs. The unitless RGDOPs were calculated assuming all carrier phase observations to have equal unit weight and the scaled RGDOPs were calculated assuming all carrier phase observations to have equal weights based on standard deviations of five mm. This latter weighting is optimistic since it does not include errors beyond the measurement accuracy, but serves as an indicator of the "best" RGDOPs achievable and will be used for comparisons in the discussion of code and carrier combination.

Note, in the program used, the variances are input for undifferenced observations. These variances are then multiplied by four to account for the propagation of errors in double differencing. Consequently, the unitless RGDOP measures shown in all the figures in this section are based on undifferenced observations of unit weight rather than double difference observations of unit weight.

Comparing Figure 4.2 with 4.1, it can be seen that RGDOP values are plotted for zero minutes in Figure 4.2 but not Figure 4.1. This is because for the former case only three double difference observations are required to solve for the coordinate unknowns, meaning only one epoch is required for a solution, whereas for the latter case eight double difference observations are needed to solve for the coordinate and ambiguity unknowns (assuming six satellites observed), meaning two epochs are required for a solution.

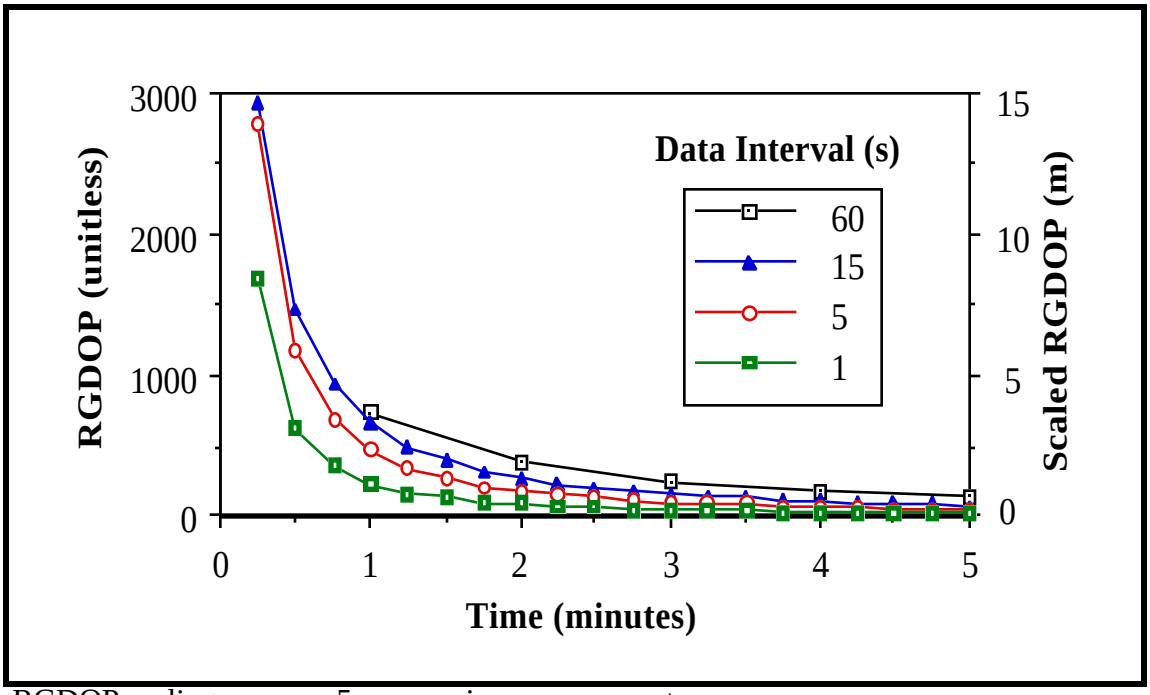

RGDOP scaling assumes 5 mm carrier measurement accuracy.

Figure 4.1
RGDOP - Carrier Ambiguities Unknown
(Feb. 12th, 350100 to 350400 s, 6 satellites)

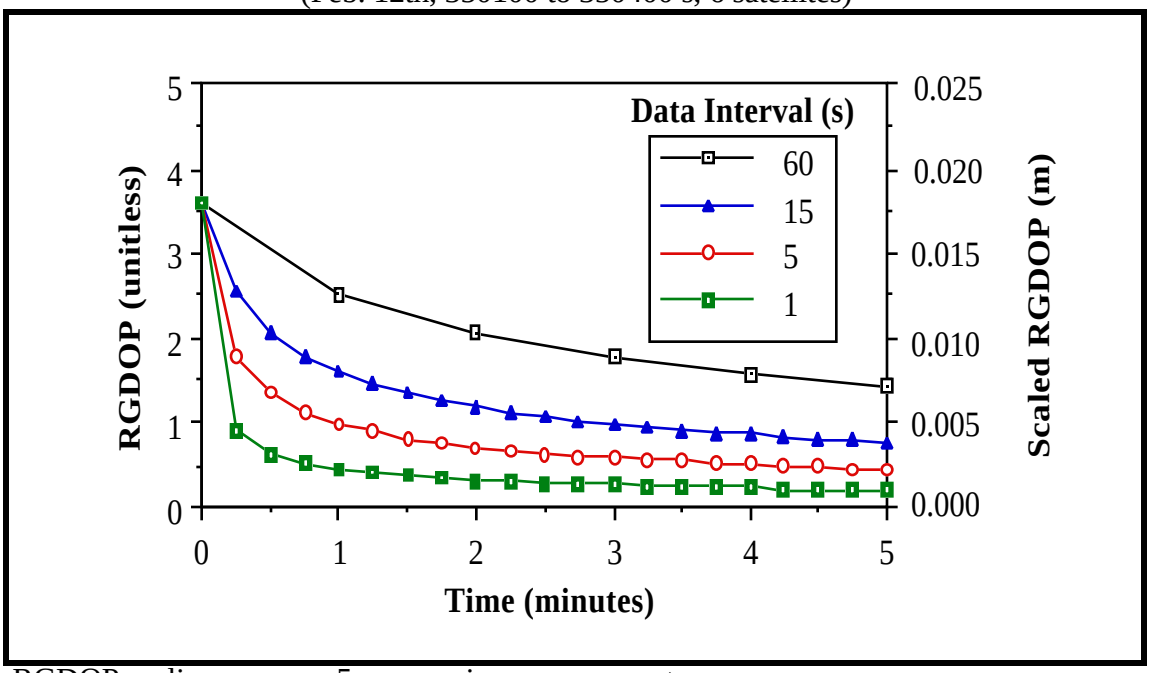

RGDOP scaling assumes 5 mm carrier measurement accuracy.

Figure 4.2
RGDOP - Carrier Ambiguities Known
(Feb. 12th, 350100 to 350400 s, 6 satellites)

Note the dramatic difference in vertical scales for the cases of ambiguities unknown and known, which illustrates the benefits of being able to compute a solution with "fixed" ambiguities. From Figure 4.2 the smaller data intervals improve the RGDOP somewhat, showing the benefit of smaller data intervals when solving only for coordinate unknowns.

RGDOP values for double difference code solutions are given in Figure 4.3. The left hand RGDOP scale is unitless and the right hand has been scaled by a 10 cm code accuracy (representative of the NovAtel GPSCard™ code accuracy). This value is optimistic since it does not include errors beyond the measurement accuracy, but serves as an indicator of the "best" RGDOPs achievable and will be used for comparisons in the discussion of code and carrier combination.

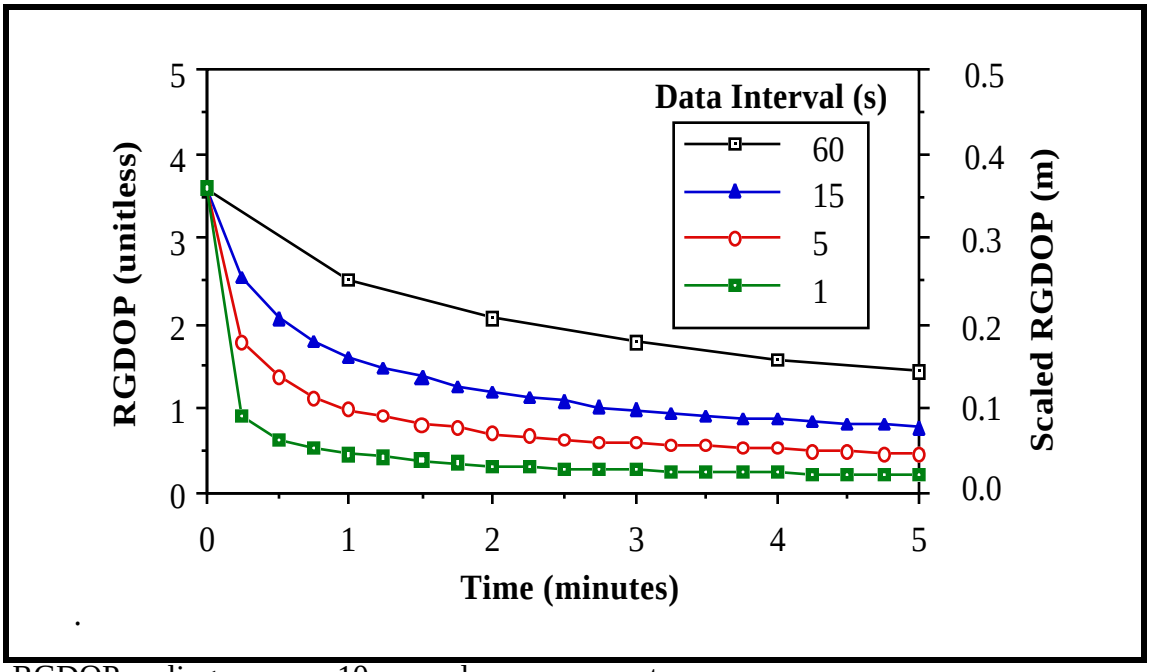

RGDOP scaling assumes 10 cm code measurement accuracy.

Figure 4.3
RGDOP - Code
(Feb. 12th, 350100 to 350400 s, 6 satellites)

As can be expected based on the formulation in Table 2.5, the RGDOP for code and fixed carrier solutions are identical with the exception of the scaling.

Figure 4.4 shows RGDOPs for code and carrier observations combined. The combination of observations was achieved using equations (2.8) and (2.9) together through summation of normal equations, based on the assumption that code and carrier observations of the same epoch are uncorrelated. The objective of forming such a combination of observations is to investigate the possibility of resolving ambiguities simply by combining very accurate code measurements (10 cm) with carrier measurements. In Figure 4.4, carrier observations are weighted with a standard deviation of 5 mm in keeping with Figure 4.1, and code observations are weighted with a standard deviation of 10 cm in keeping with Figure 4.3. The carrier data interval in all cases is 15 s and the code intervals are 15 s, 5 s and 1 s as shown in Figure 4.4.

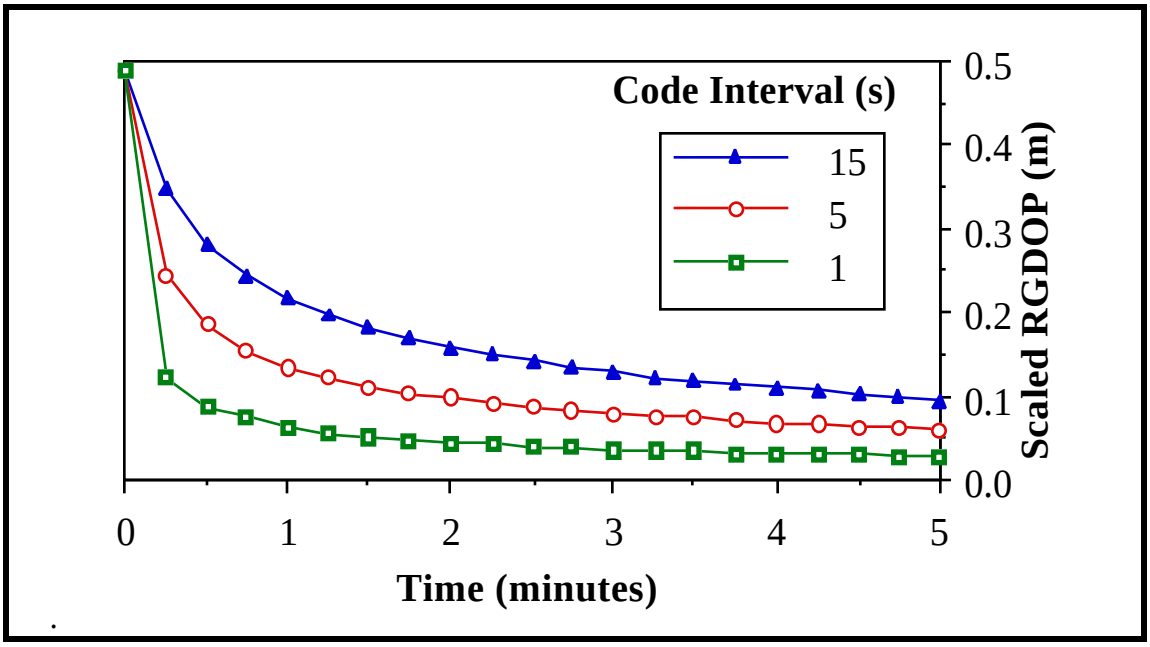

Figure 4.4
RGDOP - Code and Carrier Combined - Ambiguities Unknown
(Feb. 12th, 350100 to 350400 s, 6 satellites)
(code scaling 0.10 m, carrier scaling 0.005 m, carrier interval 15 s)

Several observations can be made regarding Figure 4.4. At the first epoch (0 minutes) a solution impossible using a carrier float solution alone (as per Figure 4.1), is possible using a combination of code and carrier measurements, albeit worse than a code solution alone as indicated by the RGDOP values. After five minutes at a 1 s code data rate the RGDOP value is 0.03 m, accurate enough to resolve integer ambiguities if all the underlying assumptions are true.

The relative weighting of code and carrier observations has significant implications on the combined solutions and RGDOPs. To combine the observations effectively, correct relative weights, determined through rigorous testing should be used. The results presented here give an indication of theoretical accuracies possible for code and carrier combinations, but optimal relative weighting has not been investigated.

To show the significance of relative weights, in Figure 4.4 code observations were given 1/20th of the weight of carrier observations. In Figure 4.5, the same code-carrier observations are shown, but with code observations holding only 1/40th of the weight of the carrier observations.

Comparing Figure 4.5 with 4.4 and paying attention to the vertical scales, it can be seen that doubling the code accuracy (halving its relative weight with respect to carrier observations) has the effect of essentially doubling the RGDOP. Based on the assumptions used, from Figure 4.5 it can be seen that with five minutes of observations using 15 s carrier data at a 5 mm accuracy and 1 s code data at a 20 cm accuracy, one should theoretically be able to achieve about 5 cm accuracy. These numbers indicate that ambiguities theoretically can be resolved using a simple combination of carrier and code measurements in an adjustment through the summation of normal equations. Shortfalls in the assumptions used, discussed in Section 4.2 and 4.3, show why this is inconsistent with results found with real data.

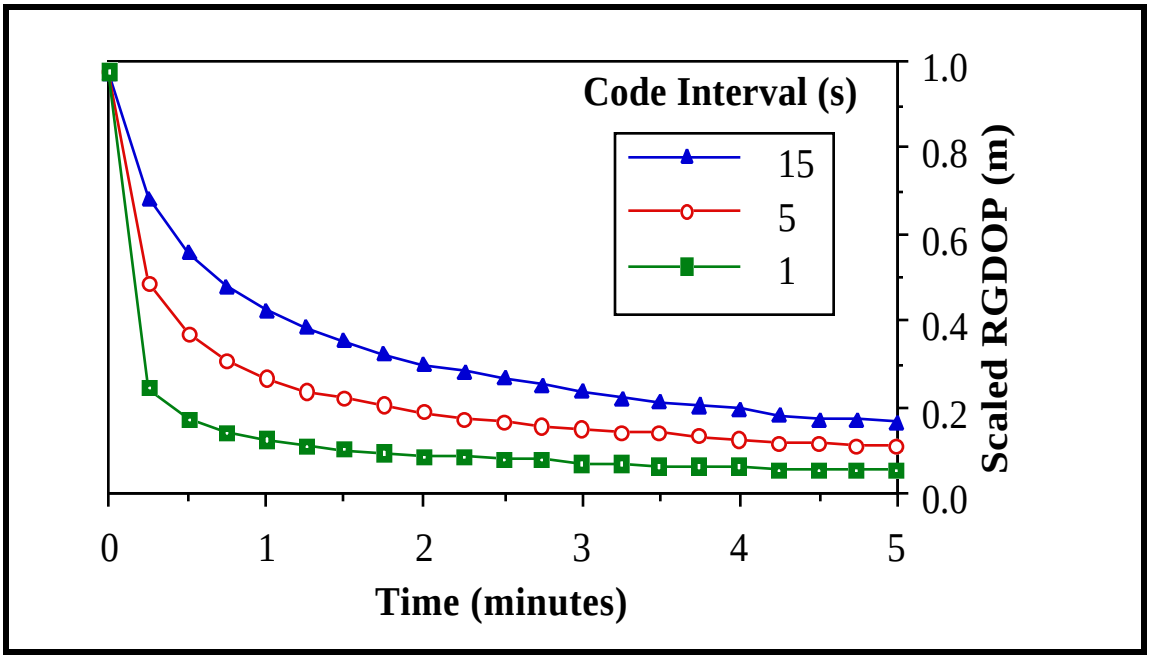

Figure 4.5
RGDOP - Code and Carrier Combined - Ambiguities Unknown
(Feb. 12th, 350100 to 350400 s, 6 satellites)
(code scaling 0.20 m, carrier scaling 0.005 m, carrier interval 15 s)

4.1.2 Reliability

Reliability measures were computed following the equations described in Section 2.4.2 over the same five minute observation span as used for the RDOP calculations shown above. In all cases reliabilities are based on accumulated rather than instantaneous solutions. To reduce the computational burden, the double difference correlations are neglected as is done in Lu (1990).

Statistical reliabilities are computed to give an indication of the quality of solutions over the short time spans which characterize rapid static surveys. Redundancy numbers, internal reliability and external reliabilities for carrier only, code only and code and carrier observations combined are presented.

Redundancy Numbers

Redundancy numbers help provide an understanding of how observations are combined within an adjustment to arrive at a solution. As explained in Section 2.4.2, observations critical to a solution will have small redundancies numbers, and those well-checked within a solution will have large redundancy numbers.

Redundancy numbers for carrier float solutions computed based on equation (2.28) over one and five minute periods are shown in Figures 4.6a and 4.6b respectively. A data interval of 15 s is used, resulting in five epochs for the one minute solution and 21 epochs for the five minute solution. The legend shows the respective SV (space vehicle, i.e. satellite) pairs used in double differencing.

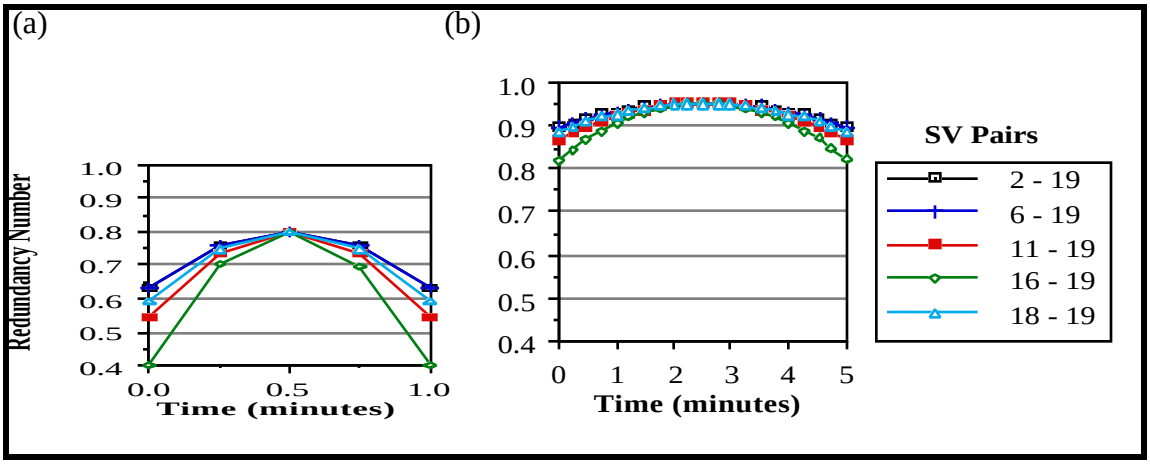

Figure 4.6
Carrier Float Solution Redundancy Numbers
(Feb. 12th, 350100 to 350400 s, 6 satellites, 15 s data interval)

In both figures, a trend where redundancy numbers are highest in the center, and lowest at the start and end of the observation periods is evident, meaning the observations at the start and end of the periods are the most critical. As can be expected and as shown

by the results in Figure 4.6, the five minute - 21 epoch solution has much higher redundancy numbers than the one minute - five epoch solution. Moreover, for the five minute solution, redundancy numbers for the different satellite pairs are closer in magnitude, showing the observations to be more consistently controlled.

Redundancy numbers for code solutions (or fixed carrier solutions since they are based on the same design matrix) computed for one and five minute periods which correspond with Figure 4.6, are shown in Figures 4.7a and 4.7b respectively.

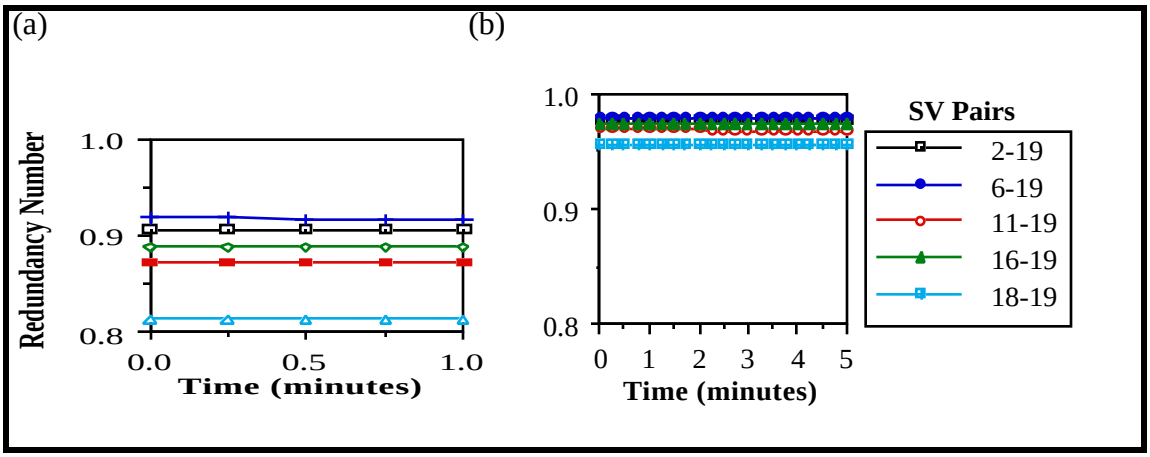

Figure 4.7
Code (or Carrier Fixed) Solution Redundancy Numbers
(Feb. 12th, 350100 to 350400 s, 6 satellites, 15 s data interval)

In both figures redundancy numbers are essentially constant across the full observation period, meaning all observations from the same satellite pair contribute equally to the solution. Similar to the carrier float solution, the five minute - 21 epoch solution has much higher redundancy numbers than the one minute - five epoch solution. The redundancy benefits of a fixed carrier solution (Figure 4.7) over a float carrier solution (Figure 4.6) can be seen.

Redundancy numbers over the same periods for combined code and carrier solutions are shown in Figure 4.8. A data interval of 15 s is used for both code and carrier observations. In the graphs for one minute and five minute solutions, the top set of lines represent redundancy numbers for code observations and the bottom set of lines represent redundancy numbers for carrier observations.

Comparing Figure 4.8a with Figures 4.6a and 4.7a, it can be seen that over a one minute period, the overall carrier redundancy is greatly improved through the combination of code and carrier observations, and the code redundancy is almost unchanged. For the five minute case comparing Figures 4.6b and 4.7b with 4.8b, one can see a small improvement of the carrier redundancy with the combined solution and an almost unchanged code solution redundancy.

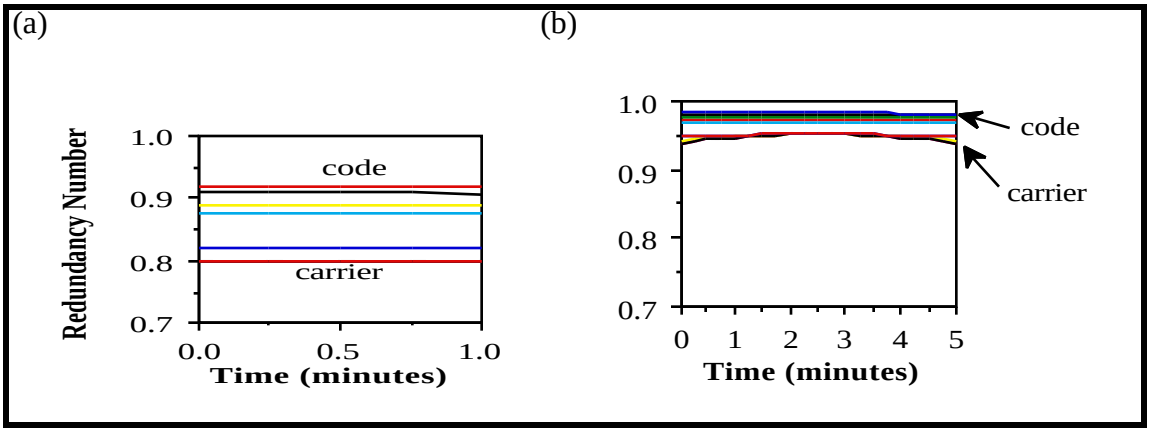

Figure 4.8
Redundancy Numbers for Combined Code and Carrier Solution

(Feb. 12th, 350100 to 350400 s, 6 satellites, 15 s code & carrier data interval, code std. dev. 10 cm, carrier std. dev 5 mm)

From examination of redundancy numbers in Figures 4.6 to 4.8, one can see that for the five minute solutions at a 15 s rate, redundancy numbers are usually above 0.9, and always above 0.8. For the one minute solutions, redundancy is good for the code only and code and carrier combined solutions where all values are above 0.8, but relatively poor for the carrier solution where values fall as low as 0.4. If fewer satellites had been used in redundancy computations, lower redundancy numbers would be expected and if higher data intervals had be used, higher redundancy numbers would be expected.

In network adjustment applications, an average redundancy number of 0.5 has been cited by MacKenzie (1985) as a criteria for judging a network to be well designed. Compared to this value, the redundancy numbers shown above are quite large, meaning that GPS baselines adjustments are generally well controlled, even over the short periods which characterize rapid static surveys.

The benefits of combined code and carrier solutions over carrier alone from a redundancy perspective are significant for very short observation periods (e.g. one minute), especially if the code observations are used at a high data interval, but become less significant as the length of the observation period increases.

Internal Reliability

Internal reliability is inversely proportional to the square root of the redundancy number (see equation (2.31)). Consequently, if one were to plot the minimal detectable errors (MDEs) for each observation over a full observation period, one would see opposite but more subdued trends of those shown in Figures 4.6 to 4.8, scaled by the standard deviation of the observation and the square root of the non-centrality parameter. For example, the carrier phase MDEs corresponding to Figure 4.6 would be highest at the

start and end of the observation period where the largest errors would go undetected, and smallest in the centre where observations are well checked. The code MDEs corresponding to Figure 4.7 would be almost constant for the full observation period.

For any given solution, the largest MDE is the most important. Consequently, rather than examining individual MDEs over a full observation period, the highest MDE for a range of solutions are examined.

The highest MDEs for solution lengths of one to five minutes and data intervals of 1, 5 and 15 seconds are shown in Figure 4.9 and 4.10 for carrier float solutions and code solutions respectively. A non-centrality parameter of 4.13^2 was used in the computations, which corresponds to a significance level of 0.001 and power of the test of 0.8 (Caspary, 1988).

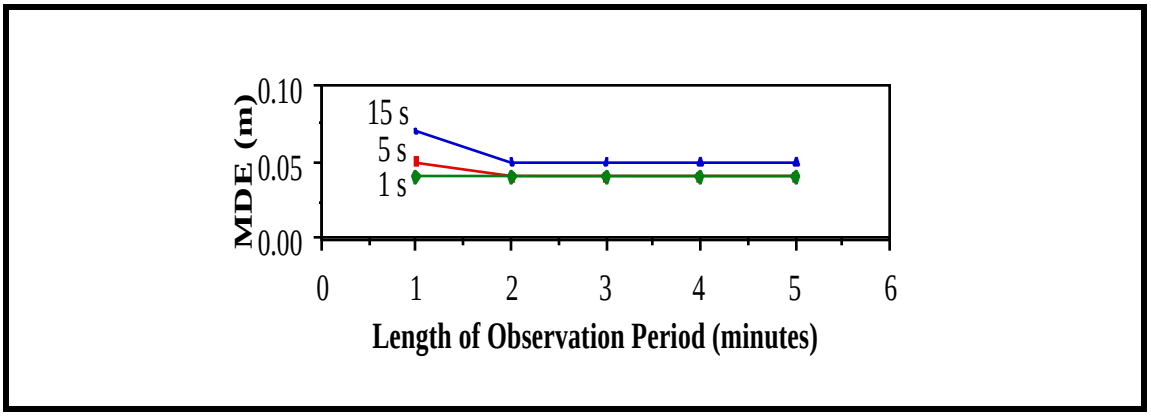

Figure 4.9
MDE for Carrier Float Solutions
(Feb. 12th, 350100 to 350400 s, 6 satellites, carrier std. dev. 5 mm)

MDEs which were computed for combined solutions (not shown here) were slightly lower than those for both code only and carrier only solutions.

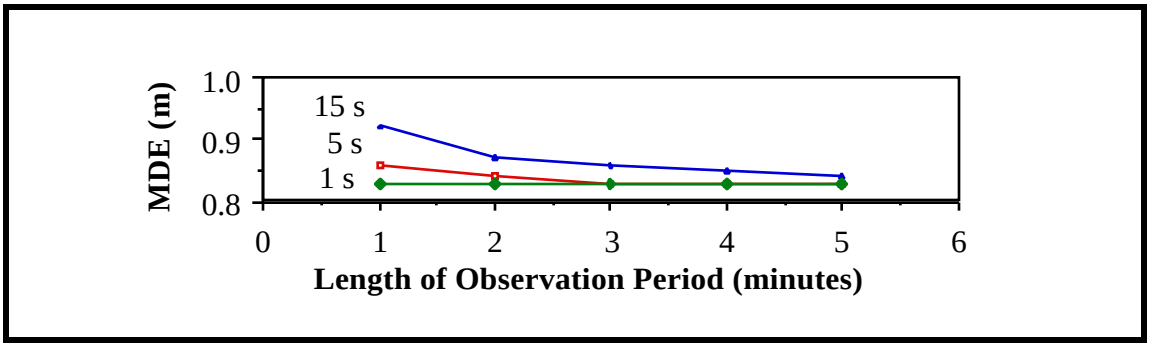

Figure 4.10
MDE for Code Solutions
(Feb. 12th, 350100 to 350400 s, 6 satellites, code std. dev. 10 cm)

Figures 4.9 and 4.10 both show the same trends of lower MDEs for smaller data intervals and longer observation periods, leading one to believe the number of observation epochs is the most significant factor for internal reliability of rapid static surveys. To investigate this, the code MDEs of Figure 4.10 were plotted against the number of epochs used in the solution rather than the length of the observation period and data intervals, as shown in Figure 4.11.

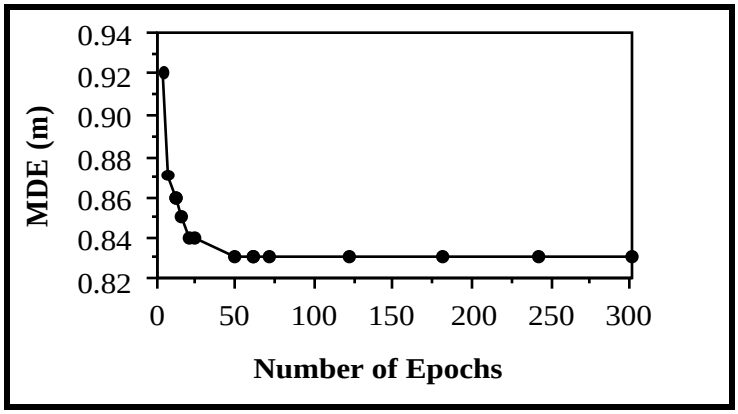

Figure 4.11
MDE for Code Solutions vs. Number of Epochs
(Feb. 12th, 350100 to 350400 s, 6 satellites, code std. dev. 10 cm)

Figure 4.11 clearly shows, based on the assumptions of equally weighted uncorrelated code observations for periods up to five minutes, internal reliability is dependent on the number of observation epochs rather than the period or interval of observations. At about 50 epochs, one sees a levelling off of the MDEs.

External Reliability

Measures of external reliability based on equation (2.34), which give an indication of the effect of an undetected observation error on the estimated parameters, are shown in Figures 4.12 and 4.13 for code and carrier float solutions respectively. Reliabilities using observation periods of one to five minutes and data intervals of 1, 5 and 15 s were computed, and the worst external reliability measure for each is plotted.

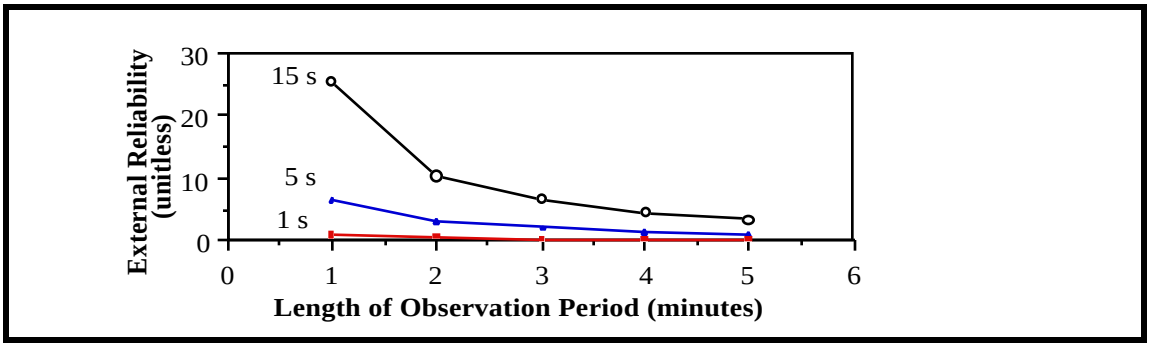

Figure 4.12
External Reliability Measures for Carrier Float Solutions
(Feb. 12th, 350100 to 350400 s, 6 satellites, carrier std. dev. 5 mm)

One can see the same general trends in Figures 4.12 and 4.13, of external reliability measures gradually diminishing with increased lengths of observation periods and decreased data intervals. Unlike the internal reliabilities which leveled off (see Figures 4.10), the external reliability measures continue to decrease as the number of

epochs increase. This is shown in Figure 4.14 where the code external reliability measures of Figure 4.13 are plotted against the number of epochs. The gradual decrease in external reliability measures is logical since more and more observations are combined to diminish an MDEs effect.

In Figure 4.15 external reliability measures for solutions using combined code and carrier observations are shown for observation periods of one to five minutes. Code data intervals of 15, 5 and 1 s are used while the carrier data interval is left at 15 s. Code standard deviations of 10 cm and carrier standard deviations of 5 mm are assumed. Since two types of observations are combined, two types of external reliabilities are shown, one based on redundancy numbers of carrier observations and one based on redundancy numbers of code observations.

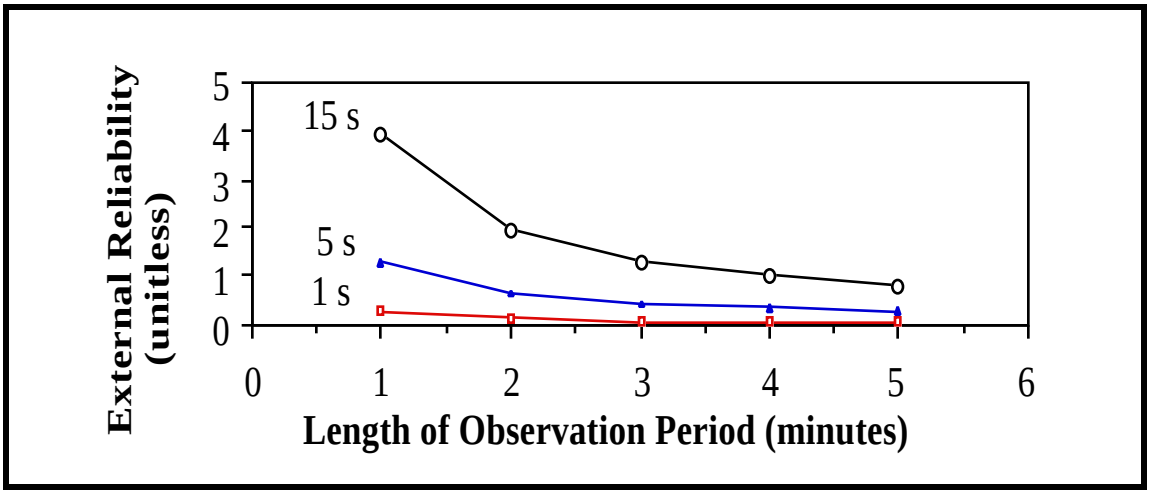

Figure 4.13
External Reliability Measures for Code Solutions
(Feb. 12th, 350100 to 350400 s, 6 satellites, code std. dev. 10 cm)

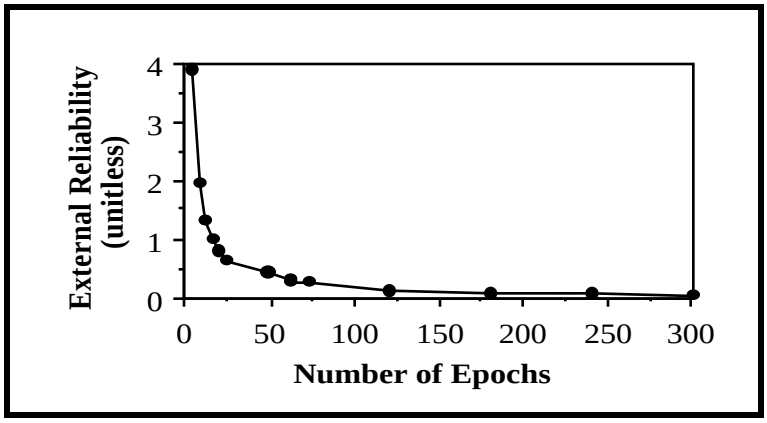

Figure 4.14
External Reliability Measures for Code Solutions vs. Number of Epochs
(Feb. 12th, 350100 to 350400 s, 6 satellites)

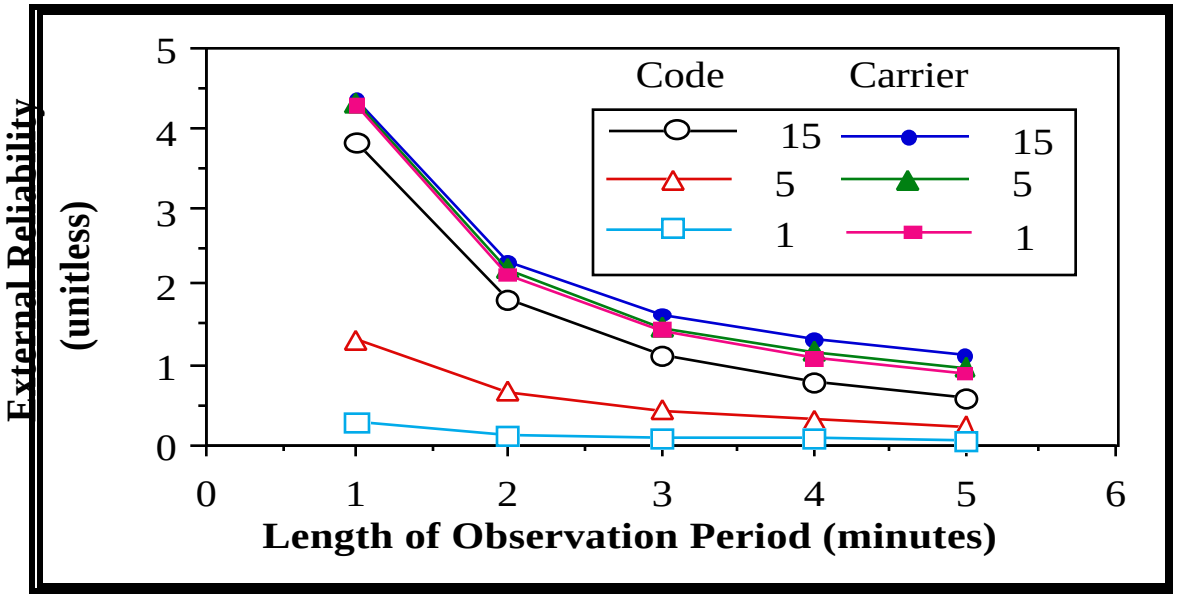

Figure 4.15
External Reliability Measures for Combined Code and Carrier Solutions
(Feb. 12th, 350100 to 350400 s, 6 satellites, code std. dev. 10 cm,
carrier std. dev. 5 mm, carrier data interval 15 s)

Comparing the code portions of Figure 4.15 with Figure 4.13, it can be seen that the addition of carrier observations and ambiguity unknowns has little effect on code external reliabilities. Comparing the carrier portions of Figure 4.15 with the 15 s data

interval external reliabilities in Figures 4.12, and noting the difference in vertical scales, it can be seen that the addition of very accurate code observations significantly improve carrier external reliabilities.

The preanalysis results represent what may be achieved under ideal conditions when all the assumptions used hold true. The validity of reliability measures is not tested through analysis of real data in this thesis, however the validity of RDOP preanalysis is tested through evaluation of real data in the following sections.

4.2 CODE DOUBLE DIFFERENCE RESULTS

Code results are presented for several solution sets for three different days of observations. The results are then compared to RDOP preanalyses, and the effect of multipath on the solutions is investigated. Results are from a program written in C-language, to compute code, carrier or combined code and carrier double difference solutions. Mathematical correlations which result from double differencing are taken into account. Variations in data intervals and observation weighting are permitted in the program.

4.2.1 Code Solutions

Sets of code double difference solutions were generated for Feb. 12th, Feb. 15th and Feb. 17th NovAtel GPSCard™ data and compared to "known" values to attain a measure of achievable code accuracies. The data sets used are described in detail in Chapter 3. Sets of solutions were computed using one epoch of data, one minute of data at one second intervals, and five minutes of data at five second intervals. Individual

results for Feb. 15th are shown in Figures 4.16 to 4.18. The root mean squares (rms) of results from all three data sets are presented in Figures 4.19 and 4.20.

Figure 4.16 shows the difference from truth of latitude, longitude and height components, when solutions are computed using a single epoch of data. The points plotted correspond to the epochs of code solutions, and the lines joining points are added to improve the graph's clarity. Each tick on the horizontal scale represents one minute. In total 11 one epoch solutions, spaced one minute apart are shown.

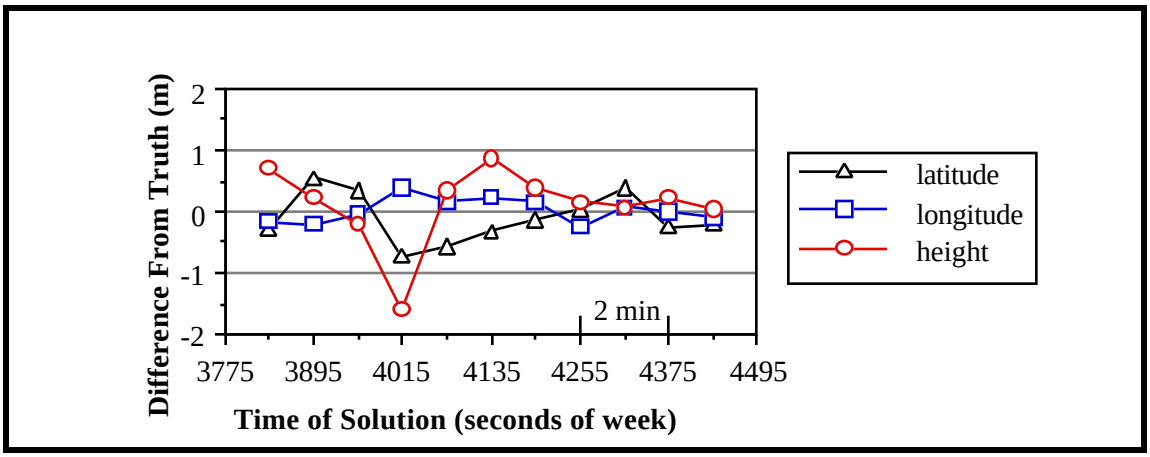

Figure 4.16
Accuracy of Code Solutions Using 1 Epoch of Data
(Feb. 15th, 6 satellites, 720 m baseline)

Figure 4.17 shows the difference from truth of latitude, longitude and height components, when solutions are computed using one minute of data at a 1 s data interval. The points plotted on the graph show the first epoch in each one minute period. The 10 solutions represented are from ten consecutive but independent minutes of data.

Comparing Figures 4.16 and 4.17, which use the same 10 minutes of data, and paying attention to the difference in vertical scales, one can see the one minute solutions are better than the one second solutions, as can be expected. The largest "difference from

truth" of the height component is 1.6 m in the one second case (Figure 4.16), and 0.8 m in the one minute case (Figure 4.17).

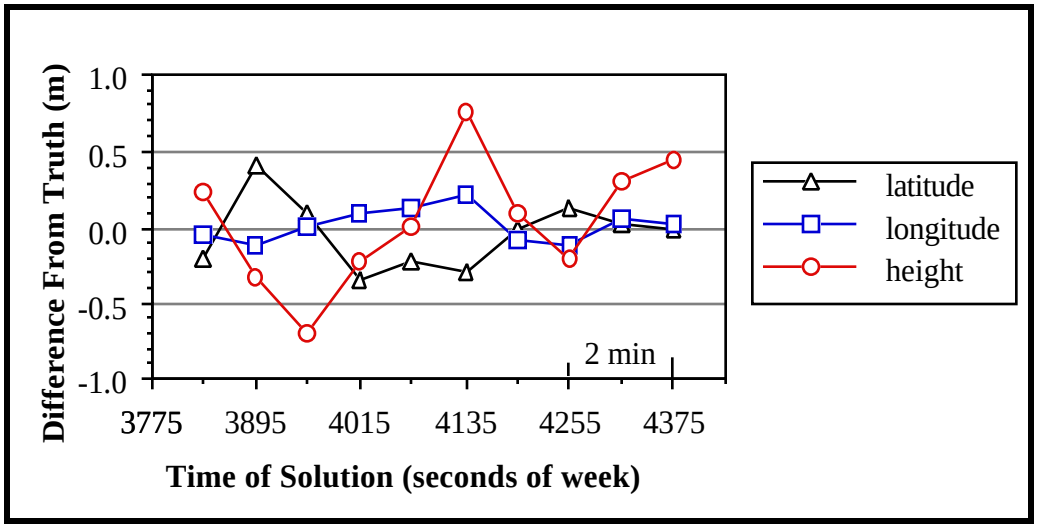

Figure 4.17
Accuracy of Code Solutions Using 1 min. of Data at 1 s Intervals
(Feb. 15th, 6 satellites, 720 m baseline)

Figure 4.18 shows the difference from truth of latitude, longitude and height components, when solutions are computed using five minutes of data at a 5 s data interval. The points plotted on the graph show the first epoch in each five minute period. The five solutions represented are from consecutive but independent blocks of data.

Comparing Figure 4.17 with Figure 4.18, one can see significant improvements in the accuracies achieved. The largest differences from truth for the 5 minute solutions (Figure 4.18) are about 20 cm, much smaller than the 80 cm from the one minute solutions (Figure 4.17).

The rms of the differences from truth for the results presented in Figures 4.16 to 4.18 are shown for latitude, longitude and height components in Figure 4.19b. The same information for solutions computed for Feb. 12th and Feb. 17th are shown in

Figures 4.19a and 4.20. The rms' of the vector distance from truth for each day and the number of solution sets used to arrive at the rms' are given in Table 4.1, columns (5) and (3) respectively.

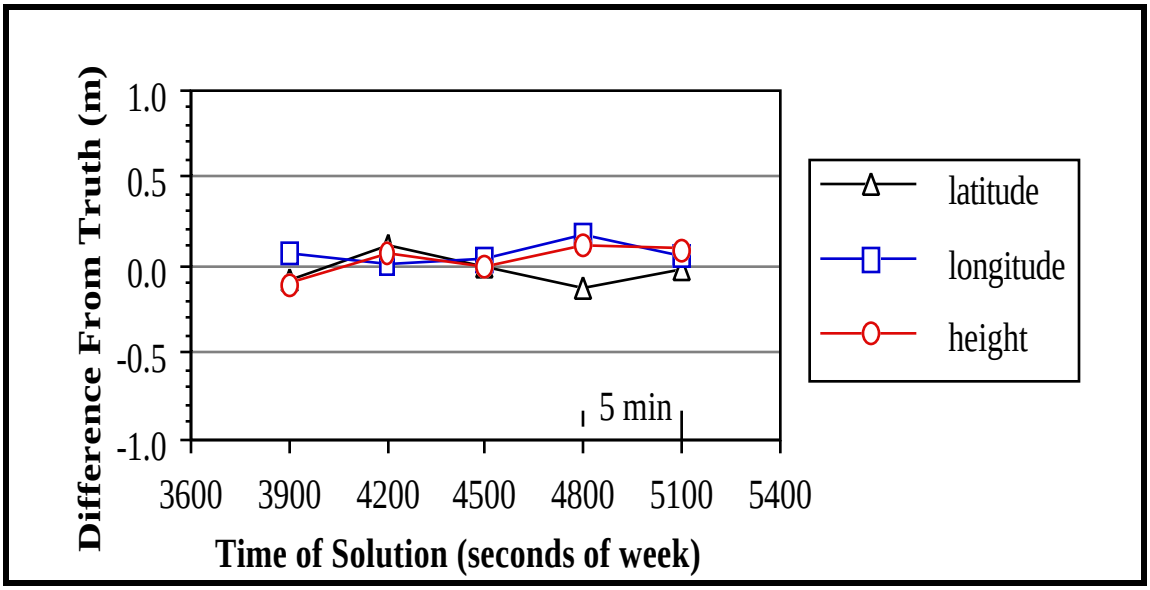

Figure 4.18
Accuracy of Code Solutions Using 5 min. of Data at 5 s Intervals
(Feb. 15th, 6 satellites, 720 m baseline)

Reviewing the rms graphs (Figures 4.19 and 4.20), it is evident that the accuracy of the height component is the weakest and the longitude component is the strongest. This is consistent with GPS solutions in general and is a function of satellite geometry.

Also evident from the rms graphs is the improvement in all components as one moves from 1 s, to one minute, to five minute solutions. The 4.1 km baseline results of Figure 4.20 are similar to the 720 m baseline results of Figure 4.19, leading one to believe code double difference accuracy is not degraded over very short baselines.

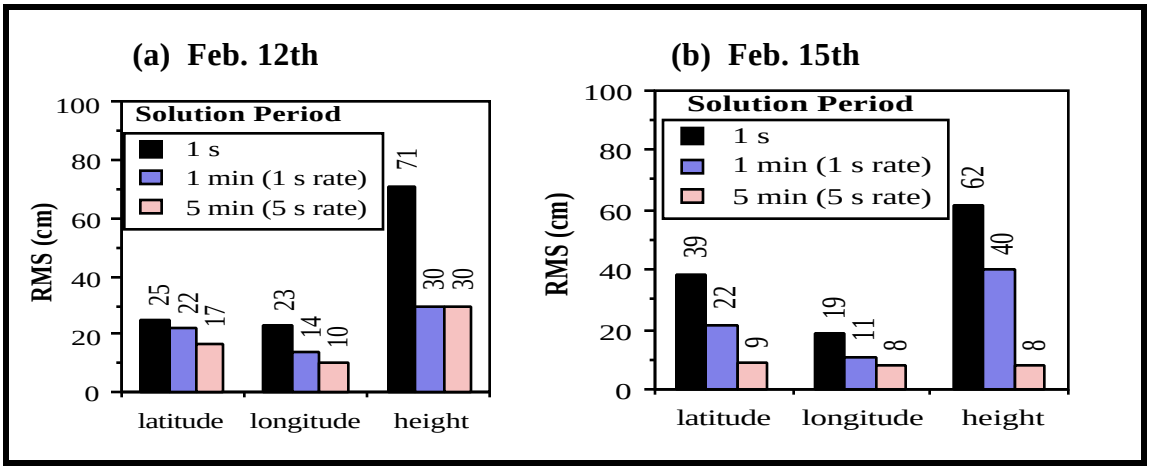

Figure 4.19
RMS of Code Solutions For a 720 m Baseline
(Feb. 12th & Feb. 15th, 6 svs in all but a few cases, exceptions:
5 satellites for 2/4 Feb. 12th 5 min. solns, 5 satellites for 2/ 5 Feb. 15th 5 min. solns)

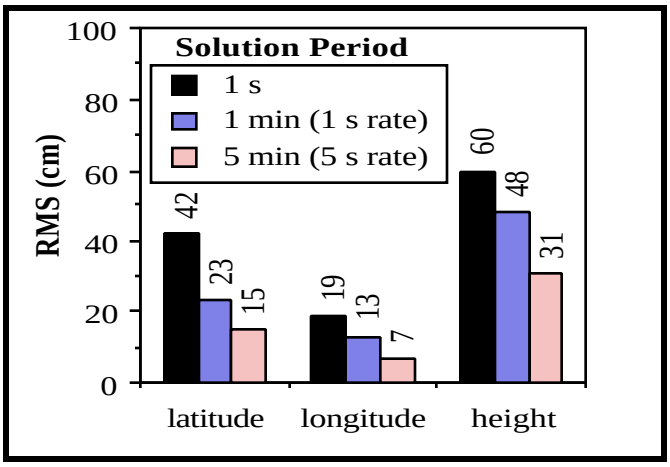

Figure 4.20
RMS of Code Solutions For a 4.1 km Baseline
(Feb. 17th, 6 satellites)

4.2.2 Comparison of RDOPs and Code Solutions

The code solutions above can be compared to the RDOP preanalysis of Section 4.1. To enhance the validity of these comparisons, RDOPs directly computed from the code solutions' covariance matrices can be used. (Recall RDOPS are merely the square root of the trace of the covariance matrix of the parameters).

The theoretical relationship between RDOPS and achieved accuracies is given by equation (2.24). Rearranging equation (2.24) to solve for the measurement accuracy, σ_{o_Δ} , gives

$$\sigma_{o_\Delta} = \frac{\sigma_\Delta}{\text{RDOP}} \quad . \tag{4.1}$$

If the assumption of observations being uncorrelated between epochs holds true then σ_{o_Δ} should yield approximately the same value for all computed solutions.

Equation (4.1) was applied to the code solution computations and results are shown in Table 4.1. In the table, the RGDOPs used are shown in column (4), achieved accuracies (σ_Δ) are shown in column (5) and the measurement accuracies (i.e. the product of equation (4.1)), are shown in column (6). Note, as explained in Section 4.1.1, these RGDOPs are based on undifferenced observations of unit weight, and consequently the measurement accuracies apply to undifferenced measurements. The tabulated RGDOPs are the averages derived from all the code solutions used in the rms computations. Since the total observation span was short and the changes in RGDOPs very small, the averaging was a reasonable approximation. The achieved accuracies (σ_Δ) were represented by the rms of the distance from the truth.

Table 4.1
Computed Code Measurement Accuracies

(1) **Solution Period**	(2) **Date**	(3) **# of Solns**	(4) **Average RGDOP (unitless)**	(5) **RMS of Dist. From Truth (cm)**	(6) **Undifferenced Measurement Accuracy (cm)**
1 s	Feb. 12	11	3.65	79	22
	Feb. 15	12	3.58	71	20
	Feb. 17	12	3.92	75	19
1 min	Feb. 12	10	0.47	40	85
(1 s rate)	Feb. 15	12	0.46	47	102
	Feb. 17	12	0.50	54	108
5 min	Feb. 12	4	0.52	36	69
(5 s rate)	Feb. 15	5	0.49	14	28
	Feb. 17	4	0.49	35	71

Perusing the results of Table 4.1, interesting observations can be made. The rms' of distances from the truth show the five minute solutions to give the best results, and the one second solutions to give the worst results, which is consistent with the results of Figures 4.19 and 4.20. Yet, the measurement accuracies from column (6) are best for the 1 second solutions and worst for the 1 minute solutions.

For the 1 second solutions, the double difference measurement accuracy is a product of the NovAtel GPSCard™ measurement accuracy and code multipath effects. For 20 cm total measurement accuracy, assuming 10 cm code receiver measurement accuracy and applying the law of propagation of errors, the multipath error is 17 cm (assuming all other errors to be negligible). For the one minute solutions, the double difference measurement accuracy is shown to be four to five times worse than for the one second solutions. For the five minute solutions, accuracies are 1.5 to 3.5 times worse.

Note the RGDOPs for the one minute and five minute solutions are very close in magnitude, which is logical since 60 epochs were used in each solution and the satellite

The results of Table 4.1 lead to the belief that the assumption of observations being uncorrelated between epochs does not hold for the sets of observations used. This would explain why the RGDOPs for the one second case, where no summations of normal equations over consecutive epochs are required, result in favorable measurement accuracies through application of equation (4.1), and the RGDOPs for the one minute and 5 minute cases do not.

To investigate the suspected correlations between epochs, multipath effects are examined. Since code observations are especially susceptible to multipath, and since receiver noise and multipath are the only significant errors not reduced or eliminated through double differencing (because residual atmospheric errors are present, but are insignificant over such short baselines), multipath is a likely cause of the correlations between consecutive epochs of observations.

4.2.3 Multipath Effects

An estimate of the magnitude of code multipath and code measurement accuracy combined may be acquired by subtracting the carrier double difference observations from the code double difference observations (Lachapelle, 1991), i.e.

$$\delta = \Delta p - (\Delta \Phi + \Delta N). \qquad (4.2)$$

This technique is valid for short baselines where ionospheric errors are negligible. The errors left in the difference, δ, include receiver noise and multipath from both code and carrier observations. With receiver carrier noise and multipath usually less than a few cm (Cannon and Lachapelle, 1992a), the contribution of carrier errors as compared to code errors is negligible. This leaves code receiver measurement accuracy and code multipath

errors. From zero baseline tests where multipath is all but eliminated in double differencing, the NovAtel GPSCards™ receivers show code double difference measurement accuracies of 20 cm (Erickson et al, 1991). Consequently, the remaining errors in δ, after consideration of the 20 cm double difference code measurement accuracy, is likely a product of multipath.

Code minus carrier differences were formulated following equation (4.2) for the data which corresponds to the Feb. 15th solutions in Figures 4.16 and 4.17. The double difference ambiguities ΔN were determined independently and the data used was cycle slip free. In all cases satellite 19, which had the highest elevation during the observation period (see Figure 3.2) was used as the base satellite in double differencing (as it was in the code double difference solutions).

The code minus carrier differences to the highest and lowest non-base satellites are shown in Figures 4.21 and 4.22 respectively. The lines on the graphs show the connection of differences, δ, at 540 epochs evenly spaced over nine minutes. The highest non-base satellite, satellite 2, had elevations ranging from 46^{o} to 50^{o}, and the lowest, satellite 18, had elevations ranging from 16^{o} to 12^{o}. Low satellites are more prone to multipath. This is well illustrated in the comparison of Figures 4.21 and 4.22, where the code-carrier difference for satellites 2-19 do not exceed 0.4 m, but for satellites 18-19 extend up to 1.7 m. Neither graph shows random noise-like behavior, instead signatures which characterize multipath are evident.

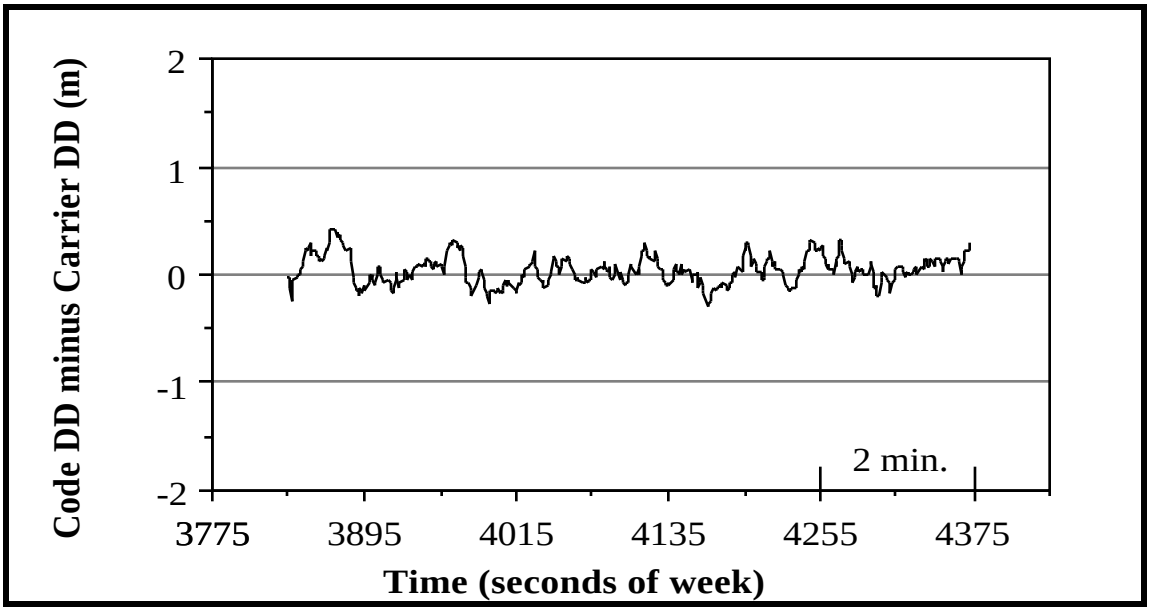

Figure 4.21
Code - Carrier Difference for Satellite Pair 2-19
(Feb. 15th, 720 m baseline, elevations: satellite 2, 46 to 50^{o}; satellite 19, 60 to 58^{o})

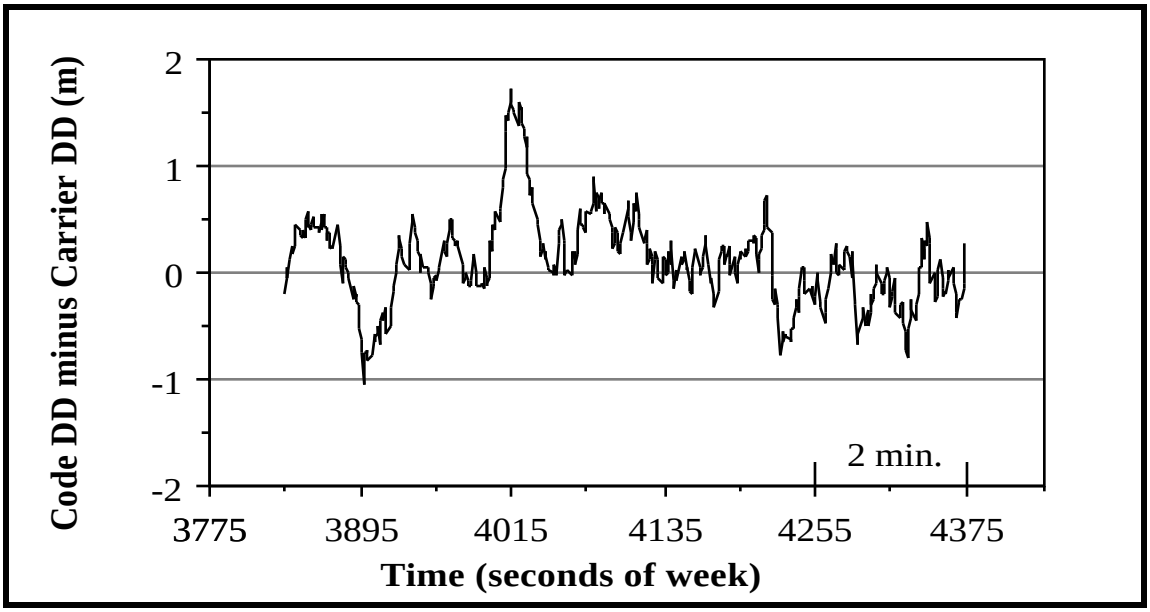

Figure 4.22
Code - Carrier Difference for Satellite Pair 18-19
(Feb. 15th, 720 m baseline, elevations: satellite 18, 16 to 12^{o}; satellite 19, 60 to 58^{o})

To see the direct effect the multipath shown in Figures 4.21 and 4.22 on the Feb. 15th code solutions, the code minus carrier differences for the same data, at the same epochs, interval and solution periods were formed.

Code minus carrier results, which correspond to the one s solutions of Figure 4.16, are plotted in Figure 4.23. Satellites 16 and 18, which are below 20^{o} and represented with hollow symbols in the figure, clearly are the most affected by multipath. The remaining satellites, which are all above 30^{o} and represented by dark filled symbols, are the least affected. Note the δ of 1.7 m for satellite 18 at 4015 seconds of week. This spike correlates with the poor code solution at the same epoch in Figure 4.16. From a visual inspection of Figure 4.16 and 4.23, one can see similar trends.

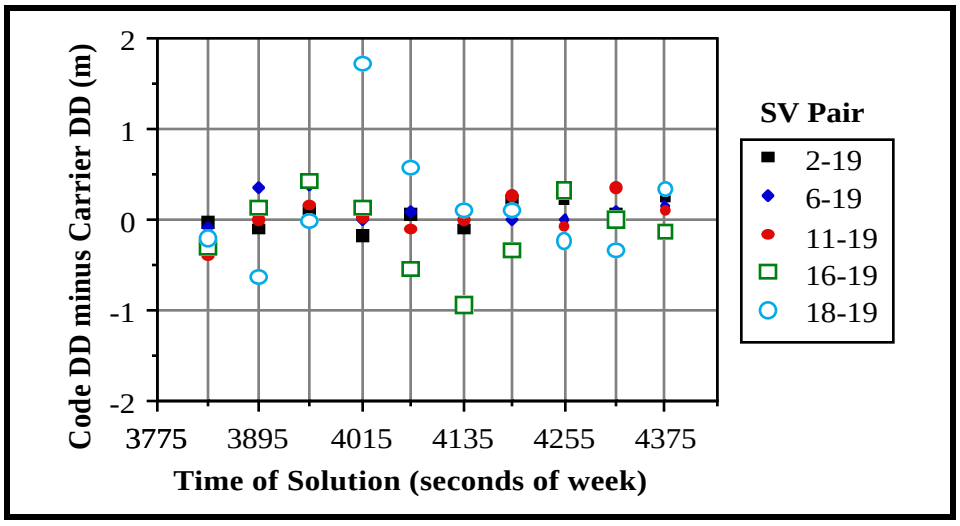

Figure 4.23
Code - Carrier Differences At Single Epochs (Feb. 15th)

It was shown that the code solution accuracy improves when using one minute of data at a 1 s interval, instead of just one epoch. To represent the one minute code-carrier differences, the means and rms' of the differences were computed using

$$\delta_{mean} = \frac{\sum (\Delta p - (\Delta \Phi + \Delta N))}{n}, \text{ and} \tag{4.3}$$

$$rms(\Delta p) = \left(\frac{\sum (\Delta p - (\Delta \Phi + \Delta N))^2}{n-1} \right)^{\frac{1}{2}} \tag{4.4}$$

(Cannon and Lachapelle, 1992a). The resulting means and rms' are shown in Figure 4.24 and 4.25 respectively. In the figures, the values are plotted at the first epoch of the minute of data they represent. For instance, the means for the minute from 4015 to 4095 s are plotted at 4015 s.

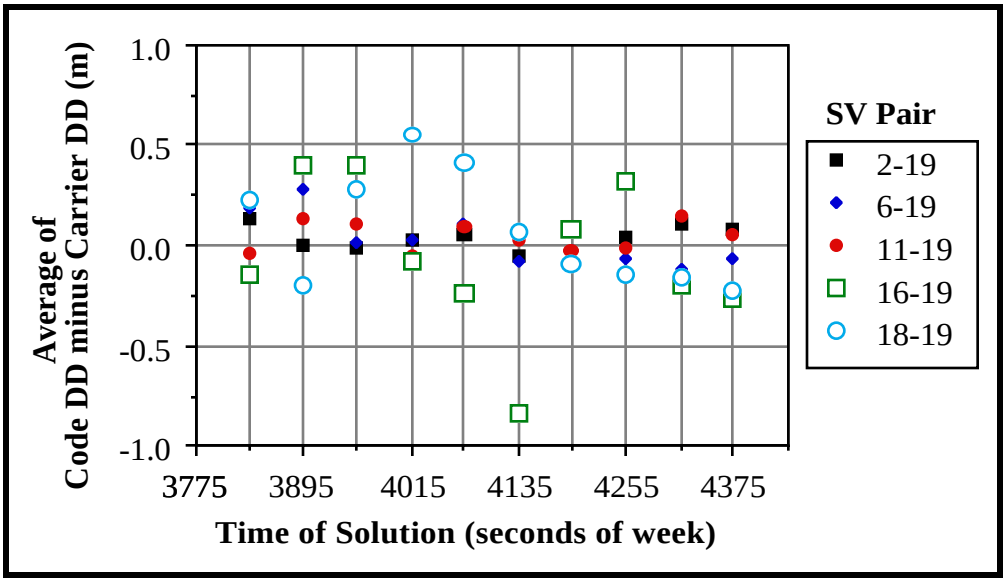

Figure 4.24
Code - Carrier Differences (Feb. 15th)
Averaged From 1 min. of Data at 1 s Intervals

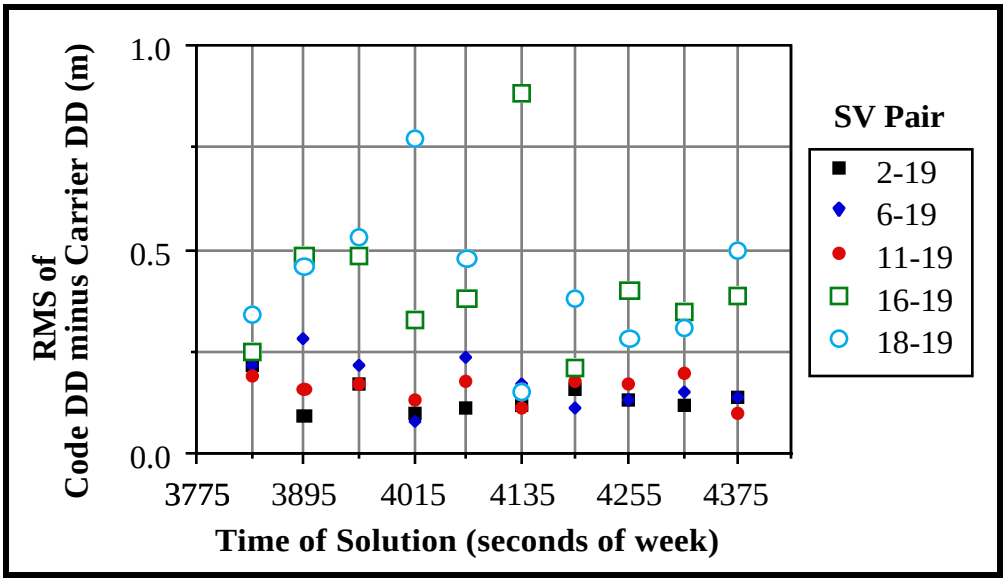

Figure 4.25
Code - Carrier Differences (Feb. 15th)
RMS' From 1 min. of Data at 1 s Intervals

Looking at the single epoch case (Figure 4.23) and the one minute epoch averages (Figure 4.24) and noting the difference in vertical scales, one can see a near two-fold general improvement in code noise through averaging over a minute. There are exceptions, such as at 4135 seconds of week, where averaging produced worse results. This exception corresponds to a very large rms for svs 16-19 for the minute following 4135 seconds of week (Figure 4.25). The rms' in general centre around 20 cm for the high satellites (sv 2, 6 and 11) and 40 cm for the low satellites (sv 16 and 18). The one minute average code-carrier differences show a near two-fold improvement over the single epoch case of Figure 4.23.

Means and rms' were calculated following equations (4.3) and (4.4) for two five minute blocks of data at 5 s data intervals. Results are shown in Figure 4.26. In the figure, the values are plotted in the centre of the five minutes they represent. Note the vertical scales. The largest average code - carrier difference over five minutes was only

some 23 cm, and the largest rms, 55 cm. These values signify a major improvement over the one minute case.

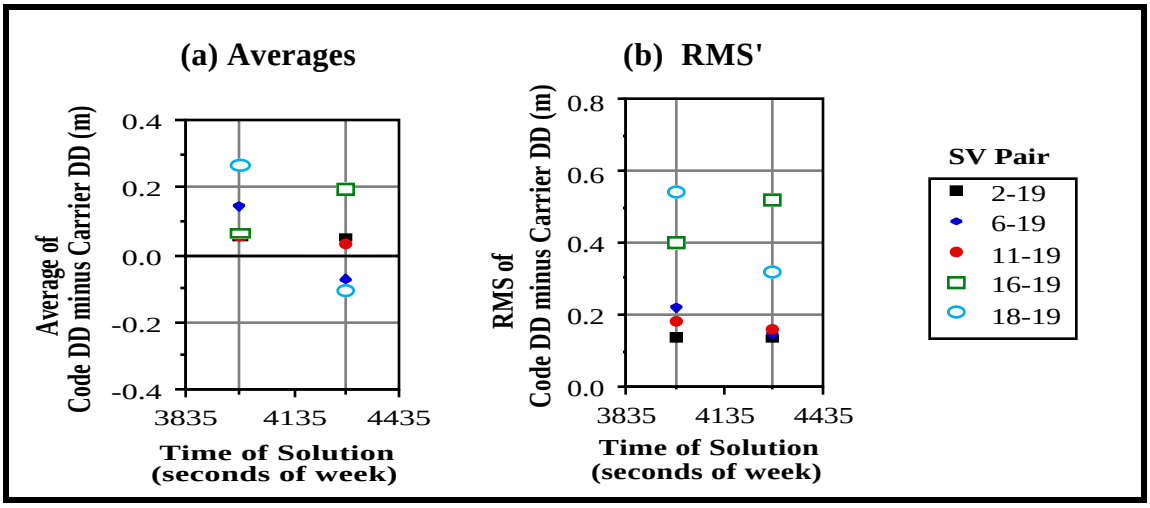

Figure 4.26
Code - Carrier Differences (Feb. 15th)
Averages and RMS' From 5 min. of Data at 5 s Intervals

The figures above show correlations between epochs of data mainly as a product of multipath. Some correlations may also exist due to the physical and electronic properties of the receiver. Because of these correlations, the direct application of RGDOPs for code observations based on the assumptions of no correlations between consecutive epochs (as shown in Table 4.1) can produce erroneous results. For code RDOPS to be used over consecutive epochs rather than a single epoch, some means must be used to handle the correlations between epochs.

Forming code solutions from adjustments over longer time periods (one minute rather than one second, five minutes rather than one minute) resulted in improved accuracies as shown in Figures 4.19 and 4.20. Forming averages and rms' of code - carrier differences, which give a measure of code multipath effects, over longer time periods resulted in comparable improvements in accuracy. Thus for rapid static surveys

based on initial code solutions, to mitigate multipath effects, code observations across the full duration of the observation period should be used.

As a caveat, for full reduction of multipath through averaging, depending on the cause and type of multipath, observation periods of up to one hour may be required (Tranquilla and Carr, 1990). This is impossible for rapid static surveys. Nevertheless, the sub-metre code noise shown above, made possible by the NovAtel GPSCard's high resistance to multipath and high code accuracy, is very small compared to amplitudes over 10 m possible on standard C/A code receivers (Lachapelle et al., 1989; Tranquilla and Carr, 1990).

Although not investigated here, based on research of others (Georigiadou and Kleusberg, 1988) one can expect similar correlations as a result of multipath for carrier phase measurements, and accordingly, similar problems.

4.2.4 Accuracy Estimates

In practical applications, there is no "truth" against which code solutions may be compared and one must rely on the accompanying covariance information for accuracy estimates. The standard deviations for the coordinates can be used to define the limits of search volumes used in the ambiguity function method (AFM) and the least squares ambiguity search technique (LSAST). For instance, with AFM Remondi (1990) suggests using a block with sides of $4\sigma_x$, $4\sigma_y$ and $4\sigma_z$ where σ_x, σ_y and σ_z are the standard deviations of the x, y and z coordinates respectively. It is therefore important, when using the code solution and its accuracy estimates to define a search block, that the accuracy estimates be realistic.

It has been shown that RDOPs give measures of achievable code accuracies that are too optimistic because of multipath correlations between consecutive epochs. Since RDOPs and parameter accuracy estimates are derived from the same covariance matrices, the accuracy estimates associated with the code solutions will also be too optimistic. If these accuracy estimates are then used to define a search volume for an ambiguity resolution technique, erroneous results may be attained. This also applies to carrier solution accuracy estimates.

One of the advantages of using covariance information rather than pre-specified dimensions to define a search block is the ability to scale the coordinate axes according to their uncertainties. The relative accuracies of the coordinate estimates are generally realistic even though their magnitudes become too optimistic over time. Thus by applying an appropriate scaling or modeling, appropriate accuracy estimates for defining a search volume may be determined. These are not investigated in this thesis, rather the intent here is to bring attention to the problem of overly optimistic code accuracy estimates.

4.3 CARRIER AND CODE-CARRIER COMBINED RESULTS

Carrier and code-carrier combined results are shown for several reasons. The carrier results show the inability to resolve ambiguities over short baselines using 5 minutes of data, hence the requirement for rapid static ambiguity resolution techniques. They also show why accurate code solutions are more desirable than carrier float solutions for initial coordinate estimates in rapid static ambiguity resolution techniques. The combined code and carrier results show the simple combination of these observation types in an adjustment is inadequate for ambiguity resolution. Float and fixed solutions

shown for both sets of results emphasize the importance of fixing ambiguities to the correct integer.

4.3.1 Carrier Solutions

Two sets of 5 minute carrier solutions were computed for Feb. 12th, 15th and 17th NovAtel GPSCard™ data and then compared to "known" values. For each, a float solution was computed and ambiguity estimates attained. The nearest integers to the float ambiguity estimates were then held as constants in a fixed carrier adjustment. The five minute solutions were computed using observations at a 5 s data interval. Results are give in Table 4.2.

In the results table, the proximity of ambiguities to the correct integer are given. The "correct" integers were determined using SEMIKIN results for the full set of observation data. For float solutions the proximity is in real values, and for fixed solutions in integer values. The observation period for each set number is shown in Table 4.3, to enable cross-referencing with the satellite elevations shown in Chapter 3.

Examining Table 4.2, one can see the correct integers are determined for all double difference pairs in only one case: Feb. 15th, set #1. The resulting coordinate difference from the truth was at the mm level for this fixed solution, compared to the 28 cm level for the float solution, illustrating the importance of a fixed solution over a float solution for precise surveys. Note for the float solution, the integers were barely rounded to the correct solution since two were at the half cycle level (satellites 11 and 12). As seen in the table, fixing ambiguities to the wrong integer can degrade results.

Table 4.2
Carrier Solutions*

Date (Feb)	**Set #**		**Proximity of Ambiguities to Correct Integer (cycles)†**					**Distance From Truth (m)**			
			2	6	11	16	12	lat.	long.	hght.	dist.
12th	1	float	-0.5	-0.2	0.2	-0.6	-0.8	-0.10	-0.06	-0.09	0.15
		fix	0	0	0	-1	-1	-0.04	0.01	-0.36	0.36
	2	float	-1.2	-0.5	1.1	-0.6	-0.2	-0.22	-0.23	0.33	0.46
		fix	-1	0	1	-1	0	-0.17	-0.21	0.17	0.32
15th	1	float	-0.2	0.0	0.5	0.4	-0.5	-0.07	-0.07	0.26	0.28
		fix	0	0	0	0	0	0.00	0.00	0.00	0.00
	2	float	1.7	0.8	-1.3	1.0	0.2	0.25	0.31	-0.39	0.56
		fix	2	1	-1	1	0	0.22	0.32	-0.46	0.60
17th	1	float	-1.1	-0.9	0.3	-1.4	-0.9	-0.05	-0.14	-0.12	0.20
		fix	-1	-1	0	-1	-1	-0.04	-0.10	-0.11	0.15
	2	float	-1.0	-0.6	0.6	-0.9	-0.7	-0.12	-0.14	0.03	0.19
		fix	-1	-1	1	-1	-1	-0.17	-0.20	0.05	0.27

***** solution period: 5 min. carrier interval: 5 s. † base satellite: 19.

Table 4.3
Solution Periods
(corresponding to Tables 4.2 & 4.4)

Date	Set #	Time (seconds of week)
Feb. 12th	1	349999-350299
	2	350299-350599
Feb. 15th	1	3835-4135
	2	4135-4435
Feb. 17th	1	175466-175766
	2	175766-176066

The float carrier phase solutions were in error by about the same magnitude as the code solutions of Section 4.2.1. For shorter periods, a rapid deterioration in carrier float results can be expected as shown for the RGDOPs of Figure 4.1. If the data had cycle slips, results would be worse. In contrast, code accuracies degrade gradually with shorter time spans (Figures 4.19 and 4.20) and are not subject to cycle slips. Since for rapid static surveys one ideally wants results in five minutes or less, and in consideration of the above discussion, accurate code solutions are superior to carrier float solutions for initial coordinate estimation.

4.3.2 Combined Code and Carrier Solutions

Code and carrier observations were combined in an adjustment to see if accurate code measurements at a high data rate could help resolve ambiguities as the RGDOP results in Figures 4.3 and 4.4 might lead one to believe. The same data sets and observation periods used in Table 4.2 were used for combined code-carrier solutions and are shown in Table 4.4. Data intervals were 5 s for carrier observations and 1 s for code observations. Carrier observations were weighted by 5 mm and code observations were weighted by 20 cm.

From the table it can be seen that in no case were the code observations sufficient to resolve the carrier ambiguities correctly. Comparing Tables 4.2 and 4.4, it can be seen that sometimes the carrier float solution is better than the combined code-carrier solution, and sometimes the reverse is true. Further investigations of code-carrier combinations would require testing several different code-carrier relative weighting schemes and data intervals. This is not pursued here.

Table 4.4
Code and Carrier Combined Solutions*

Date (Feb)	Set #		Proximity of Ambiguities to Correct Integer (cycles)†					Distance From Truth (m)			
			2	6	11	16	12	lat.	long.	hght.	dist.
12th	1	float	-0.3	-1.3	-0.4	-0.9	1.1	0.28	-0.12	0.04	0.30
		fix	0	-1	0	-1	1	0.23	-0.12	-0.03	0.26
	2	float	-0.6	-1.0	0.2	-1.1	0.2	0.12	-0.12	-0.04	0.17
		fix	-1	-1	0	-1	0	0.02	-0.16	0.08	0.18
15th	1	float	-0.1	-0.1	0.0	-0.2	-0.6	-0.06	0.00	-0.11	0.13
		fix	0	0	0	0	-1	-0.1	0.04	-0.14	0.17
	2	float	0.3	0.4	0.2	1	0.6	-0.01	0.03	0.20	0.20
		fix	0	0	0	1	1	0.03	0.00	0.32	0.32
17th	1	float	0.4	0.7	-0.1	0.8	-0.2	-0.07	0.09	0.05	0.13
		fix	0	1	0	1	0	-0.10	0.08	0.18	0.22
	2	float	0.2	1.0	0.9	1.4	0.2	-0.20	0.02	0.38	0.43
		fix	0	1	1	1	0	-0.22	-0.01	0.31	0.38

† base satellite: 19
* solution period: 5 min, carrier interval: 5 s, code interval: 1 s,
carrier std. dev.: 5 mm, code std. dev.: 20 cm

The limited results in Table 4.4 show the code-carrier combinations tested to be unsuccessful for resolving carrier phase ambiguities over short time periods. A few explanations for the success of this technique suggested by the RGDOP Figures of 4.4 and 4.5 and the lack of success here can be put forward. To start with, the same between-epoch multipath code correlations shown in Section 4.2.3 apply in the code observations used for code-carrier combined solutions. Correlations between consecutive epochs of carrier phase data are also probable. Code-carrier divergence (Hatch, 1982) due to the opposite effect the ionosphere has on each observation type should not be a problem for

the short baselines investigated, but differential multipath effects of the two are a problem. The lack of success of combined code and carrier solutions gives impetus for more rigorous rapid static ambiguity resolution techniques, such as the ambiguity function method, addressed in Chapter 5, and the least squares techniques, addressed in Chapter 6.

CHAPTER 5

CARRIER PHASE AMBIGUITY RESOLUTION USING THE AMBIGUITY FUNCTION METHOD

The ambiguity function method (AFM) is unique compared to other ambiguity resolution techniques because it is cycle slip invariant. It was originally introduced for GPS data processing by Counselman and Gourevitch (1981) and later developed by Remondi (1984). Only in recent years, with the advent of more powerful computers and the development of precise kinematic applications, has the application of the ambiguity function method become more prevalent (Remondi, 1990; Mader, 1990; Remondi, 1991; Lu, 1991).

The ambiguity function method is used to arrive at a correct set of integer ambiguities, by following four steps:

(1) initial coordinates of an unknown point are estimated;

(2) a neighbourhood of points (potential solutions) around the initial point are defined by a specified set of criteria;

(3) the "ambiguity function" is calculated for each potential solution and the one with the maximum value is saved; and

(4) the integer ambiguities are computed using coordinates of the "best" solution.

The initial coordinates may be estimated using triple difference solutions (Remondi, 1984), double difference carrier phase solutions with real ambiguities, or double difference pseudorange solutions. The latter two methods are discussed in Chapter 4. Defining a neighbourhood of points to be tested may be accomplished by grid searches or double difference plane intersections as described in Section 5.2. Means for ensuring the certainty of AFM solutions are given in Section 5.3 and AFM results are given in Section 5.4. The crux of the ambiguity function method lies in the computation of the ambiguity function itself.

5.1 THE AMBIGUITY FUNCTION

The ambiguity function (AF) is described geometrically in a manner similar to that used by Remondi (1984), followed by its mathematical formulation and practical implementation.

For the sake of explanation, consider an errorless carrier phase observation transmitted from one GPS satellite to a receiver, on a single frequency at one epoch. The equation representing this observation would be the error free form of equation (2.5), i.e.:

$$\Phi = \rho + \lambda N. \qquad (5.1)$$

Here the carrier phase ambiguity, N, and the receiver coordinates of the satellite-receiver range, ρ, are unknown, the carrier phase, Φ, is observed and the carrier wavelength, λ, is a constant. This observation alone gives little useful information for finding the correct receiver coordinates or carrier phase ambiguity. The information contained here is illustrated in Figure 5.1. It is evident from Figure 5.1 that potential solutions for the

receiver coordinates must lie along the arcs, separated by the wavelength, radiating from the satellite to the receiver. Each arc represents a different ambiguity value, hence the one wavelength (λ) spacing.

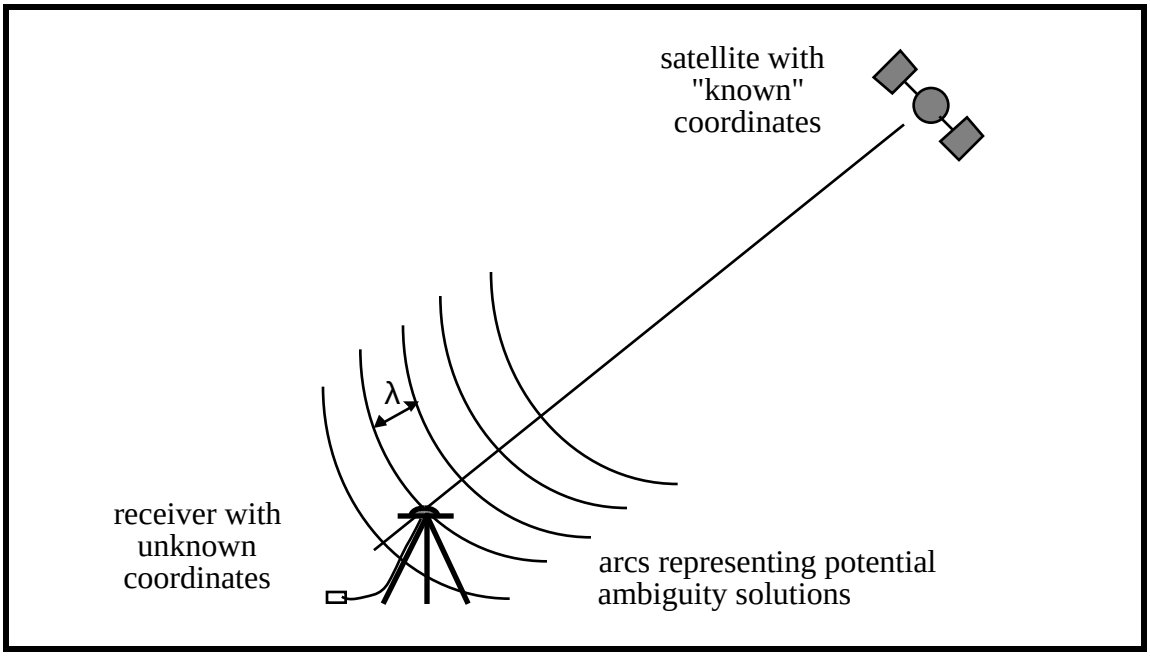

Figure 5.1
One Satellite-Receiver Carrier Phase Geometry

With two satellites instead of one at a single epoch, Figure 5.1 is transformed to Figure 5.2. The extra satellite adds both an unknown ambiguity term and a carrier phase observation. From a geometrical perspective, the two satellites in Figure 5.2 provide a richer source of information since instead of potential coordinate solutions lying at all points along one set of arcs, they must lie at the intersection of arcs radiating from the two satellites.

One can envision with each addition of a satellite, the number of points of intersection of all satellite arcs would decrease meaning fewer potential solutions. Similarly, if observations at a second epoch were added (after a period long enough to ensure substantial change in satellite geometry), fewer intersections of arcs would result.

Intersections alone are not useful since infinite space may need to be searched to locate them. However, if the solution is known to lie within a bounded region, the number of potential solutions (or intersections) to be considered are limited. The first two steps in the ambiguity function method mentioned above (finding a good initial coordinate approximation and setting a criteria for testing neighbouring points) serve to define a bounded region thereby restricting the number of potential solutions. Points within the bounded region may then be tested to see if they mark a strong positive intersection of all satellite arcs. With sufficient satellite geometry a unique point which clearly intersects "better" than any other in the region should be discernible.

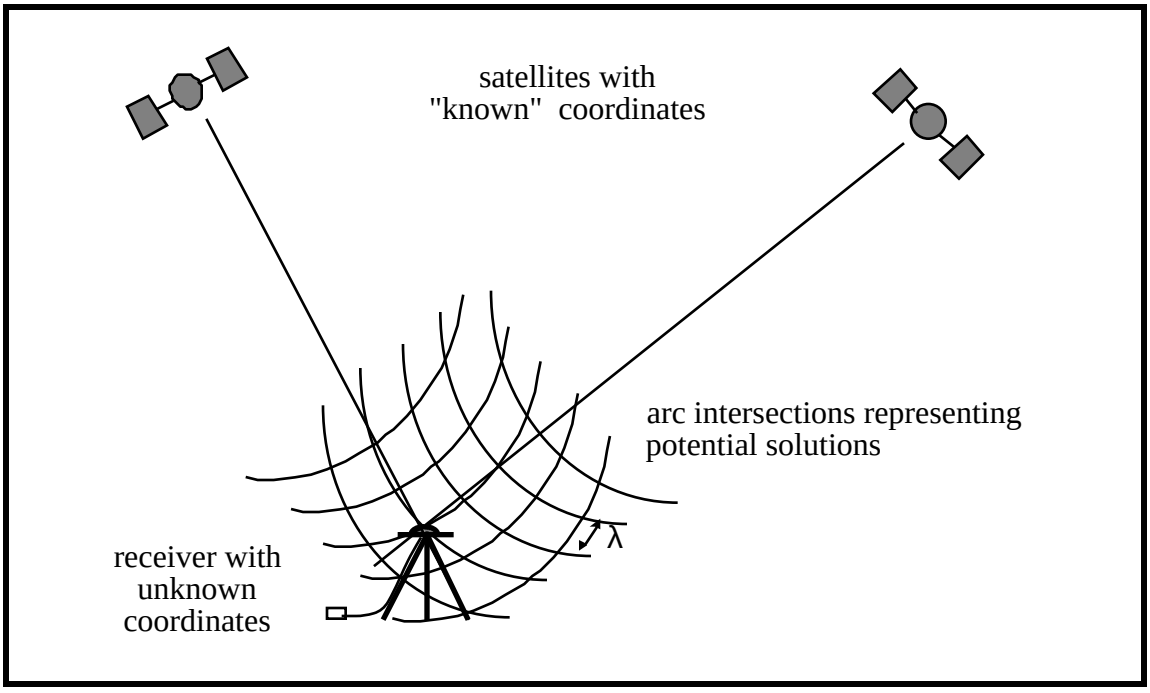

Figure 5.2
Two Satellite-Receiver Carrier Phase Geometry

It is interesting to consider hypothetically if a unique AFM solution could exist in infinite space. Moreover, a theoretical formulation of the number and type of observations

that would be required for a unique solution in any given volume would provide guidance for practical AFM applications. Elements in the functional relationship between the observations required and the volume size would include the number of satellites, satellite geometry, the length of observation period, the carrier wavelength(s) and the distance between the satellite and the receiver. Some characteristics of AFM over physical space are developed by Counselman and Gourevitch (1981) through the use of Fourier Transforms. These theoretical developments are not dealt with in this thesis but deserve investigation.

Up to this point only the geometric relations for undifferenced observations have been discussed; yet the ambiguity function may be applied to single difference carrier phase observables as is done in Remondi (1984) or double difference carrier phase observables as is done in Mader (1990), Lu (1991) and as will be done herein. For the case of double difference observations, the undifferenced satellite-receiver range vector shown in Figure 5.1 is replaced by the vector resulting from double differencing. The unknowns are the double difference ambiguities and receiver coordinate portion of the double difference range. Maintaining the error-free assumptions represented above, this is formulated as

$$\Delta \Phi_L = \Delta \rho_L + \lambda \Delta N, \tag{5.2}$$

where the subscript L denotes units of length.

The mathematical realization of the ambiguity function method for the double difference observable can be developed starting with equation 5.2. At any given epoch and for any satellite pair the double difference carrier phase observable, $\Delta \Phi$, may be determined and the double difference satellite-receiver range, $\Delta \rho$, may be computed

(using trial receiver coordinates x,y,z). If $\Delta\ \Phi$ and $\Delta\ \rho$ are scaled to cycles by factoring out λ, and equation 5.2 is rearranged, then

$$\Delta\ N = \Delta\ \Phi_C - \Delta\ \rho_C, \tag{5.3}$$

where the subscript c indicates units are in cycles. In other words, the observed double difference carrier phase minus the calculated double difference range should give the double difference ambiguity. If the true receiver coordinates are used to calculate $\Delta\ \rho$, then $\Delta\ N$ should be an integer. In reality, the "correct" point will approach but not give an exact integer due to atmospheric, measuring noise, carrier phase multipath and other errors which were ignored in the above geometrical development. To check a test point with a given double difference observation, one needs to measure how well the double difference ambiguity computed using equation (5.3) approaches an integer. This can be done by using phasors, which have the properties needed for the desired testing.

The term phasor describes a complex vector of the form

$$e^{i\theta} = \cos\theta + i \sin\theta, \tag{5.4}$$

where θ is the angle in the counter-clockwise direction from the positive real axis (see Figure 5.3). Phasors have the property of yielding the same value for any number of cycles (or full rotations) given the same fractional cycle value. Thus by letting θ be the observed minus calculated double difference from equation 5.3 (converted to radians) the phasor can be used to compute how well a given test point satisfies the requirement for an ambiguity to be an integer. The unique test point for which all double difference observables closely approximate integers would be considered the "correct" point at which "true" ambiguity values may be calculated.

This leads to the formulation of the ambiguity function, which is written as

$$AF(x,y,z) = \sum_{k=1}^{nepoch} \sum_{j=1}^{nsat-1} e^{2\pi i \left(\Delta \Phi_{obs}^{kj} - \Delta \rho_{calc}^{kj}(x,y,z) \right)}, \qquad (5.5)$$

where AF(x,y,z) is the ambiguity function for the test point (x,y,z), $\Delta \Phi_{obs}^{kj}$ is the observed double difference range for the "true" point and $\Delta \rho_{calc}^{kj}(x,y,z)$ is the calculated double difference range for the test point (x,y,z). Summations are made for all nsat-1 double difference observations (where nsat is the number of satellites) and all epochs (where nepoch is the number of epochs). Only the real (cosine) portion of $e^{2\pi\theta i}$ need be computed since its maximization will correspond with the closest proximity of an ambiguity to an integer value.

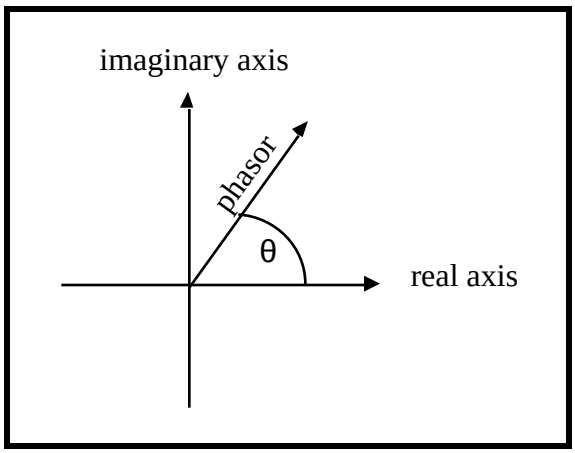

Figure 5.3
Phasor Diagram

Note that if dual frequency carrier phase data is available (squaring or P-code types), summations may be performed over the two frequencies providing additional information to isolate a maximum. The two frequencies may also be used to compute ionospheric correction terms, which are very important for AFM applications on longer baselines (e.g. over 10 km). Dual frequency data is not dealt with in this thesis, but is discussed in relation to the ambiguity function method in Mader (1990).

A variation of equation (5.5) which accounts for weighting of observations as a function of satellite elevation angles was given by Counselman and Gourevitch (1981) and discussed by Remondi (1984). Although not considered in this thesis, it holds merit, especially since access to six, seven or eight satellite constellations will often require the use of low elevation satellites, which are subject to a greater portion of atmospheric and multipath distortions than their higher elevation counterparts.

The computation of the ambiguity function is rather simple to implement. The algorithm used herein follows Mader (1990) and is illustrated in Figure 5.4. For each test point (x,y,z), all epochs and all double difference observations are looped through. For each individual observation the cosine of the observed minus calculated double differences are computed. If this value falls below a threshold (here set to 0.7), the test point is immediately rejected and the next test point is examined. If this value passes the threshold test its value is accumulated along with all other cos(obs - calc) observations for the test point. Once all observations have been checked, the average value (referred to as the ambiguity function in Figure 5.4 and elsewhere for brevity, but it really is the normalized ambiguity function) is calculated and its value and corresponding coordinates are written to file for later examination. The maximum value is saved along with its coordinates. These coordinates are then used to compute the double difference range which is used together with the observations to compute the unknown ambiguities of equation (5.3).

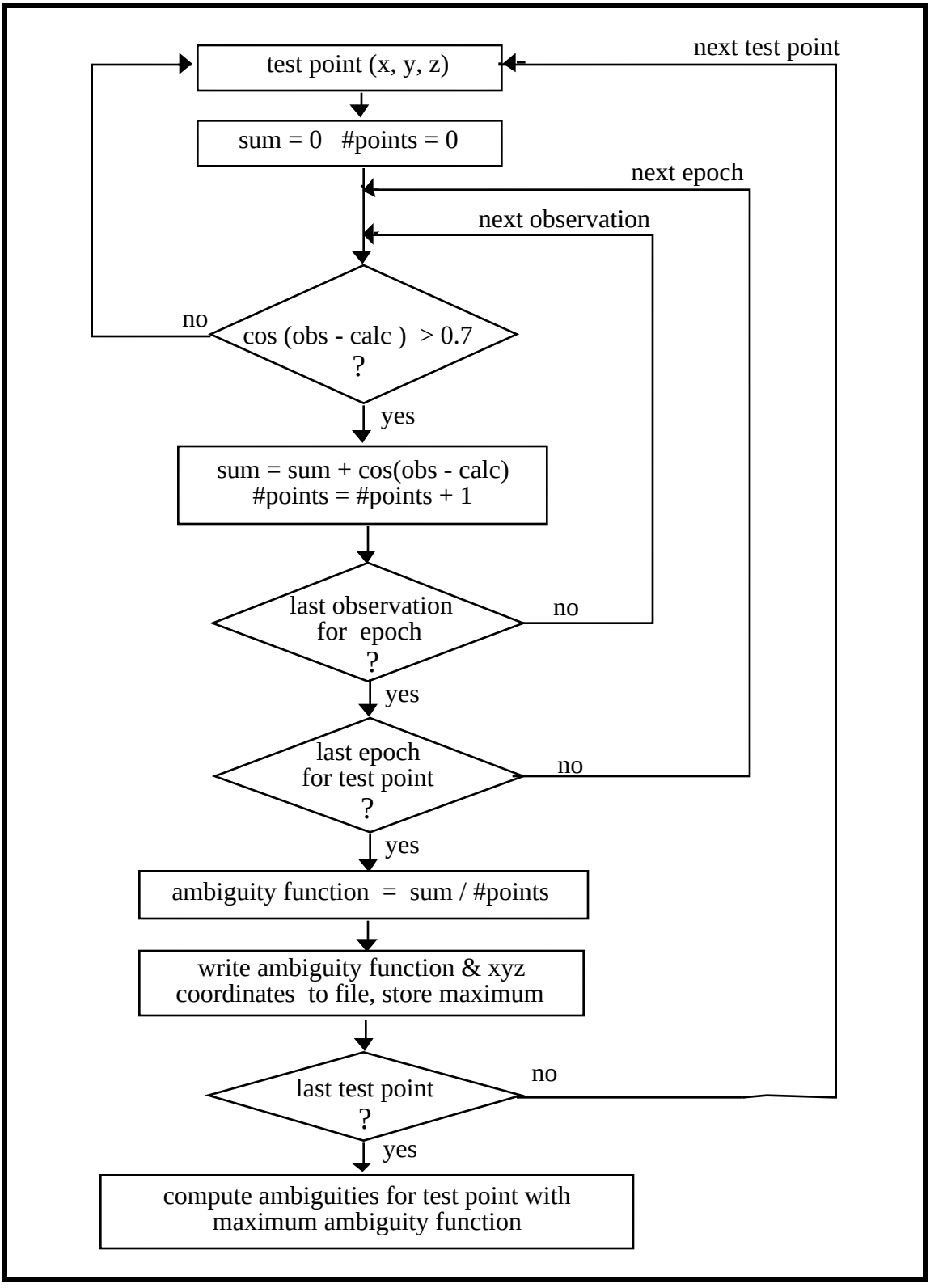

Figure 5.4
Ambiguity Function Algorithm

The relation between maximizing cos(obs - calc) and maximizing the proximity of an ambiguity to an integer is illustrated by the cosine function of Figure 5.5. Here three horizontal scales are given, one in degrees, one in cycles, and one in cm of L1 carrier observations. It can be seen that the 0.7 threshold given in Figure 5.4 corresponds to the observed minus calculated double differences coming within at least 0.12 cycles of an integer. This corresponds to 2.3 cm of L1 carrier observations. Results have shown that the maximum calculated ambiguity function for a given data set is usually above 0.9. This value is also shown in Figure 5.5, and corresponds with 0.07 cycles from an integer or 1.3 cm of carrier phase observations.

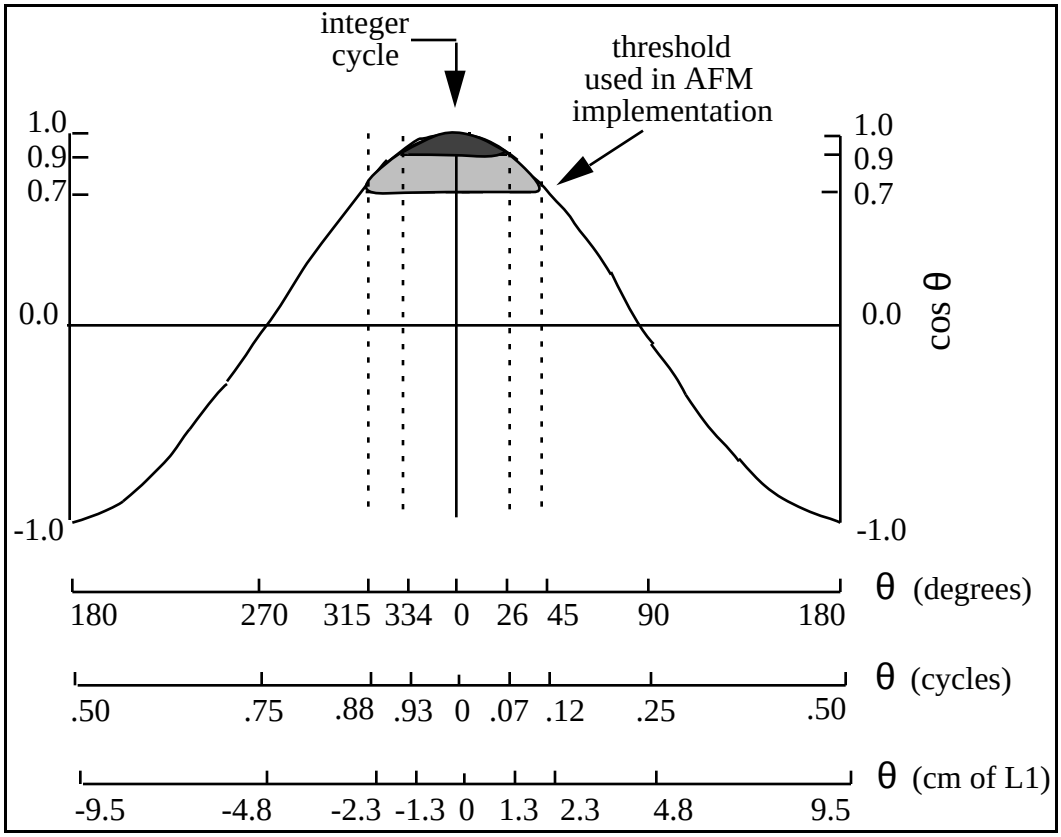

Figure 5.5
Relationship Between Cosine Function and Proximity to an Integer Cycle

The computation of the ambiguity function itself is straight forward and objective. The same cannot be said about the search patterns required to identify test points and the decision of whether the maximum ambiguity value is trustworthy.

5.2 SEARCH PATTERNS

The ambiguity function method requires that a series of test points around an initial point be defined by a specified set of criteria. Each point is then evaluated using the algorithm of Figure 5.4 following some search pattern. In this section two main search patterns are examined, the grid search and the double difference plane intersection.

5.2.1 The Grid Search

In the grid search, a volume around an initial point is searched by stepping through equally spaced points (see Figure 5.6). The initial point is situated at the centre of the volume, and the "true" point must lie somewhere within. The search volume may be cubic as shown in the figure, with all dimensions of equal "block size", or it may have different dimensions along each coordinate axis proportional to the uncertainty of the initial coordinate estimates. At each grid intersection the AF is calculated. As described in Mader (1990), the grid search technique may be implemented using nested loops to increment the x, y and z coordinates respectively.

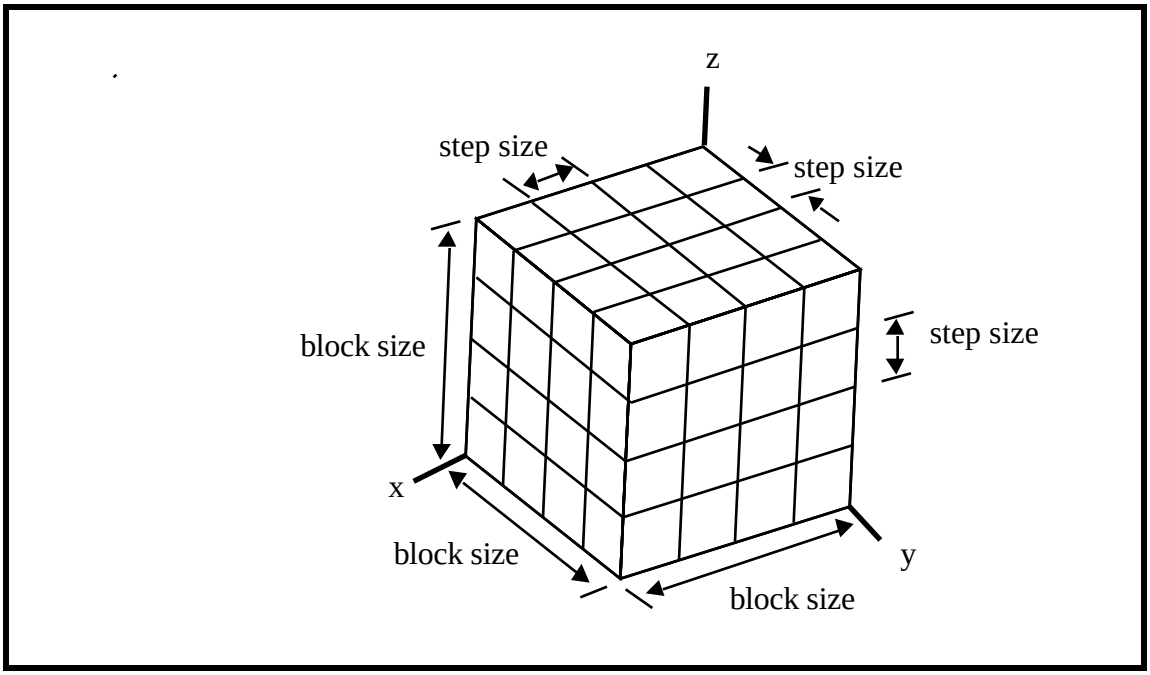

Figure 5.6
Grid Search For a Cube

The grid search may be made much more efficient by first searching with a coarse grid to isolate the general location of the maxima, and then searching with a finer grid in a block around the point found by the coarse grid. This concept was described by Remondi (1984) in relation to search volumes of a few metres and observation periods spanning over hours. At that time he warned that too large an observation period would result in a very narrow peak that a coarse grid might miss, and recommended that short periods (and a consequently broader peak) be used with the coarse grid and the large periods be used with the fine grid. In his 1990 publication on pseudo-kinematic GPS (Remondi, 1990), he advocated using a coarse grid of 0.33 to 0.25 cycles as a first pass with the ambiguity function.

When searching with a finer grid in a block around the point found by the coarse grid, the block size should exceed that of the coarse grid step size, to ensure a true point is not overlooked. In the coarse-fine grid implemented for results in this thesis, the fine grid

block was bounded by dimensions twice the coarse step size. The advantage of a 2 x coarse step size grid over a 1 x coarse step size grid for a hypothetical two dimensional case is shown in Figure 5.7. It can be seen that if only one coarse step size around an initial point was searched with a fine grid, a true point just over the search boundary would be rejected, whereas the use of two step sizes would include it.

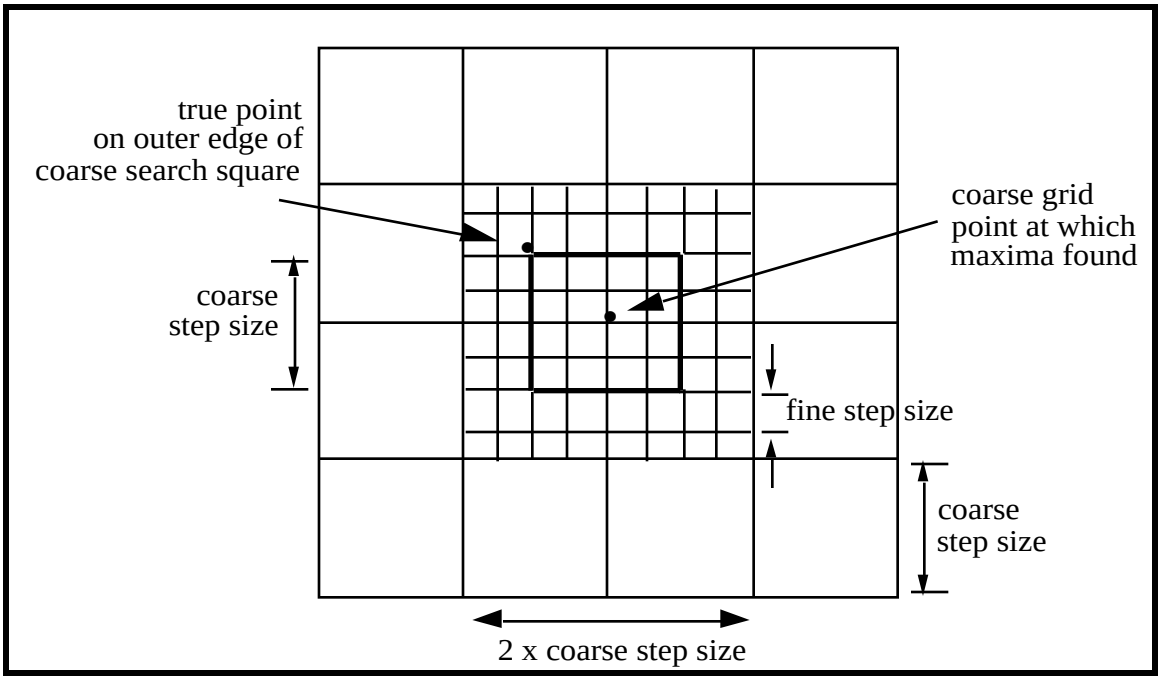

Figure 5.7
Coarse-Fine Grid Search - showing benefits of fine grid being bounded by 2 x instead of 1 x coarse step size

One may desire to lower the cos(obs - calc) rejection criteria of 0.7 given in Figure 5.4 when using larger grid sizes. The reason for this is evident through examination of Figure 5.5. When using a larger grid, the proximity of a test point to the true point is potentially reduced and the chance of the cos(obs - calc) falling below 0.7 increases. Hence a lower threshold may be warranted to avoid rejecting a good test point. Carrier multipath is another reason for reducing the rejection criteria. If double difference multipath exceeds 2.3 cm (from Figure 5.5), a good test point may be rejected.

The advantage of using a coarse-fine grid instead of a uniform grid is the great reduction of test points to be examined and the corresponding reduction in computation time. This is shown in Table 5.1 where the number of points for uniform and coarse-fine grids for 1 m and 0.5 m cubes are shown. Here a coarse grid size of $\lambda/4$ and a fine grid size of $\lambda/10$ are assumed.

Table 5.1
Comparison of Uniform vs. Coarse-Fine Grid Search Techniques

Grid Type		Step Size	Cube Size	No. of Points†
Uniform		$\lambda/10$ (1.9 cm)	1.0 m	157,464
		$\lambda/10$ (1.9 cm)	0.5 m	19,683
Coarse-Fine	Coarse	$\lambda/4$ (4.8 cm)	1.0 m	10,648
	Fine	$\lambda/10$ (1.9 cm)	9.6 cm	216
	Total	---	---	10,864
	Coarse	$\lambda/4$ (4.8 cm)	0.5 m	1,728
	Fine	$\lambda/10$ (1.9 cm)	9.6 cm	216
	Total	---	---	1,944

† number of steps on cube sides always rounded up before computing number of points

The table shows that for 1 m and 0.5 m cubes, only 7% and 10% of the points respectively, needed for a fine uniform grid search, need be considered for a coarse-fine grid search. Corresponding computation times are not given. However, using Mader's claimed ability to compute one million points in 55 seconds using a Compaq 386 with 25 Mhz clock speed and an 80387 and Weitek math co-processor (Mader, 1990) as a benchmark, the relatively small number of points for the limited search regions given above (made possible by the accurate code solutions discussed in Chapter 4), shows that

computation time is no longer a limiting factor for applying the AFM for post-mission static and rapid static applications.

The grid search technique, whether used uniformly or via the coarse-fine technique, does not take advantage of the one wavelength spacing between potential ambiguity solutions. Only every 19 cm of space (one L1 wavelength) need be searched rather than the full volume as is done using the grid search techniques. The needless searching of space between potential solutions may be eliminated using the double difference plane intersection search technique.

5.2.2 The Double Difference Plane Intersection Search

The geometrical concepts underlying the double difference plane intersection were presented by Hatch (1991a) as the first steps in his Least Squares Ambiguity Search Technique and applied by Remondi (1991) with the AF for kinematic applications without static initialization. The double difference plane intersection uses the observations from four satellites (three double differences) with sets of potential ambiguities to generate positions. Each satellite double difference with its trial ambiguity defines a plane in 3-dimensional space. By finding the intersection of the planes from three double differences the coordinates of a potential solution are found. All potential solutions are then tested by computing the AF, following the routine shown in Figure 5.4.

Sets of potential ambiguities may be generated in two ways. First, a double difference carrier phase solution with real ambiguities and statistics representing their accuracy may be used. This method will not be mentioned again with respect to the ambiguity function method, but will be discussed in relation to the fast ambiguity resolution approach (FARA) in Chapter 6. Second, the limits of a block around an initial

point may be specified as done for the grid search technique, and the ambiguities for each double difference observation for each corner point may be calculated. This is illustrated for a simplified 2-dimensional case with undifferenced observations in Figure 5.8. In the 2-dimensional case, the real ambiguity terms are calculated for the four corners of the square for one satellite-receiver observation. The figure shows the calculations for the minimum and maximum ambiguities.

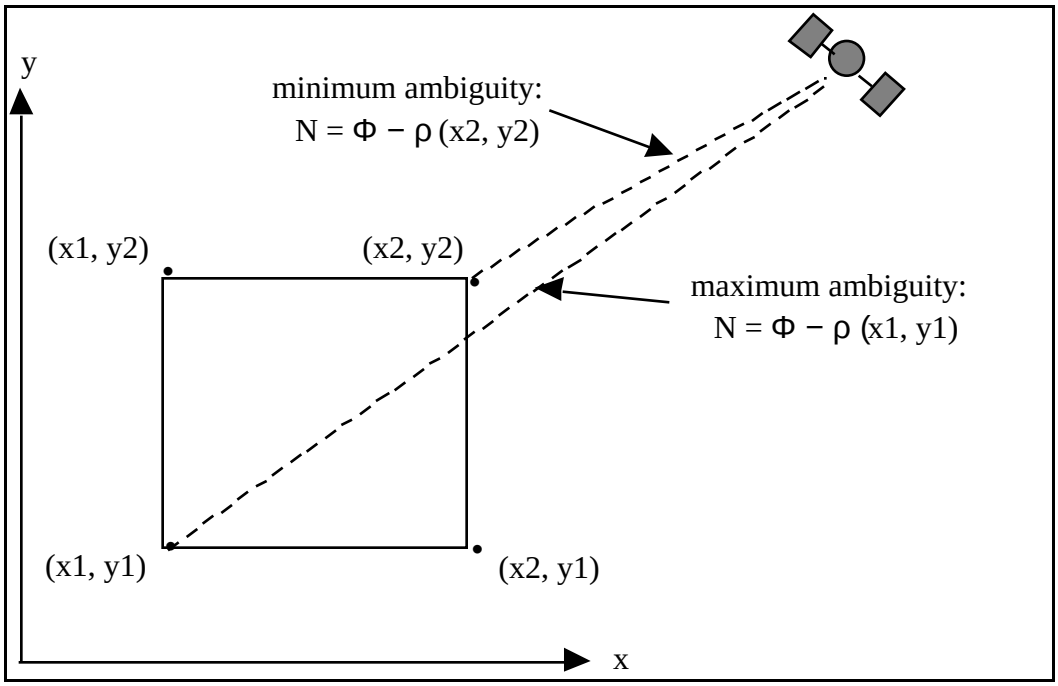

Figure 5.8
Computation of Maximum and Minimum Ambiguities for 2-D Space

In AF applications, the ambiguities for the eight corners of a block are calculated for three double difference pairs. The maximum and minimum ambiguity for each is saved. The resulting ranges may be zero to several cycles depending on the size of the search block and its orientation with respect to the double difference vectors. Sets of potential ambiguities are then generated using nested loops to increment between the

maximum and minimum of each ambiguity. An arbitrary example of ambiguity ranges and their sets of generated ambiguities are given in Tables 5.2 and 5.3 respectively.

Table 5.2
Ambiguity Ranges

SV Pair	Minimum	Maximum
19-2	-3	-2
19-6	8	9
19-11	4	4

Table 5.3
Generated Ambiguity Sets

Set	19-2	19-6	19-11
1	-3	8	4
2	-3	9	4
3	-2	8	4
4	-2	9	4

The smaller the ambiguity ranges, the fewer the number of points that need be considered as test points. The number of ambiguity sets to be considered may be computed as

$$\#\text{ sets} = \prod_{i=1}^{nsat-1} [(\text{max. ambiguity} - \text{min. ambiguity}) + 1]_i. \qquad (5.6)$$

where nsat is the number of satellites. For example, in Table 5.2 the number of sets is computed as 2 x 2 x 1 = 4, hence the 4 sets in Table 5.3.

The maximum and minimum ambiguities computed as per Figure 5.8, will almost never be exact integers and will require rounding of some sort. One may round the real ambiguities "in" so they fall within the cube, or "out" so they fall outside the cube, or they may be rounded to the nearest integer. Even though block corners may be used to find ambiguity ranges, this does not imply that all generated test points (or ambiguity intersections) will fall within the block. This is illustrated in Figure 5.9 for a simplified 2-dimensional case with the intersection of undifferenced observations from two satellites.

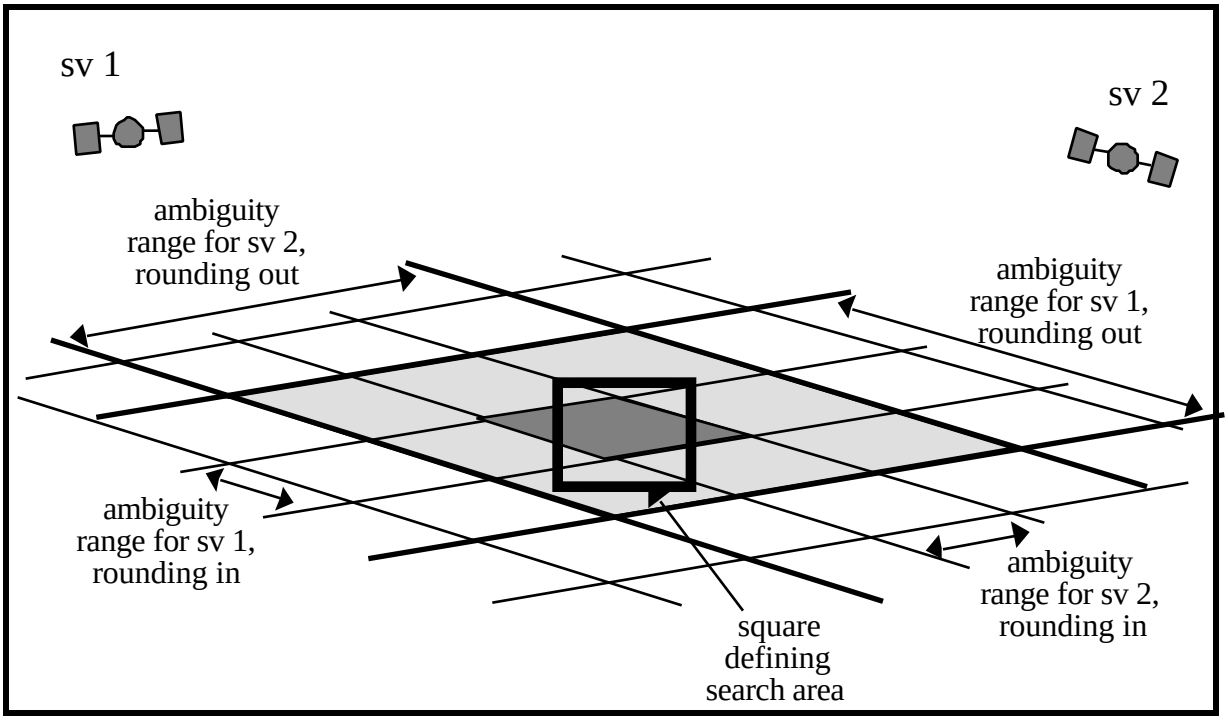

Figure 5.9
Ambiguity Intersections Outside Search Square

In the figure, the inner darkly shaded region demarcates the area bounded by maximum and minimum ambiguities that were rounded "in" and the surrounding lightly shaded area demarcates the maximum and minimum ambiguities that were rounded "out". The darkly outlined square represents the search region. It can be seen that even when rounding ambiguities "in" the test points may lie outside the search region.

To avoid testing points outside the search cube, test points generated using the double difference plane intersection techniques should be checked to see if they fall within the search cube. If not, they should be rejected from further consideration. This step can considerably reduce the number of test points to be evaluated, and at the same time reduce the potential for false ambiguity determinations.

Since only three double difference observations are required to compute a test point solution, some consideration must be given as to which satellites should be used.

From Hatch (1991b), Figure 5.10 shows that poor geometry would result in fewer intersections (and candidate test points), than would good geometry.

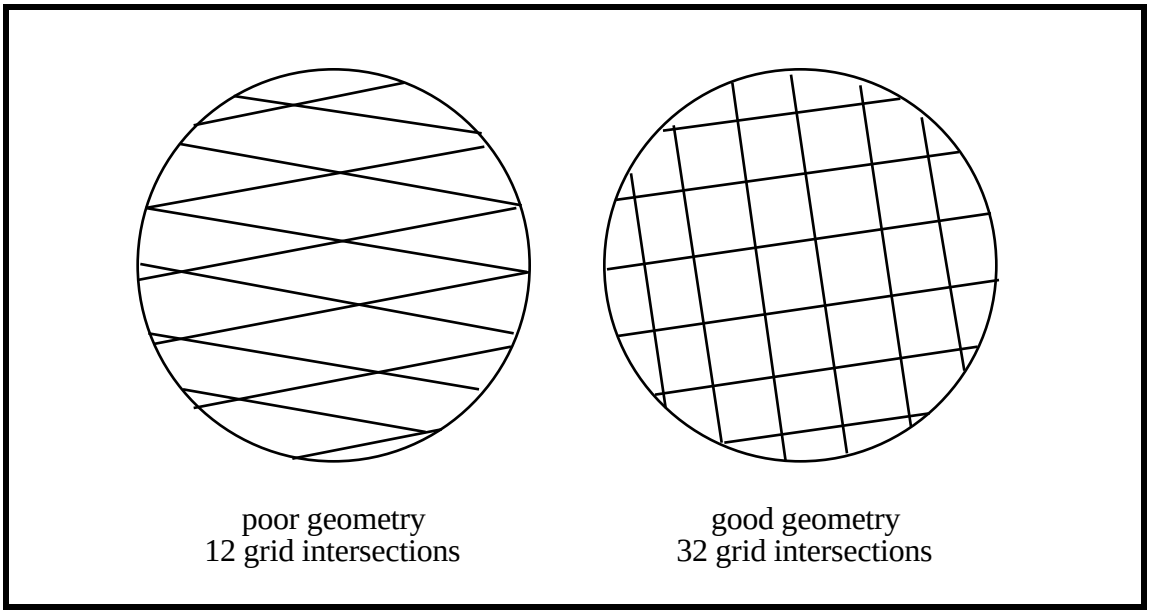

Figure 5.10
Number of Intersections With Poor Geometry Compared to Good Geometry
(Hatch, 1991b)

The trade off against fewer intersections to compute with poor geometry, is a less accurate test point to evaluate using the ambiguity function. If the test point is too far from the "true" point, a peak may be missed (similar to the risk of missing a peak using Remondi's course grid technique (Remondi, 1984)). For rapid static applications using AF and the small search volumes made possible by accurate code solutions, the advantage of poor geometry for computational efficiency is negligible, but the importance of being close enough to the true point to detect an AF peak is critical. Consequently the use of satellites which yield the best geometry is recommended for the AF.

For the double difference observations used in this thesis, the relative dilution of precision (RDOP) as discussed in Section 2.4, is the best tool to quantify geometry.

However, since PDOP measures are much more familiar and accepted by most working in the GPS industry, and since there is a general trend for PDOP values to correspond with RDOP values, PDOP values are given with results in Section 5.4.

Unless one is sure there are no cycle slips in a given set of data, only a single epoch of observations should be used in the computation of test points using double difference plane intersections. Using a single epoch of observations however, opens the risk for bad position estimates due to carrier phase outliers or poor geometry. This risk could be alleviated by computing independent tests point solutions (e.g. at sequential epochs) and cross-checking them, or by using mini-grid cubes around the point determined through double difference plane intersection. The development of the former point is straight forward, but the latter point will be expanded upon.

Instead of having to be sure a double difference plane intersection test point is determined accurately enough to find a maxima, a cube around the point (one step size out in all coordinate directions) may be used to generate surrounding points for testing, as shown in Figure 5.11. Although this would mean 27 test points to check for each double difference plane intersection point instead of one, the greater chance of finding the true point may outweigh the added computational burden.

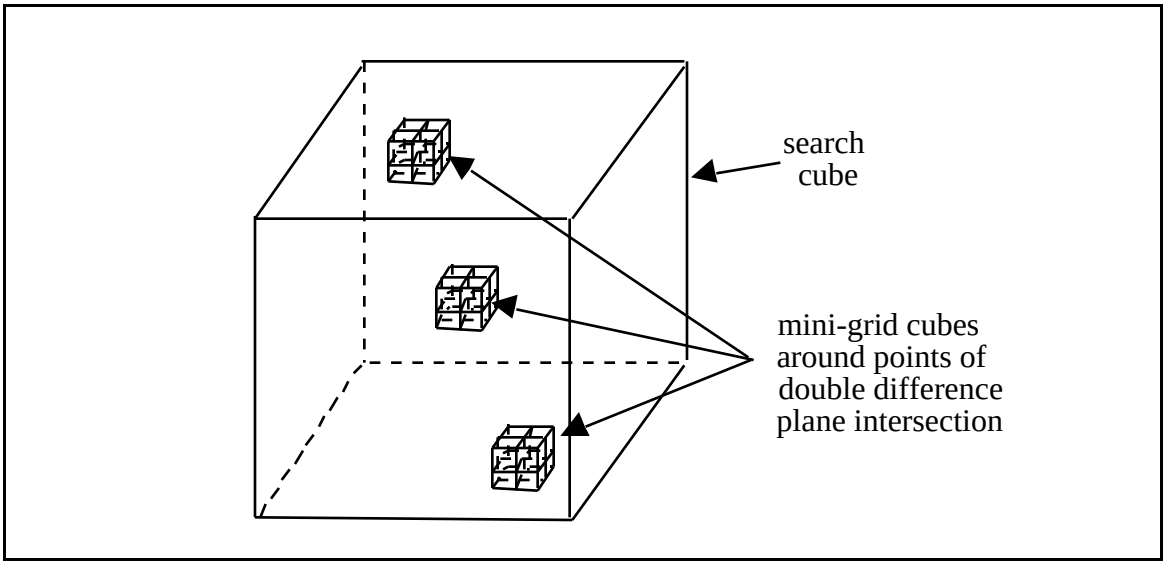

Figure 5.11
Mini-Grid Cubes Around Points of Double Difference Plane Intersection

The significance of the grid search and double difference plane intersection techniques, and variations thereof, will become apparent with the analysis and discussion of results of processed GPS data, but first it is important to develop means to assess the certainty of results.

5.3 AFM RELIABILITY

One of the pitfalls with the ambiguity function method to date has been the lack of robust means to assess if the resulting solution is reliable. In this section, reliability is used to mean a measure of certainty of the results attained, rather than the more narrow definition of statistical reliability given in Chapter 2. Unlike the least squares ambiguity search technique (Hatch, 1991a) or the fast ambiguity resolution approach (Frei and Beutler, 1990) which use statistical tests based on generated residuals, no rigorous testing has accompanied results of the AF. Hatch (1991a) argues this point as an indication of the superiority of the least squares ambiguity search technique over the ambiguity

function method. However, some certainty of AF results can be attained by limiting the observation conditions under which the AF is applied, being aware of the effect of search volumes and techniques on AFM solutions, and developing criteria for assessing results.

5.3.1 AFM Observation Conditions

Errors which affect all GPS observations, namely ionospheric, tropospheric, residual orbital errors, measurement and multipath errors, affect the ability of AFM to arrive at the correct solutions. Similarly, the geometry and redundant observations which lead to improved least squares GPS solutions also correlate with increased ability for the AFM to give good results.

Using only the single frequency data dealt with in this thesis, it is difficult to resolve ambiguities to the correct integers over long baselines (>15 km) using any ambiguity resolution technique, mainly due to errors resulting from decorrelation of the ionosphere with distance. Testing in different ionospheric conditions is needed to validate what baseline lengths are reasonable for AFM applications, but as a preliminary guideline in Canada, one would be wise not to exceed 10 km.

Low elevation satellites are subject to greater atmospheric errors because they map a longer signal path through the atmosphere, and are subject to greater multipath because their signal paths come closer to reflective multipath causing surfaces. The errors will have the effect of distorting the double differences such that when they are combined together, they may not yield a "clean" intersection. The AFM, which measures how well the double difference ambiguities intersect, may then fail by not detecting a point of intersection as a maxima, or be weakened and outweighed by a false maxima. To reduce the chance of low elevation satellites corrupting the power of the AFM, very low satellites

(below 10^{o}) should not be used, and low satellites (below 15^{o}) should be used with caution. An alternative not addressed in this thesis would be to use an elevation weighting function as described by Counselman and Gourevitch (1981), and Remondi (1984).

The ambiguity function method is similar to least squares techniques, in that the more significantly different good observations available, the greater the chance of attaining good results. Significantly different is intended to mean observations which contribute new information, not more of the same. Observations from more satellites or from dual frequency receivers constitute significantly different observations which would aid in the solution determination. Observations from the same satellite would not constitute significantly different information unless a sufficient change in satellite geometry had occurred. Observations five minutes apart, the time frame over which one would typically desire to have completed a rapid static survey, would correspond to less than a 3^{o} change in satellite elevation, meaning the added observations would have negligible geometrical implications for the AFM, although they would improve somewhat its statistical reliability. It is for this reason that Remondi (1990) recommends pseudo-kinematic surveys based on AFM have visits to the same station separated by at least an hour in time, which corresponds to about a 30^{o} change in satellite elevation. Greater satellite coverage constitutes significantly different information.

From the above discussion, the rapid static application of the AFM almost reduces to a one epoch solution problem from a geometrical perspective. However, by using several epochs instead of one, reduction in carrier phase measurement noise and multipath effects through averaging is possible.

A description of achievable AFM results for one epoch of observations is given by Mader (1990). Mader showed that for a cube with 1 m edges with 5 satellites at one epoch, ambiguity resolution by the AFM is impossible since several peaks of comparable

magnitude are present. He further showed that with addition of either L2 observations or an epoch of observations two hours later, the false peaks are suppressed and the true position is easily distinguished. Using eight satellite dual frequency data at one epoch he showed that only one peak would be detected in a cube bounded by 2 m edges. Since the scope of this thesis is limited to the single frequency case, most of his findings are not directly applicable. However two fundamentals can be built upon, the greater the satellite coverage, the greater the chance of success using AFM, and the smaller the search block, the greater chance of success using AFM. This latter point will soon be expanded upon.

In summary, for the greatest chance of success with AFM using single frequency data, observation conditions should be limited to

1) short baselines (<10 km),
2) satellites > 15^{o}, and
3) as great a satellite coverage as possible.

These are general guidelines, not steadfast rules; and exceptions are plentiful. The satellite coverage required has not been quantified, since it is closely linked to the size of the search volume.

5.3.2 The Influence of Search Volumes and Techniques on AFM

Two general situations may apply when using the AFM in a specified search volume. A single unique peak may exist in the volume or more than one peak may exist. The former case is ideal and sought after. The latter case is apt to occur and may pose significant problems. In the latter case it is important to understand two factors which influence the success of the AFM or lack thereof. These are

(1) the closest test point to the true point must be close enough to detect a maxima relative to other test points, and

(2) the search volume must be small enough for the corresponding satellite coverage and geometry to rule out from consideration, all peaks of comparable size except the peak at the true point.

The proximity of a test point to a true point is dictated by step-size when using the grid search technique, and the accuracy of the computed test points when using the double difference plane intersection technique. The arbitrary designation of grid points relative to the true point, may result in a true point exactly coinciding with a grid point, being equidistant between grid points (as shown in Figure 5.12) or being somewhere between these two extremes. (It is assumed the true point falls within the search cube.) The closer the true point is to a grid corner or to a test point computed using the double difference plane intersection technique, the higher the AF that will be found. Consider the case when a primary and secondary peak exists in a search volume. If the primary peak was equidistant between grid corners (as in Figure 5.12), the test points (grid corners) surrounding the primary peak may be rejected from consideration over a test point which happened to coincide exactly with the location of the secondary peak.

To give an indication of the type of values one might expect at test points separated from the "true point" by a range of distances, AFM results using a uniform grid with a 1 cm step size ($\lambda/20$) for one epoch of the January 25th, five satellite zero baseline data set were computed. (See Chapter 3 and Figure 3.1 for data set details.) From the listing of test point coordinates and normalized AF, sample results at different distances from the truth were extracted and are tabulated in Table 5.4. The algorithm used to produce data shown had its cos(obs - calc) threshold set at 0.0 instead of 0.7.

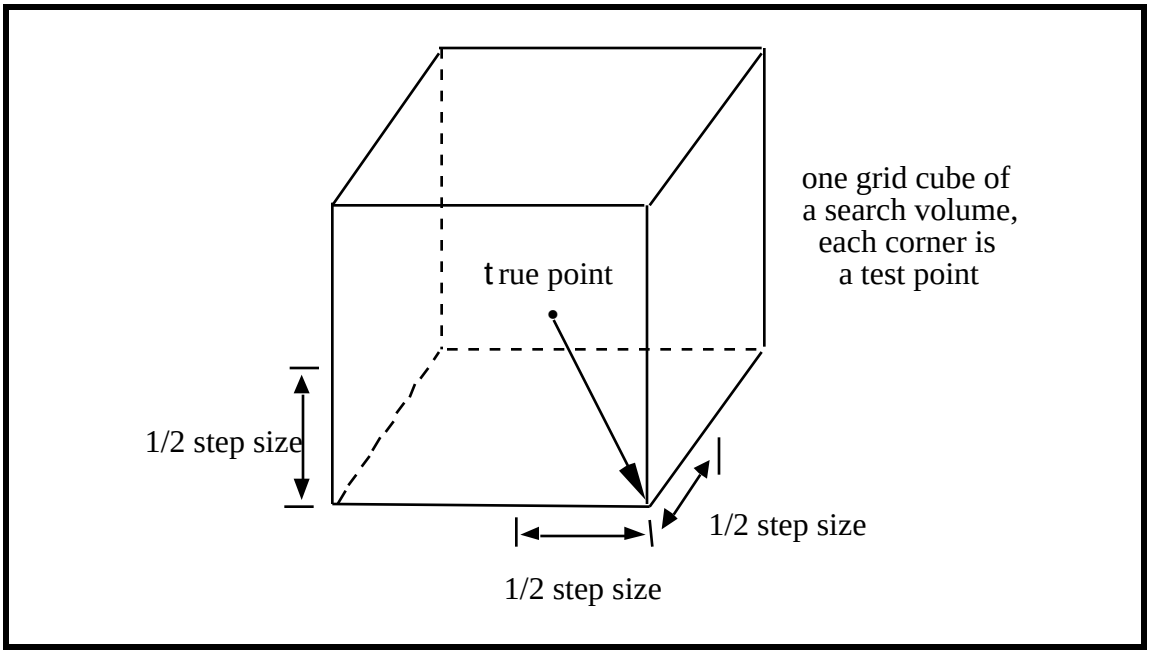

Figure 5.12
True Point Equidistant Between Grid Corners

The first column in Table 5.4 gives a range of step sizes as fractions of wavelengths that correspond to the second column's maximum distances of the closest grid corner to the truth. (Recall from Figure 5.12, the distance is the length of the vector from the test point to a grid corner.) The third column gives sample ambiguity function values for respective distances from the truth.

One could interpret Table 5.4 by saying at a $\lambda/2$ grid spacing, the AF expected at a true point may range anywhere from 0.73 (at the most distant point) to 1.00 (collocated with the true point). For a $\lambda/2$ spacing, a false peak could be easily thought of as a true point if it coincides with the test point, and the closest test point to the true point was 8 cm away.

Table 5.4
Typical Ambiguity Function Values for Varied Step Sizes
(Jan. 25 - zero baseline - epoch 576460 - 5 satellites)

Step Size (λ = 19 cm)	Maximum Distance Between Closest Grid Point and True Point	Normalized Ambiguity Function Value
$\lambda/2$	8.2 cm	0.73
$\lambda/4$	4.1	0.90
$\lambda/7$	2.4	0.93
$\lambda/10$	1.6	0.97
$\lambda/20$	0.8	1.00

The significance of Table 5.4 should not be misconstrued. It has been provided for no purpose other than to illustrate the potential for choosing an incorrect point over a correct point. It is shown in Section 5.4 that the AF values surrounding true points show oriented patterns rather than concentric patterns, as the misinterpretation of Table 5.4 might lead one to believe. Also, since Table 5.4 is based on zero baseline data, the results are more optimistic than under normal conditions.

The above discussion brings about the observation that a test point must be close enough to a true point (as compared to other test points) to yield good results no matter what search technique is used, if there is more than one peak within the search volume.

The size of a search volume has significant implications since smaller search volumes not only dramatically reduces the number test points (as shown in Table 5.1), but also have the potential for ruling out secondary peaks from consideration. This was mentioned in Mader (1990) and is demonstrated in Section 5.4.

Looking at the extreme case, if an initial coordinate estimate was known with a certainty of ±2.75 cm, implying a search cube of with 5.5 cm edges, with only one double difference observation, the ambiguity would be immediately determined as illustrated in

Figure 5.13. Note how the numbers in Figure 5.13 were arrived at. The solution must lie within 9.5 cm (half a wavelength) of the truth for its correct integer ambiguity to be chosen. Transferring this length to a cube's diagonal results in cube edges of 5.5 cm, and a required initial point accuracy of ±2.75 cm.

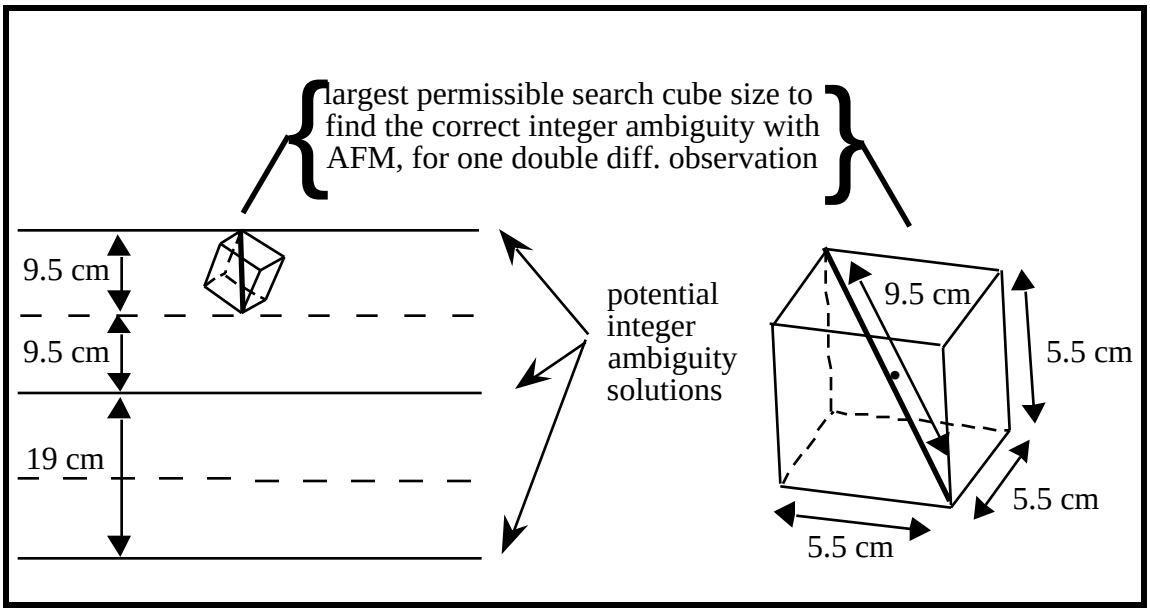

Figure 5.13
Maximum Cube Size To Find Integer Ambiguity With One Double Difference Observation

In typical applications for rapid static surveys, five to seven satellites might be visible. Each could be used for rapid static ambiguity resolution if the initial search area is well enough determined to eliminate false peaks. One can envisage the general trend, that an increase in the number of satellites will correspond with an increase in the allowable uncertainty of the initial search volume. This trend is illustrated graphically in Figure 5.14. The word "general" is important here. Many considerations including satellite geometry have an intertwined relationship with the size of the AFM search cube. Two entries have been made in Figure 5.14, a 5.5 cm cube size for one satellite as shown in

Figure 5.13, and a 40 cm cube size for 6 satellites as results of Section 5.14 tend to show. All others are left with question marks, to be determined through empirical testing.

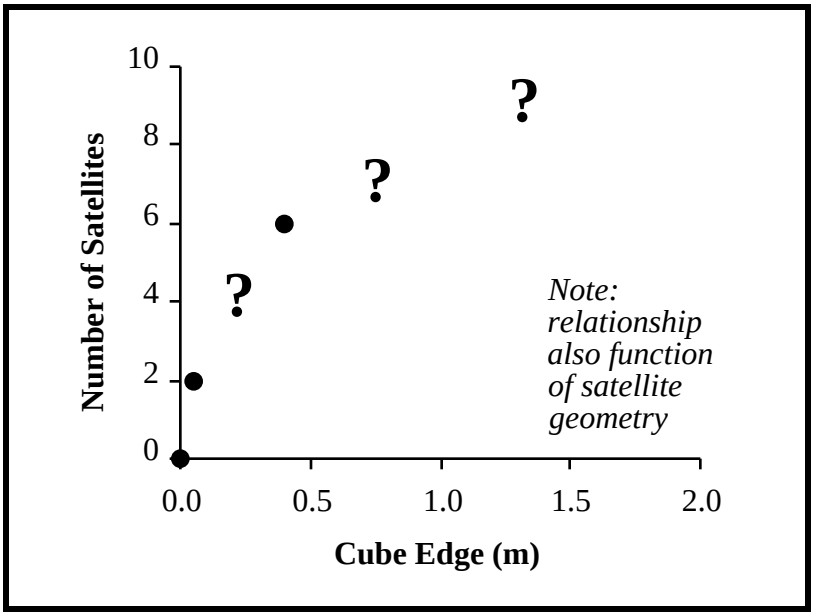

Figure 5.14
Satellites Required vs. Search Cube Size

In designing production AFM algorithms and assessing AFM results, it is important to know the behavior of peaks for a given satellite coverage and configuration, and know the corresponding ability or lack thereof to isolate a correct peak for a specific search cube size. A figure such as 5.14 would be of assistance. One shortcoming of this figure is its limitation to cubic dimensions. In production one is more apt to define blocks proportionally to the accuracy of initial coordinate estimates, which in turn is a function of code accuracy, errors and satellite geometry. Variations of the information of Figure 5.14 may be required in these instances.

Ensuring good observation conditions and checking that search techniques and volumes are compatible with the satellite coverage are prerequisites which eliminate

situations where the AFM is not apt to succeed. Means to reject or accept AFM results assuming all the above have been taken into consideration are still required.

5.3.3 Acceptance Criteria

Acceptance criteria for AFM solutions fall into two basic categories; first, checks that are made on the integrity of an individual solution and second, checks that are made against sequential but independent solutions. Before discussing details of these two categories of acceptance criteria, it is informative to review techniques other authors have used to evaluate the certainty of AFM results.

Mader (1990) wrote a 3-dimensional colour plotting program to plot AFM "peaks". Through this technique, he could visually see the number and location of peaks and make a decision based on human intelligence if the solution was good. This is an effective method, but not practical for production applications.

Remondi (1990) spoke of predominant peaks which are clearly greater than other peaks, as being distinct enough to identify the correct peak for pseudo-kinematic GPS surveys. He also gave a clever method to verify the identification of the correct peak. He recommended the coordinates at the candidate peak be used to correct cycle slips and then the cycle slip corrected data be used in a float double difference solution. If the cycle slips were correctly fixed (meaning the candidate point was correct), the real ambiguity estimates would be almost perfect integers on short baselines. This would not be the case with incorrectly fixed cycle slips. If no cycle slips were present in the data, false cycle slips could be introduced. The drawback with this method is that observations with sufficient change in satellite geometry are needed to make a float double difference carrier

phase solutions feasible. (Remondi was applying this to the pseudo-kinematic case where the geometrical requirements are well fulfilled.)

The checks that are made on the integrity of an individual solution proposed here extract some basic concepts from Mader (1990) and Remondi (1990). Before delving into these, an important pattern of AF's needs to be clarified.

The normalized ambiguity function (AF) may have several "peaks" in a given search volume. These "peaks" generally consist of a point with the highest local AF value surrounded by points with lesser AF values, oriented in some direction in 3-dimensional space. Two errors could occur in isolating the "true" solution. First, the correct peak could be isolated, but a point other than its highest point may be chosen (perhaps as a consequence of a search pattern). This error is almost always acceptable since the point will be close enough to the true point to ensure the correct integer ambiguities are computed. Second, the wrong peak could be isolated. This error has grave repercussions since it could result in one or more ambiguities being fixed to the wrong integer. It is this second error that the checks presented aim to avoid.

A scheme for checking individual AFM solutions is presented in Figure 5.15. The algorithm is used to validate that the point with the largest AF is the solution. One begins with a file of all test points generated following the ambiguity function algorithm of Figure 5.4. The points with the highest and second highest AF values are extracted, and in the figure are referred to as points 1 and 2 respectively. The AF of point 1 is checked to see if it is greater than 0.92. If not, no solution is deemed to be found. Next, the AF of points 1 and 2 are differenced. If their difference exceeds 0.08 a solution is said to be isolated. (This is a quantification of Remondi's method of distinguishing points with clearly larger AF.) If not, the length of the vector between points 1 and 2 is calculated. If the distance between the points is greater than 10 cm they can be thought of

as belonging to different "peaks", hence a solution cannot be isolated. If the distance between points is less than 10 cm, the second point can be disregarded. (This is done by Mader through visual inspection of the results of his 3-D plots.) The file is then checked for the next largest point. If there are no more points in the file, point 1 has been isolated as the solution. If there are more points in the file, the point with the second largest AF is extracted, and the routine is repeated with this new point as point 2.

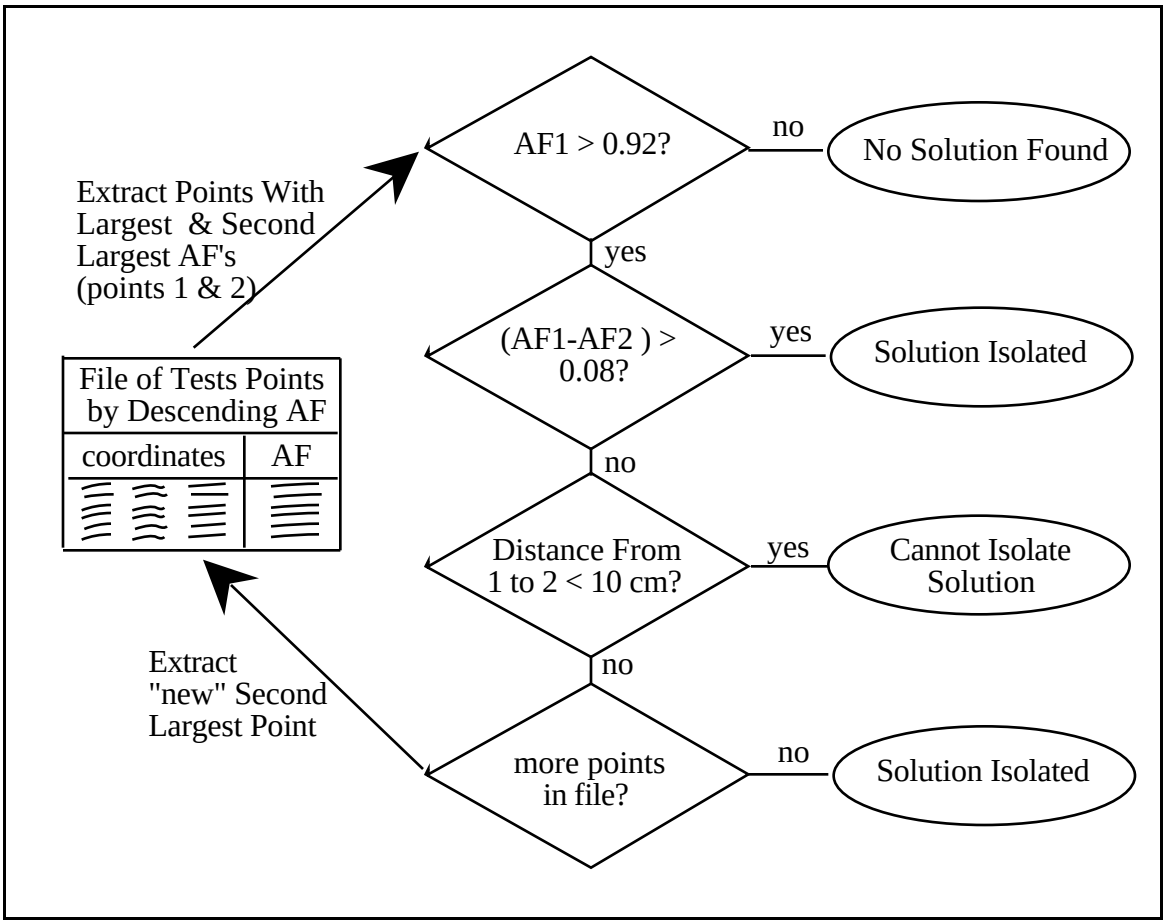

Figure 5.15
AFM Integrity Checks For a Single Solution

The (AF1 - AF2) threshold of 0.8 given is quite pessimistic, but specified as such to avoid identification of false peaks as the correct solution. It is set with the assumption that the single solution being tested is one of a set of independent solutions used to resolve ambiguities.

The AF algorithm is unforgiving of bad carrier phase observations. From Figure 5.3, if an individual cos(obs - calc) falls below a threshold of 0.7, the test point is immediately rejected. Hence, one outlier of one observation at one epoch could cause the rejection of a "good" solution. In tests carried out this has not posed a problem. Nevertheless, this dilemma along with noise due to receiver hardware or multipath may invalidate good results either in the AF algorithm or the AFM integrity checks for a single solution. To mitigate these effects, several independent solutions may be computed using neighbouring epochs of observations. Even if the AFM was calculated over 5 minutes using observations every 20 s for the sake of statistical reliability, several independent solutions could be computed at the same data rate but each offset by 1 second from the previous solution. The consistency of the independent results may then be assimilated to validate the correct isolation of a solution or the inability to do so. This concept is illustrated in Figure 5.16.

One begins with a file of results which contains products of the individual ambiguity checks of Figure 5.15. The overall success rate of isolating a solution is checked against a threshold success rate value. In the figure an 80% success rate has been shown, but this may be modified based on the sample size (i.e. the number of results

used), statistical assumptions and experience. If less than 80% of the solutions are successfully isolated, the data is presumed too weak to isolate a correct solution. If over 80% of solutions are successfully isolated, they are checked to ensure they apply to the same peak. If they do, a correct solution is said to be isolated and ambiguities can be computed from the x, y and z coordinates.

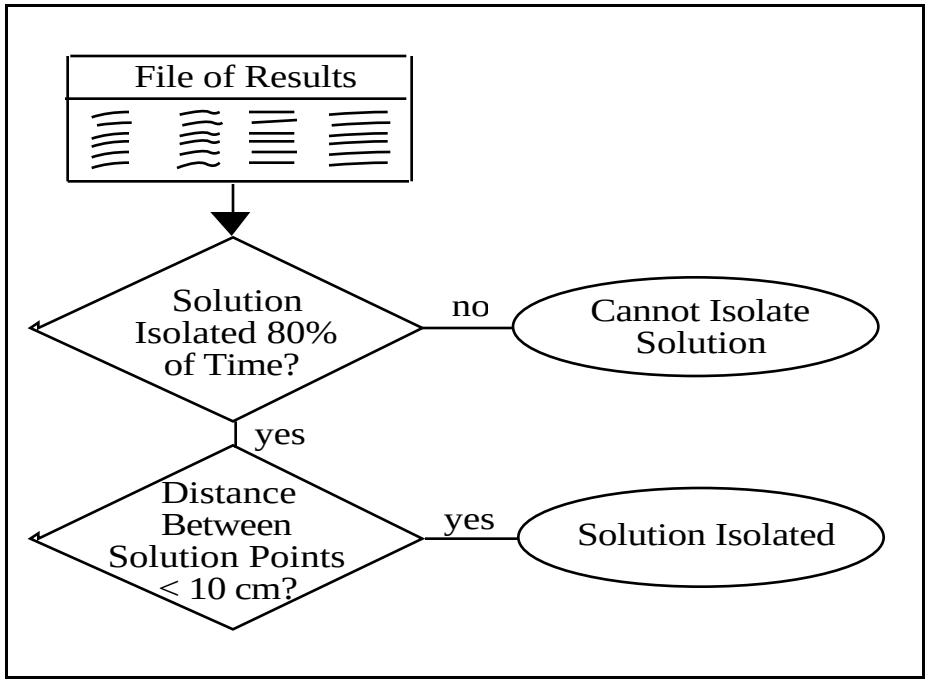

Figure 5.16
AFM Integrity Checks For Result Intercomparison

The integrity checks shown above for individual solutions and result intercomparisons, are one set of acceptance criteria that may be used with the ambiguity function method. Numerous developments and variations of the above algorithm are possible. Different thresholds, based on statistics, experience or catered to a specific observing environment, may be used. Each technique will surely have merits for different situations and for the incorporation in different GPS processing packages. Hence, it is

not the intent here to suggest a "best" technique, but rather to show that criteria to assess the results of the ambiguity function method are available.

The results presented in the latter portion of Section 5.4 were assessed using the criteria given in Figures 5.15 and 5.16.

5.4 AFM RESULTS

The results presented herein serve two purposes. First, they provide a better understanding of the concepts described in Sections 5.1 to 5.3. Second, they show results attainable with single frequency data using AFM under varying conditions. As described in Section 5.1, the ambiguity function method is comprised of initial point estimation, defining a search volume and test points, and then computing the normalized AF value. Results on initial point estimation and boundary definition are described in Section 4.2 and are not addressed here. Results of tests of cubic volumes around "true" points are presented. Output listings generated and used to produce the reported results include the normalized ambiguity function values, the x, y and z coordinate differences from the truth, and the vector distance from the truth.

The initial discussion of results is based on a single epoch over two days of observations. The single epoch results can be thought of as a "raw" form of AF since they are unaltered by averaging and rejections over successive epochs. Single epoch AFs are then compared to AFs accumulated over several epochs. Following, a detailed examination of these results show the patterns of AF for different search techniques, different numbers of satellites and different cube sizes. The latter portion of the discussion of results examines several AFM solutions for three different data sets using different search techniques.

5.4.1 AF Patterns - Using Grid Search Techniques

The pattern of AFM peaks are best seen plotted in three dimensions using colour graphics as done by Mader (1990), but this is not practical or meaningful for two colour representation. Information presented below, plotted in one and two dimensional space, effectively shows subsets of AF patterns. One should bear in mind when reviewing these graphic representations, that they are only part of the full 3-dimensional picture.

The pattern of AFM peaks is shown with normalized ambiguity function values plotted against the distance from the true point. Jan. 25th, 5 satellite, zero baseline data is shown in Figure 5.17, and Feb. 12th, 6 satellite, 700 m baseline data is shown in Figure 5.18. In both cases only one epoch of observations was used and a uniform grid search with a 1.9 cm step size over a cube with 1 m edges was carried out.

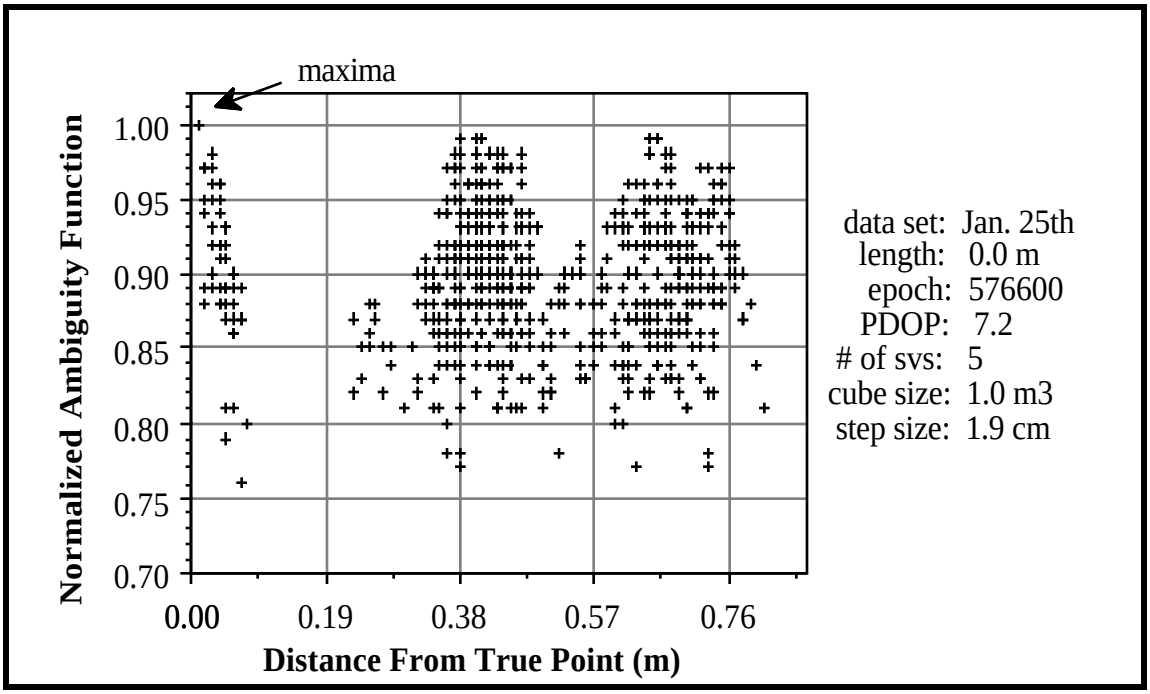

Figure 5.17
1 Epoch AF for 5 Satellite Data Using a 1.9 cm Grid Over a 1.0 m Cube

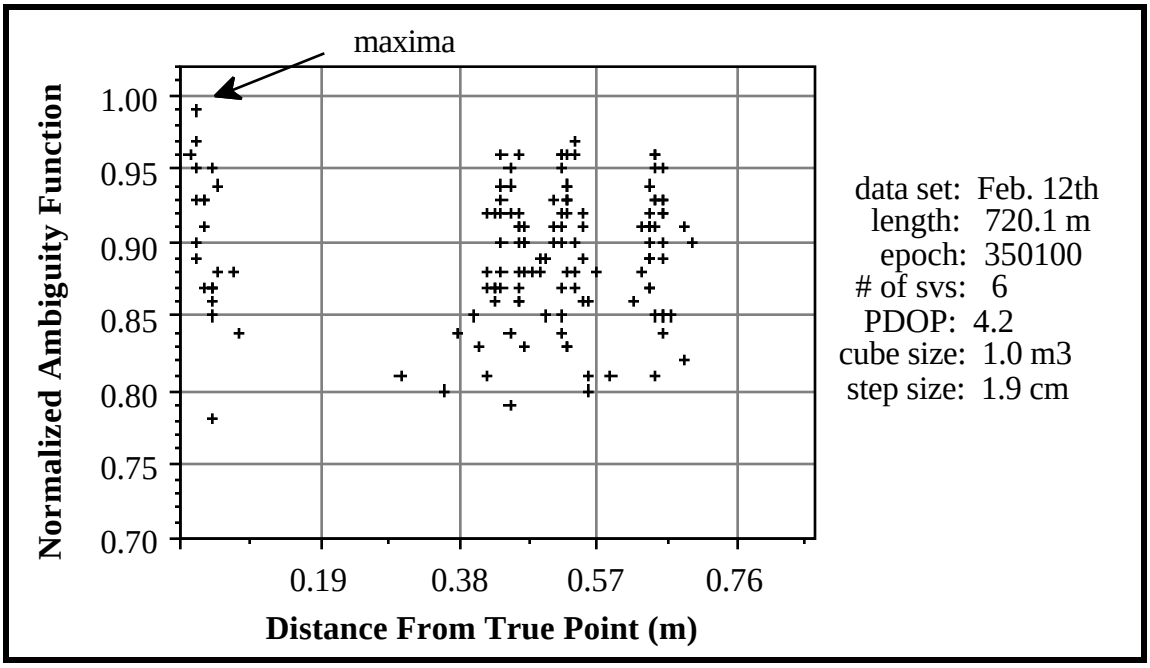

Figure 5.18
1 Epoch AF for 6 Satellite Data Using a 1.9 cm Grid Over a 1.0 m Cube

For the 5 satellite data in Figure 5.17, the location of peaks are centered at about 0.0 cm, 38 cm and 66 cm from the truth. From Figure 5.18, it can be seen that the sixth satellite ruled out many points found with five satellite data. A clear peak is evident at 0.0 cm, with less distinct peaks stretching from about 38 cm to 67 cm from the truth. In both the five and six satellite case, the largest and secondary AFM peaks are too close to distinguish the true point.

Up to a distance of about 9 cm from the true point in both Figures 5.16 and 5.17, one can see a gradual decrease in the ambiguity function values determined. It is interesting to see this same pattern in 2-dimensional space. To show this, a slice in the y-z plane was taken out of the 3-dimensional data corresponding to Figure 5.17 for x = 0. All normalized ambiguity function values for the corresponding y and z coordinates are plotted in Figure 5.19.

Y (cm) \ Z (cm)	-4	-2	0	2	4
-4			.89	.94	.90
-2			.97	.97	.88
0		.95	1.00	.95	
2	.89	.98	.97		
4	.91	.95	.89		

data set: Jan. 25th
length: 0.0 m
epoch: 576600
# of svs: 5
PDOP: 7.2
cube size: 1.0 m
step size: 1.9 cm

Figure 5.19
Ambiguity Function Values Around True Point For The Plane x = 0

Note for x, y and z = 0 (i.e. at the true point) the ambiguity function is 1.00 as expected. The values gradually decrease as one moves away from the true point, with a marked orientation extending from the positive y to the positive z axis. The same gradual decrease in values from the true point, and notable orientations are present in plots for y = 0 and z = 0, which have not been shown because they do not add to what can be learned from Figure 5.19.

All ambiguity values which cross the x = 0 axis and passed the individual rejection test of cos(obs - calc) > 0.7 (from Figure 5.4), are shown in Figure 5.19, yet they only extend ±4 cm from the true point. In vector length, the greatest distance from the true point in Figure 5.19 is about 5.7 cm (for y = 4 and x = -4). This means points extending out to about 9 cm in Figure 5.17 must be on planes where $x \neq 0$. Tests carried out have shown that when the (obs - calc) threshold is reduced, the same trend as shown in Figure 5.19 prevails, with the differences being the extension to lower normalized ambiguity function values occurring at further distances from the truth.

Note Figure 5.19 is almost symmetrical about zero. One of the characteristics of the ambiguity function is its symmetry. Theoretical explanations and discussions in relation to this are given in Counselman and Gourevitch (1981) and Remondi (1984), and are not reiterated here.

One of the dangers of non-uniform grid search techniques is evident through analysis of Figure 5.18. If a double difference plane intersection search yielded a test point at x = 0, y = -2, and z = -2, which is less than 3 cm from the truth, no solution would be found. It is this type of occasion that a mini-grid search around a double difference intersection point as illustrated in Figure 5.11 would be needed.

All results presented to this point have been based on a single epoch. Results for Feb. 12th data using several epochs are shown in Figures 5.20 to 5.23.

In Figure 5.20, the results from a uniform grid search over a 1.0 m cube, but using 61 epochs over one minute instead of a single epoch are shown for Feb. 12th data. Comparing the 61 epoch results of Figure 5.20 with the one epoch results of Figure 5.18, one can see the same values for the maxima (0.99) and the secondary peak (0.97). The difference between the two sets of results is that for the one epoch case, AF extends down to 0.78, and for the latter case, AF only extends down to 0.90. This suggests that many marginal test points which passed the cos(obs - calc) threshold of 0.7 for a single epoch, failed to pass it for one of the other 60 epochs. Note that most of the points rejected by using several epochs would not be considered when using a double difference plane intersection search.

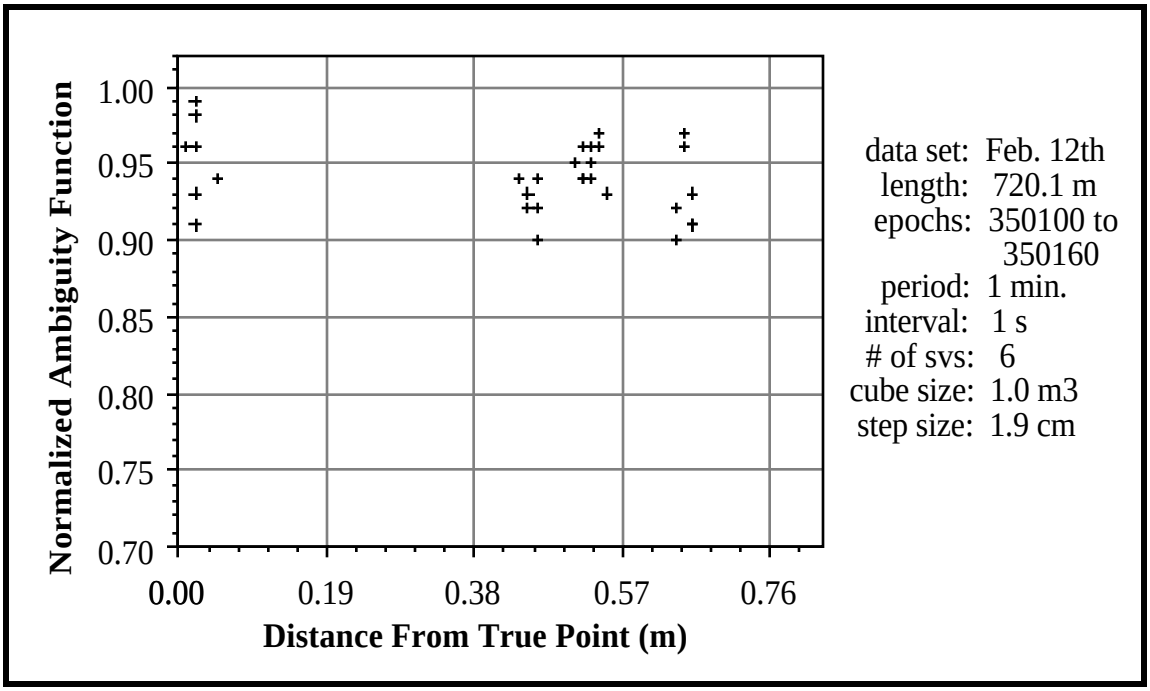

Figure 5.20
61 Epoch AF for 6 Satellite Data - 1.9 cm Uniform Grid Over a 1.0 m Cube

AF results for six epochs over five minutes, with all other parameters as described for Figure 4.20, are shown in Figure 5.21. Comparing this figure with Figure 5.18, one can see the maxima AF is 0.98 instead of the 0.99 seen in Figure 5.18, and the secondary AF is 0.95, instead of the 0.97 seen in Figure 5.18. Comparing Figures 5.21 and 5.20, it can be seen that using six epochs over five minutes had the effect of reducing the number of test points which failed the threshold test by more than the 61 observations over one minute did. A probable cause for both of these observations is the greater variation in carrier multipath effects over five minutes than over one minute. The small change in geometry is not a likely cause, since the same primary peaks and secondary peaks formed are close to the same magnitude and distance from the truth as for the single epoch case. The geometrical change over five minutes however, likely does influence multipath.

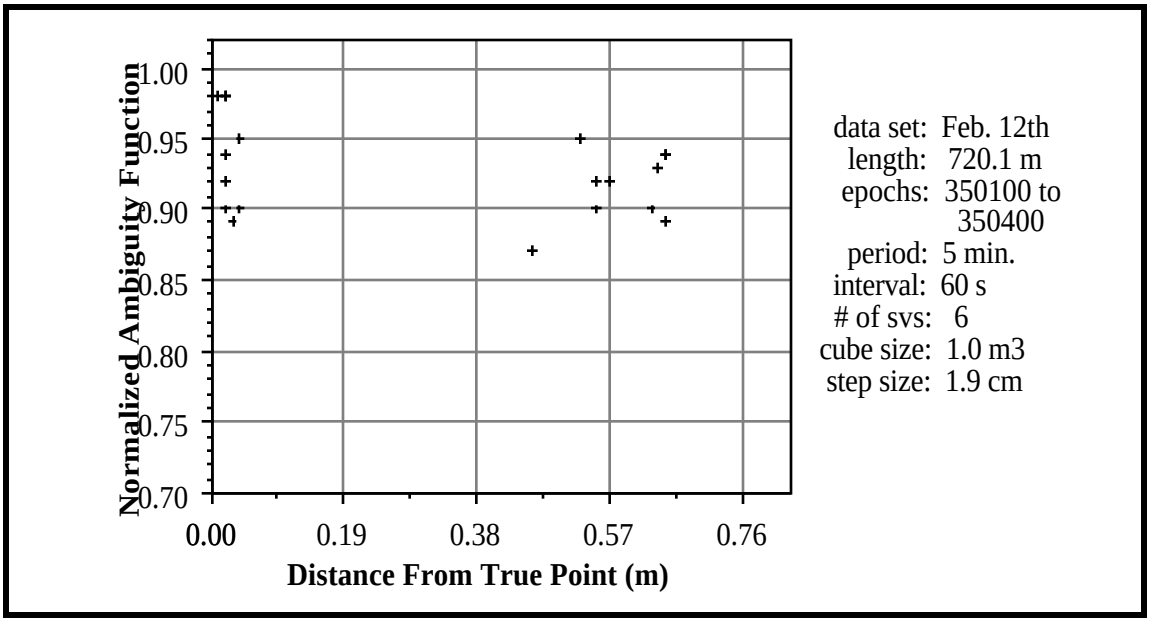

Figure 5.21
6 Epoch AF for 6 Satellite Data - 1.9 cm Uniform Grid Over a 1.0 m Cube

Figure 5.22 shows the same data as Figure 5.21, but instead of using a data interval of 60 s, a data interval of 1 s is used, meaning 301 epochs over five minutes. As can be see in the figure, only three points survived the rejection criteria for all 301 epochs, and these 3 points all occur near the truth. At first glance one might assume from these results, that the best procedures using AF is to use all possible epochs of observations at the smallest data interval possible. The danger with this approach is that all test points could potentially be rejected and no solutions found. Furthermore, there is no guarantee only one peak will remain as in Figure 5.22, because as seen in Figure 5.21, secondary peaks still do occur over five minutes of data using six satellites in a 1 m cube.

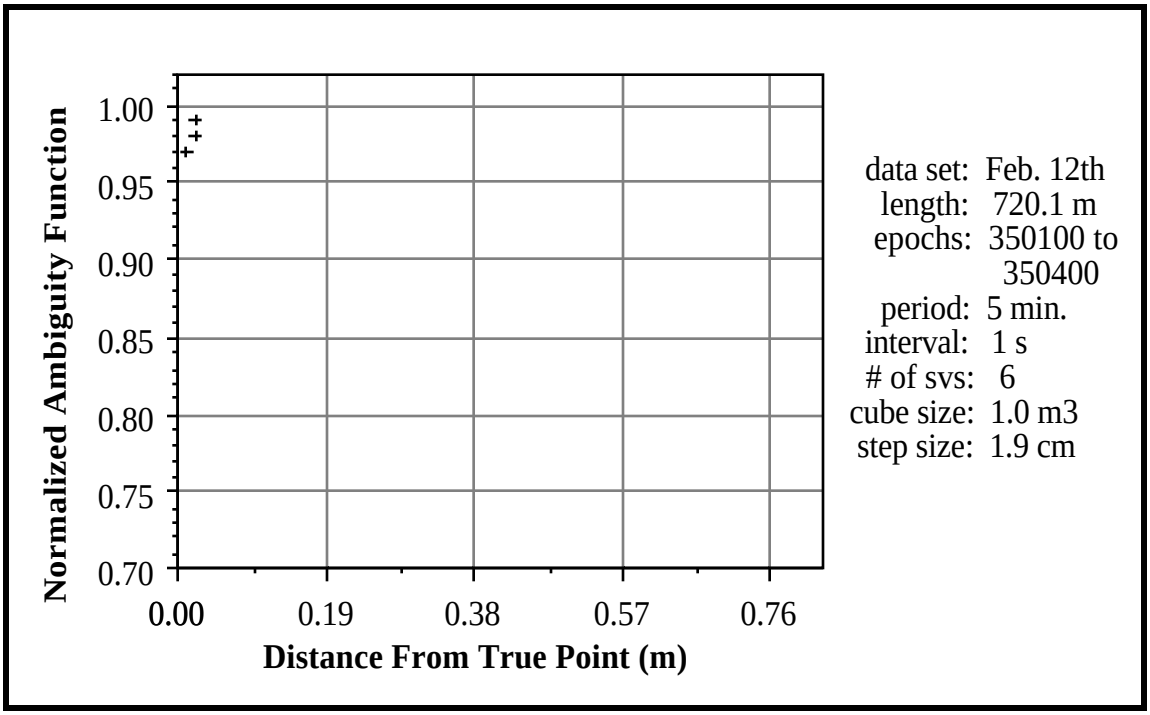

Figure 5.22
301 Epoch AF for 6 Satellite Data -
1.9 cm Uniform Grid Over a 1.0 m Cube

Variation in Cube Size

To see the effect of a smaller cube size on the AF, the single epoch data for Figures 5.17 and 5.18 is shown again in Figures 5.23 and 5.24 respectively, but for cubes with 0.5 m edges instead of 1.0 m edges. Note in each figure, only one clear peak is evident, centred around 0.0 cm from the truth, showing that the correct point is easily discernible using a cube with 0.5 m edges instead of 1.0 m edges. Fewer points are present in the six satellite data than the five satellite data as expected.

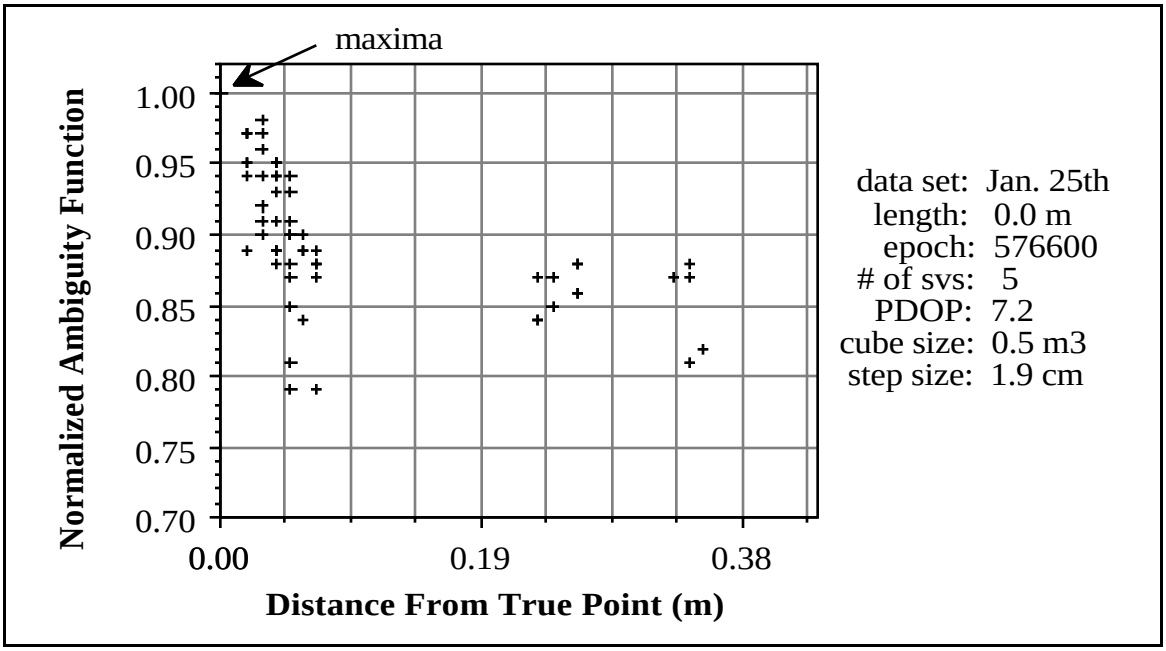

Figure 5.23
1 Epoch AF for 5 Satellite Data Using a 1.9 cm Grid Over a 0.5 m Cube

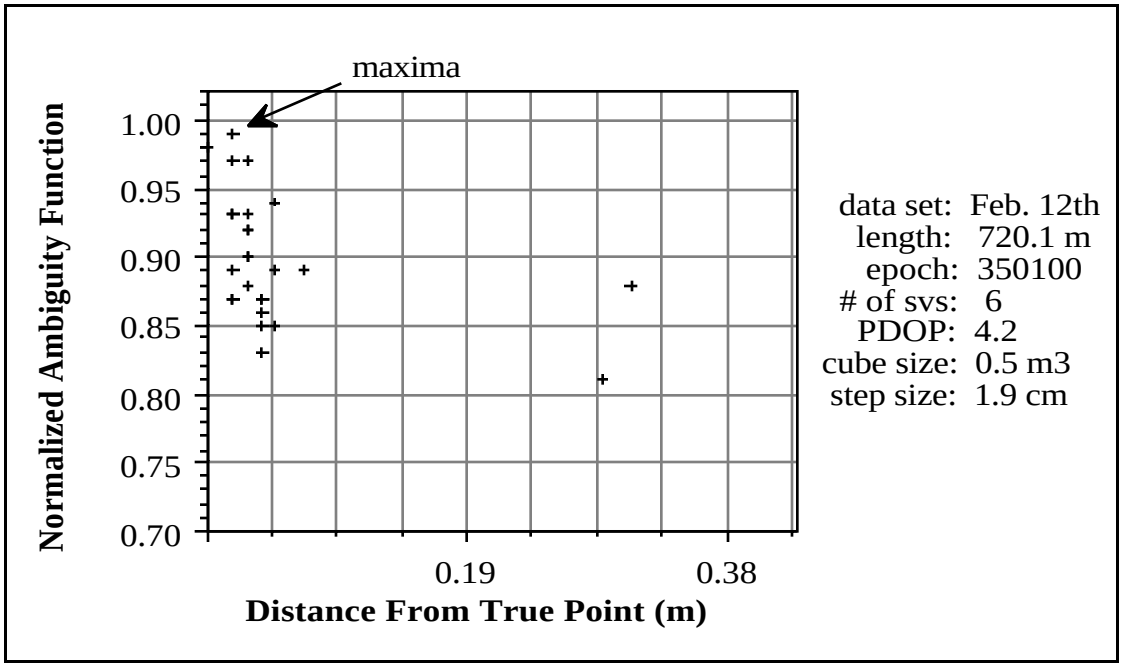

Figure 5.24
1 Epoch AF for 6 Satellite Data Using a 1.9 cm Grid Over a 0.5 m Cube

At first glance one may wonder why the peaks at 38 cm in Figures 5.17 and 5.18 are not present in Figures 5.23 and 5.24. The explanation for this lies in the transformation from the one-dimensional vector lengths shown in these figures to the 3-dimensional blocks for which AF values are calculated. These 38 cm peaks in the earlier figures were products of x,y,z coordinates where at least one coordinate laid outside ±0.25 m from the true point. Different orientations of the search cube, or different orientations of the pattern of peaks could result in some points near the borderline ruled out in these 0.5 m cube examples, not being ruled out in other cases using the same cube size.

As discussed in Section 5.3, and as illustrated above, the dimensions of the search cube are very significant as to whether ambiguities can be correctly resolved or not. The specific results shown above illustrate that with a 1 m search cube, ambiguities would not be resolved whereas for 0.5 m they would be.

Variation in Step Size

All the results shown above are based on a 1.9 cm uniform grid. However using the coarse-fine grid technique described in Section 5.1.2, one initially uses a coarse grid. To see the effect of using larger step-sizes that characterize coarse grids, the AF for uniform grids over a 1 m cube with step sizes of 4.8 cm ($\lambda/4$) were computed using the same five and six satellite data, and are shown in Figures 5.25 and 5.26 respectively.

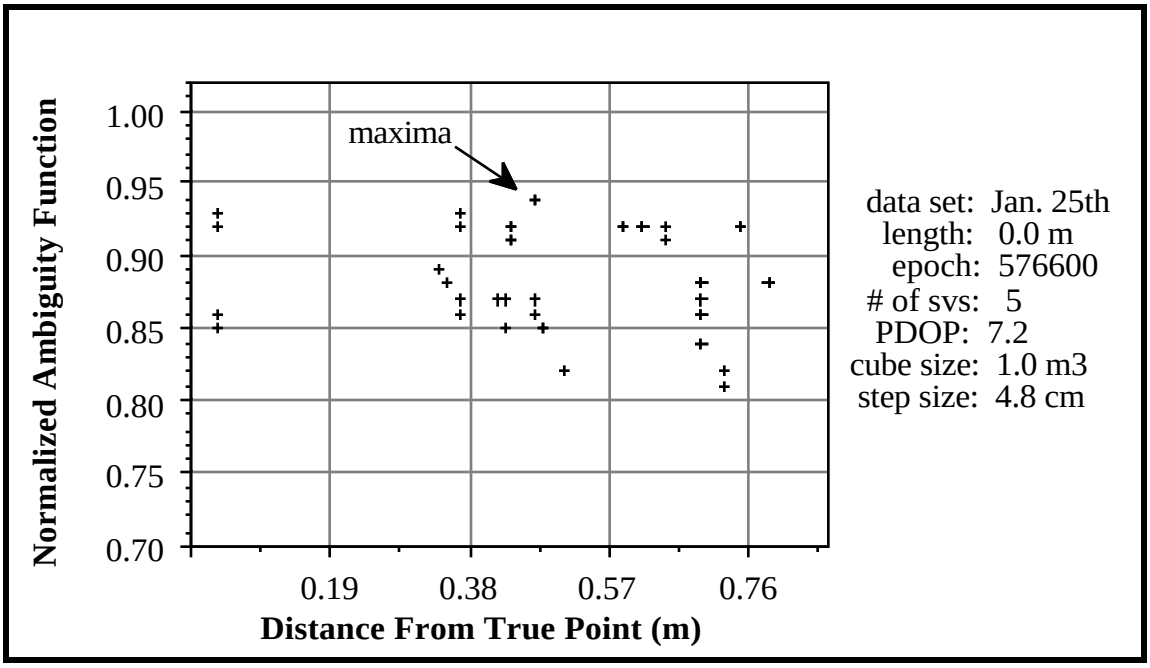

Figure 5.25
1 Epoch AF for 5 Satellite Data Using a 4.8 cm Grid Over a 1.0 m Cube

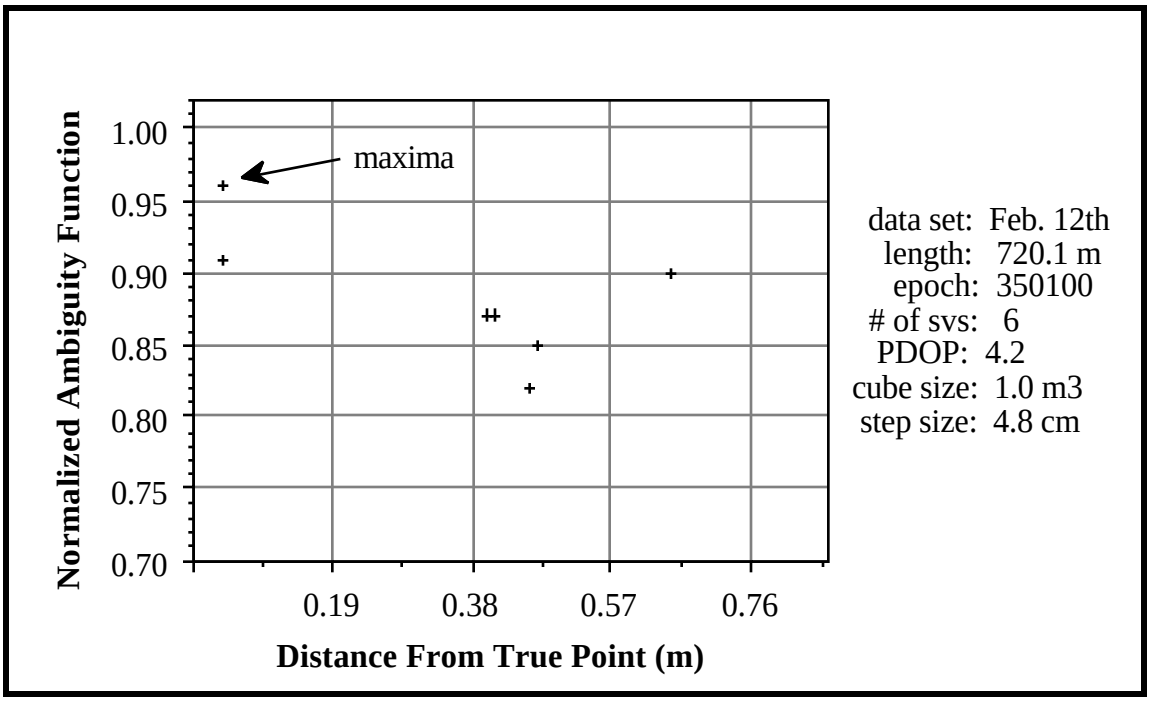

Figure 5.26
1 Epoch AF for 6 Satellite Data Using a 4.8 cm Grid Over a 1.0 m Cube

As can be seen in the figures, larger step-sizes result in sparser AF points with smaller magnitudes in general. The results in Figure 5.25 agree with those in Figure 5.16, i.e. the five satellite data is insufficient to isolate a maxima over a cube with 1.0 m edges.

The results in Figure 5.26 for the six satellites appear inconsistent with those of Figure 5.18 because the correct maxima is well separated in magnitude from an incorrect maxima using the 4.8 cm step size (a 0.06 separation), but not using the 1.9 cm step size (a 0.02 separation). The results in Figure 5.26 are a product of chance, not rigour. If the 4.8 cm test points had been aligned to coincide exactly with the maxima for a false point and not a true point, these results may have been reversed. Note that following the algorithm to check solution integrity shown in Figure 5.15, the 0.08 peak separation threshold would have correctly identified the data of Figure 5.26 as being too weak to isolate a solution.

Ambiguity function values were also plotted with step-sizes of 4.8 cm over cubes with 0.5 m edges for the Jan. 25th and Feb. 12th data, but are not shown here. Results were completely consistent with those of Figure 5.23 and 5.24, but with sparser AF values of lower magnitudes. For the six satellite case, only a single point, with a magnitude of 0.94 and located 4 cm from the true point, was detected.

5.4.2 AF Patterns - Using Double Difference Plane Intersections

The double difference plane intersection search technique was carried out for the same epoch of data as used for the Feb. 12th results of Figures 5.18, 5.24 and 5.26. Search cubes of both 1.0 m and 0.5 m were tested. The details for each run are given in Table 5.5. In this table, the second column gives the total number of test points generated from sets of trial ambiguities. (Ambiguities were rounded to the nearest integer from the

cube corners.) The third gives the number of points remaining after the rejection of those which did not fall within the search cube. (Figure 5.9 illustrates how points found through double difference intersection may fall outside search cube limits.) The fourth column gives the distance between the true point and the closest test point to the double difference solution. For the given data set and epoch, the computed test point was poor (4 cm away from truth), which can be attributed to the bad PDOP of 74.9 for the four satellites used in the double difference plane intersection. (It is known that satellites with the best RDOP or PDOP should be used, but the program used was not modified to accommodate this.) Upon testing all points using the ambiguity function algorithm of Figure 5.4, no points passed the rejection criteria, hence no ambiguity function values were found (as indicated in the fifth column) and no solutions were found.

Table 5.5
Double Difference Plane Intersections For Varied Cube Sizes - Results

(1) **Cube Size**	(2) **Total # of Test Points**	(3) **# of Test Points in Cube**	(4) ***Distance to Closest Test Point**	(5) **# of AF Values**	(6) **Soln**
1.0 m	495	20	4 cm	0	none
0.5 m	75	3	4 cm	0	none

data set: Feb. 12th
length: 720.1 m
epoch: 350100
# of svs: 6
PDOP: 4.2

***** based on 4 satellite double difference solution with PDOP of 74.9

When no AFM solution was found for either case, the double difference plane intersection search technique with mini-grid cubes around each point (as illustrated in Figure 5.11) was successfully employed. Around each double difference plane intersection within the cube, 26 other test points were generated. Results are shown in Table 5.6. The mini-grid cubes brought test points within 2 cm of the true point. A number of AF values were determined for both the 1.0 m and 0.5 m cube cases. For the

1 m cube size, the solution was unresolved because there were two peaks of comparable magnitude over 10 cm apart. For the 0.5 m case, one peak was uniquely determined. These results are in keeping with those found using the uniform grid technique.

Table 5.6
Mini-Grid Cubes - Results

Cube Size	# of Test Points in Cube	*Distance to Closest Test Point	# of AF Values	Soln
1.0 m	540	2 cm	16	unresolved
0.5 m	81	2 cm	5	good

data set: Feb. 12th
length: 720.1 m
epoch: 350100
# of svs: 6
PDOP: 4.2

*using mini-grid cube of ±2.7 cm around double diff. test point

The ambiguity function values for the 1 m cube, double difference plane intersection with mini-grids is plotted in Figure 5.27 against the distance from the truth. Note the similar but sparser pattern of this figure as compared to Figure 5.18 where results with a uniform grid with 1.9 cm spacing are shown. From Figure 5.23, the AF magnitude at the true point (at 0.0 cm) of 0.99 is too close in magnitude to the secondary peak (at about 0.47 cm) of 0.96 to resolve the ambiguities.

As can be seen from these results, the double difference plane intersection technique produces essentially the same results as the grid technique, albeit more efficiently since it checks points spaced by ambiguities, not by an arbitrary grid.

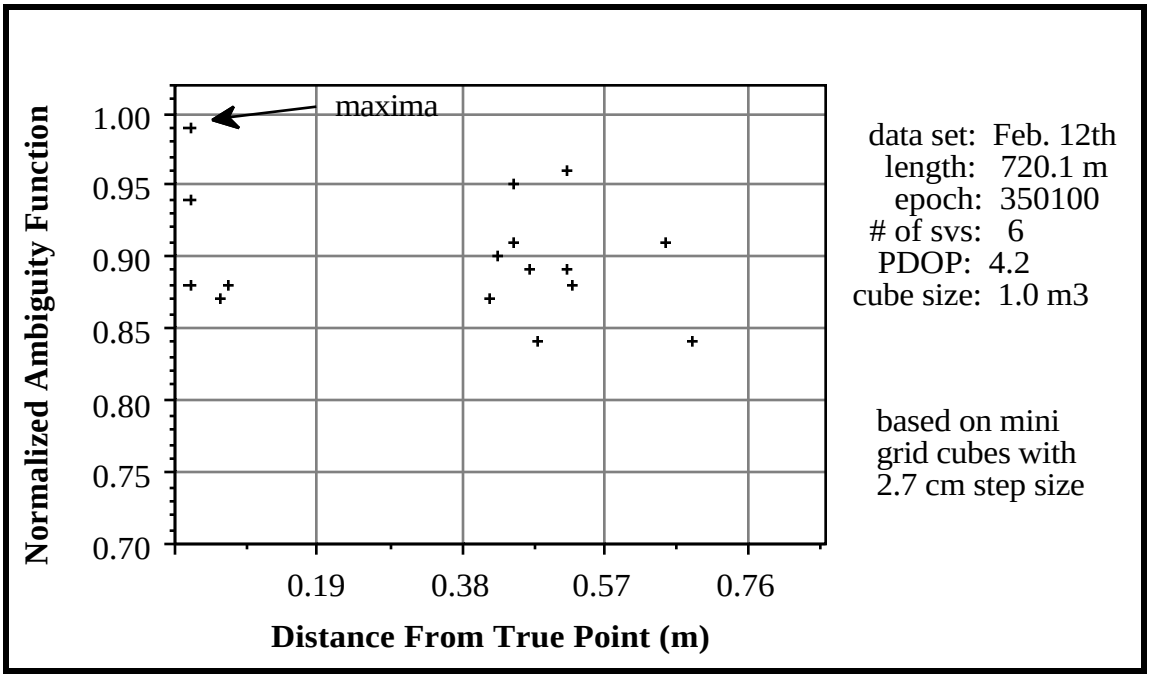

Figure 5.27
1 Epoch AF for 6 Satellite Data Using Mini-Grid Cubes Around Points of Double Difference Plane Intersection

5.4.3 AFM Baseline Results

The results presented so far have been limited to small samples from two data sets. When evaluating processing algorithms, one needs to look at the consistency with which comparable results may be achieved. For this reason, a series of results are given for two data sets of the same 720 m baseline (Feb. 12th and Feb. 15th) and one data set of a 4.1 km baseline (Feb. 17th). Detailed descriptions of these data sets are given in Chapter 3.

All results shown are based on the ambiguity function method applied over two minute data samples using two epochs of data; the first and the last. The use of two minute data samples was chosen to investigate two minute solutions rather than

five minute solutions, and a 120 s data interval was chosen to moderately reduce the number of points under consideration while minimizing the chance of rejecting good points. All solutions are based on six satellite data and a search cube with 0.5 m edges. Results for coarse-fine grid tests (using a $\lambda/4$ coarse step size), double difference plane intersections, and double difference plane intersections with mini-grid cubes are given for the three data sets in Tables 5.7 to 5.9.

In each table the second column gives the time of the first epoch of the two minute sample in GPS seconds of week. For double difference plane intersections results, the PDOP of the four satellites used is given in the third column. Note, the software used was not modified to choose the best DOP, hence the poor DOP used for some solutions. The column headed "# of AF Values" gives the number of test points which survived the 0.7 rejection criteria of the AF algorithm (Figure 5.4). The AF and distance from truth for the test point with the largest AF are given in the next two columns followed by the same information for the test point with the second largest AF. If a secondary peak was evident, the second largest AF column was filled with the values for the highest point of the secondary peak instead. For the coarse-fine grid results, the largest and second largest AF values and distances correspond to coarse grid results. The final column indicates if the solution found was "good" (solution could be clearly and correctly isolated), "unresolved" (solution could not be isolated), "false" (the incorrect solution was isolated), or not found ("none"). The integrity check algorithm of Figure 5.15 was used to arrive at the solution classifications.

Table 5.7
Feb. 12th AFM Results (720 m Baseline, 6 Satellites, 0.5 m Cube)

(a) Coarse-Fine Grid

	Time (sec)	# of AF Values	Largest AF	Largest Dist.	2nd Largest AF	2nd Largest Dist.	Solution
1	349999	1	.91	.05 m	---	---	none
2	350119	2	.94	.04	.91	.05 m	good
3	350239	0	---	---	---	---	none
4	350359	1	.95	.02	---	---	good
5	350479	1	.96	.02	---		good
6	350599	2	.95	.02	.92	.28	unresolved

(b) Double Difference Plane Intersection

	Time (sec)	4 sv PDOP	# of AF Values	Largest AF	Largest Dist.	2nd Largest AF	2nd Largest Dist.	Solution
1	349999	70	1	.99	.01 m	---	---	good
2	350119	85	1	1.00	.01	---	---	good
3	350239	103	1	.98	.01	---	---	good
4	350359	127	0	---	---	---	---	none
5	350479	157	1	.95	.03	---	---	good
6	350599	196	1	.99	.00	---	---	good

(c) Double Difference Plane Intersection With Mini-Grid Cubes

	Time (sec)	4 sv PDOP	# of AF Values	Largest AF	Largest Dist.	2nd Largest AF	2nd Largest Dist.	Solution
1	349999	70	6	.99	.01 m	.96	.04 m	good
2	350119	85	6	1.00	.01	.95	.04	good
3	350239	103	4	.98	.01	.95	.04	good
4	350359	127	3	.95	.02	.92	.29	unresolved
5	350479	157	4	.97	.01	.95	.03	good
6	350599	196	9	.99	.00	.93	.28	unresolved

Upon perusal of results, it is evident that the integrity check algorithm of Figure 5.15 was effective, as no false solutions were accepted. Most solutions are good, with some unresolved and some not found.

Table 5.8
Feb. 15th AFM Results (720 m Baseline, 6 Satellites, 0.5 m Cube)

(a) Coarse-Fine Grid

	Time (sec)	# of AF Values	Largest AF	Largest Dist.	2nd Largest AF	2nd Largest Dist.	Solution
1	3835	1	.90	.31 m	---	---	none
2	3955	0	---	---	---	---	none
3	4075	0	---	---	---	---	none
4	4195	0	---	---	---	---	none
5	4315	2	.90	.26	.83	.19	none

(b) Double Difference Plane Intersection

	Time (sec)	4 sv PDOP	# of AF Values	Largest AF	Largest Dist.	2nd Largest AF	2nd Largest Dist.	Solution
1	3835	10.4	1	.99	.01 m	---	---	good
2	3955	9.8	1	.97	.01	---	---	good
3	4075	9.3	1	.98	.01	---	---	good
4	4195	8.9	1	.99	.01	---	---	good
5	4315	8.5	1	1.00	.01	---	---	good

(c) Double Difference Plane Intersection With Mini-Grid Cubes

	Time (sec)	4 sv PDOP	# of AF Values	Largest AF	Largest Dist.	2nd Largest AF	2nd Largest Dist.	Solution
1	3835	10.4	6	.99	.01 m	.94	.03 m	good
2	3955	9.8	5	.97	.01	.97	.01	good
3	4075	9.3	5	.98	.01	.95	.02	good
4	4195	8.9	7	.99	.00	.90	.32	unresolved
5	4315	8.5	8	1.00	.01	.94	.28	unresolved

Results using the three different search techniques were consistent for the most part, with the exception of Table 5.8a and 5.8b, where no solutions were found using the coarse-fine grid, but good solutions were found using the double difference plane intersection.

Table 5.9
Feb. 17th AFM Results (4.1 km Baseline, 6 Satellites, 0.5 m Cube)

(a) Coarse-Fine Grid

	Time (sec)	# of AF Values	Largest AF	Largest Dist.	2nd Largest AF	2nd Largest Dist.	Solution
1	175466	2	.92	.02 m	.90	.09 m	none
2	175586	2	.94	.02	.90	.09 m	good
3	175706	2	.94	.02	.88	.09	good
4	175826	1	.94	.02	---	---	good
5	175946	1	.97	.02	---	---	good
6	176066	1	0.96	.02	---	---	good

(b) Double Difference Plane Intersection

	Time (sec)	4 sv PDOP	# of AF Values	Largest AF	Largest Dist.	2nd Largest AF	2nd Largest Dist.	Solution
1	175466	35	0	---	---	---	---	none
2	175586	41	1	.99	.04 m	---	---	good
3	175706	48	2	.96	.04	.93	.37 m	unresolved
4	175826	57	1	.95	.04	---	---	good
5	175946	68	1	.96	.03	---	---	good
6	176066	82	0	---	---	---	---	none

(c) Double Difference Plane Intersection With Mini-Grid Cubes

	Time (sec)	4 sv PDOP	# of AF Values	Largest AF	Largest Dist.	2nd Largest AF	2nd Largest Dist.	Solution
1	175466	35	4	.98	.05 m	.95	.03 m	good
2	175586	41	6	.99	.04	.95	.04	good
3	175706	48	7	.98	.05	.93	.37	good
4	175826	57	3	.97	.04	.96	.02	good
5	175946	68	5	.96	.03	.93	.04	good
6	176066	82	2	.96	.04	.91	.29	unresolved

From Table 5.8a, one can see that no AF maxima were detected around the true point. To see if the cause of no solutions being found was due to the cos(obs - calc) threshold at 0.7 being too stiff, the data was reprocessed with a threshold of 0.5. With the lower threshold, two peaks were detected for all solutions, one at the true point and one at a false point. The magnitudes of the AFs were comparable, meaning the solution integrity checks resulted in unresolved solutions in all cases. Consequently, using the lower cos(obs-calc) threshold was of no assistance in finding a "good" solution.

Based on these findings, it is believed that the coarse-fine grid, with a coarse grid of $\lambda/4$ is not suited for situations where peaks are in close proximity, as they are using 6 satellite single frequency data. It is believed that Remondi's success of this technique for his pseudo-kinematic work was due to a larger physical separation of peaks, made possible by a larger mix of significantly different observations. The relative success of the coarse-fine technique for the Feb. 12th data and Feb. 17th data may be attributed to higher satellite elevations and grid corners closer to true points (as a product of chance).

Looking at double difference plane intersection results, one can see that for Feb. 12th, four of the six solutions had test points within 1 cm of the truth, and all of Feb. 15th double difference plane intersections were within 1 cm of the truth. The better results for Feb. 15th correlate with the greatly improved four satellite PDOP value, and give incentive for future double difference plane intersection software to incorporate a feature to check DOPs. The Feb. 17th data showed poorer results, with solutions within 4 cm of the truth. A few factors could be contributing here; poor PDOPs, the longer baseline length and chance.

It should be noted that there were only three points of double difference plane intersection within each search cube. If the cube had been reduced to having 0.4 m edges instead of 0.5 m edges, only one point would have been detected in most cases (explaining the 6 satellite - 0.4 cm cube edge plotted in Figure 5.14).

In all cases where the double difference test point solution was within 1 cm of the truth, good unique solutions were found. When points in a mini-grid cube around the point of double difference intersection were tested (Tables 5.7c, 5.8c and 5.9c), in almost all cases results were consistent with those of simple double difference plane intersection, but instead of one AF value being found, several belonging to the same correct peak were found. On occasion, solutions otherwise rendered good, were rendered unresolved using

mini-grid cubes. In all the results presented, only on one occasion did the mini-grid cubes resolve a solution that could not otherwise be resolved, and that was for the sixth result tabulated in Figures 5.9b and c.

Results such as the fourth result in Table 5.7b and c may seem somewhat baffling when all neighbouring points have been well resolved. It is this type of a situation, where a solution stands out as an abnormality, that a technique such as that described in Figure 5.16 becomes important for intercomparisons. To assess whether solution 4 in Table 5.7c was truly unreliable or just an outlier, solutions starting each second for the 15 seconds before and 15 seconds after the two epochs were computed. Of the 30 solutions 26 (87%) of the solutions could be isolated. From this (following Figure 5.16) it can be concluded that solution 4 was just an outlier. The test point coordinates for any of the other 26 successful solutions at surrounding epochs may be used to compute ambiguity terms.

As can be seen from the results shown, the AFM is an effective technique for ambiguity resolution, but needs to be used with care to ensure reliable solutions are attained. Some basic findings include:

(1) Individual integrity checks, as shown in Figure 5.15, and solution intercomparisons as shown in Figure 5.16, are very important for ensuring reliable AFM solutions.

(2) The coarse grid searches are not well suited for data where peaks are relatively close together.

(3) The four satellites with the best geometry should be used for the double difference plane intersection.

(4) Mini-grid cube searches using double difference intersections can be used in cases where the double difference plane intersection does not yield good results, but such occasions are apt to be rare.

CHAPTER 6

CARRIER PHASE AMBIGUITY RESOLUTION USING LEAST SQUARES TECHNIQUES

Least squares ambiguity resolution techniques have been used with conventional static GPS surveys for a number of years. When used in a rudimentary sense, ambiguities estimated in a least squares float carrier phase solution are rounded to their nearest integer as done in Section 4.3.1. In more sophisticated routines, sets of integer ambiguities around the initial ambiguity estimates may be tested by carrying out several fixed carrier phase solutions. The computed variance factors from each solution are then compared. If one estimated variance factor can be found to be smaller than and statistically independent of all others, the ambiguities are said to be resolved. This procedure is often referred to as an "integer search". The drawback with such integer search routines is their high computational requirements.

The techniques proposed by Frei and Beutler (1990) and Hatch (1991a), namely the fast ambiguity resolution approach (FARA) and the least squares ambiguity search technique (LSAST), are similar to conventional integer search routines, but have modifications which greatly enhance their efficiency by reducing the number of sets of integer ambiguities which need to be searched. The underlying theory for each of these

techniques is reviewed, followed by results. The relation between AFM and LSAST is discussed. A comparison of AFM, LSAST and FARA is then presented.

6.1 FAST AMBIGUITY RESOLUTION APPROACH

The fast ambiguity resolution approach (FARA) requires only carrier phase data. This differs from AFM and LSAST which, as presented herein, use double difference code observations to find an initial solution. The FARA algorithm is presented followed by results.

6.1.1 FARA Algorithm

A summary of the steps used in FARA as described by Frei and Beutler (1990) are given in Table 6.1. Detailed explanations for each step follows.

The first step involves the computation of a double difference carrier float solution following the observation equation (2.9). The appropriate parameter vector and design matrix are given in Table 2.3(c) and the least squares solution is computed following equation (2.14). The adjusted residuals, $\hat{v}$, are computed as

$$\hat{v} = A\hat{\delta} + w, \tag{6.1}$$

where A is the design matrix, $\hat{\delta}$ is the vector of corrections to the parameter vector and w is the misclosure vector. Since the a priori variance factor is unknown, the covariance matrix of the observations, C_l, is derived using a unit a priori variance factor, and the a posteriori variance factor, $\hat{\sigma}_o^2$, is estimated as

$$\hat{\sigma}_o^2 = \frac{\hat{v}^T C_l^{-1} \hat{v}}{n-u} \quad , \tag{6.2}$$

where n is the number of observations and u is the number of unknown parameters. The covariance matrix of the adjusted parameters can then be scaled by the a posteriori variance factor to give

$$\hat{C}_{\hat{x}} = \hat{\sigma}_o^2 C_{\hat{x}} \, . \tag{6.3}$$

Table 6.1
Summary of Steps in the Fast Ambiguity Resolution Approach

(1) Compute Float Carrier Phase Solution

- estimate real values for each double difference ambiguity
- compute residuals and a posteriori variance factor
- scale covariance matrix of the parameters with a posteriori variance factor

(2) Choose Ambiguity Sets to be Tested

- choose individual integer ambiguities which fall within the confidence range of the real estimates to form sets of potential integer solutions
- reject ambiguity sets which have ambiguity pairs with differences which exceed the confidence range of the differences of the real ambiguity estimates

(3) Compute Fixed Solution for Each Ambiguity Set

- compute fixed solutions, variance factors and parameter covariance matrices

(4) Statistically Test the Fixed Solution with the Smallest Variance

- test if fixed and float solutions are compatible
- test variance factor for normal distribution (χ^2 test on the variance factor)
- compare smallest variance factor with second smallest

The covariance matrix of the parameters, $\hat{C}_{\hat{x}}$, along with the estimated parameters, $\hat{x}$, provide the information needed to choose sets of integer ambiguities to be tested.

In the second step this information is used following the criteria in Table 6.1 to choose which ambiguity sets should be tested through fixed least squares solutions. The fewer the ambiguity sets which need be tested through a least squares solution, the greater the overall computational efficiency of FARA. For the first criteria, the integer ambiguity ranges are determined based on confidence intervals around the real ambiguity solutions using the appropriate diagonal components of $\hat{C}_{\hat{x}}$. Letting N_j represent an adjusted real value ambiguity from the float solution and NA_j represent a potential integer value for the same ambiguity, then

$$P_j \{N_j - \xi_{t,df,1-\alpha/2} \bullet \sigma_{N_j} \leq NA_j \leq N_j + \xi_{t,df,1-\alpha/2} \bullet \sigma_{Nj} \} = 1 - \alpha. \qquad (6.4)$$

Here $P\{\ \}$ represents the probability for a certain confidence level $1-\alpha$ and $\xi_{t,df,1-\alpha/2}$ represents the student t distribution for df degrees of freedom and a significance level of α. The standard deviation of the float solution ambiguity, $\sigma_{Nj,}$ is the square root of the appropriate diagonal component of the covariance matrix, $\hat{C}_{\hat{x}}$. Integer ambiguities which fulfill the probability statement (6.4) are used to generate potential sets of ambiguities as illustrated in Tables 5.2 and 5.3.

The second criteria given for choosing ambiguity sets to be tested makes FARA unique as compared to other rapid ambiguity resolution techniques. In each set of potential ambiguity solutions, pairs of ambiguities are considered. The difference between two real ambiguities and the difference between two corresponding potential integer ambiguities are formed as follows:

$$N_{ij} = N_i - N_j \qquad (6.5)$$

$$NA_{ij} = NA_i - NA_j \tag{6.6}$$

The standard deviation of the real ambiguity differences N_{ij} is

$$\sigma_{N_{ij}} = \sqrt{\sigma_{N_i}^2 - 2\sigma_{N_i N_j} + \sigma_{N_j}^2} \tag{6.7}$$

where $\sigma_{N_i}^2$, $\sigma_{N_j}^2$ and $\sigma_{N_i N_j}$ are extracted from $\hat{C}_{\hat{x}}$.

The probability statement relating the real ambiguity differences with potential ambiguity differences is then written as

$$P_j \{N_{ij} - \xi_{t,df,1-\alpha/2} \bullet \sigma_{N_{ij}} \leq NA_{ij} \leq N_{ij} + \xi_{t,df,1-/2} \bullet \sigma_{N_{ij}} \} = 1 - \alpha. \tag{6.8}$$

Ambiguity sets with pairs of ambiguities which do not fulfill equation (6.8) are rejected from consideration. Note that since the same potential ambiguity pairs may occur in several ambiguity sets, a well designed routine will minimize the amount of searching using equation (6.8) as detailed in Frei and Beutler (1990).

The third step in FARA requires computing batch least squares solutions with fixed ambiguities for all potential ambiguity sets which survived the probability statements of equations (6.4) and (6.8). The required formulation is described in Section 2.3. The adjusted parameters and a posteriori variance factors from the fixed solutions are used in the fourth and final step of FARA.

The fourth step tests the fixed solution for the ambiguity set which yields the smallest variance factor. The fixed position vector $\hat{x}\,A$ is compared to the float position vector $\hat{x}$ to check for compatibility. Although not explicitly given in Frei and Beutler (1990), this may be formulated for each coordinate i as

$$P_i \{ \hat{x}_i - \xi_{t,df,1-\alpha/2} \bullet \sigma_{\hat{x}_i} \leq \hat{x}\,A_i \leq \hat{x}_i + \xi_{t,df,1-\alpha/2} \bullet \sigma_{\hat{x}_i} \} = 1 - \alpha, \tag{6.9}$$

assuming the standard deviation of $\hat{x}_{A_i}$ is much smaller than $\hat{x}_i$. The a posteriori variance factor is checked for compatibility with the a priori variance factor by performing a χ^2 test of the variance factor (Vanicek and Krakiwsky, 1982). This is formulated as

$$\frac{\xi\chi^2_{df;\alpha/2}}{df} \leq \frac{\hat{\sigma}_o^2}{\sigma_o^2} \leq \frac{\xi\chi^2_{df;1-\alpha/2}}{df}, \qquad (6.10)$$

where $\xi\chi^2_{df;\alpha/2}$ and $\xi\chi^2_{df;1-\alpha/2}$ denote the chi-squared distribution with df degrees of freedom. The fixed solutions with the smallest and second smallest variance factors are then computed to ensure their independence. This comparison is given as

$$\frac{\hat{\sigma}_o^2}{\hat{\sigma}_o^{2'}} \geq \xi F_{df1;df2;\alpha}, \qquad (6.11)$$

where $\hat{\sigma}_o^{2'}$ is the smallest variance factor, $\hat{\sigma}_o^2$ is the second smallest variance factor, and $\xi F_{df1;df2;1-\alpha/2}$ is the F (Fisher) distribution for df1 degrees of freedom (for the solution with the smallest variance factor) and df2 degrees of freedom (for the solution with the second smallest variance factor) and with a significance level α. If the fixed solution with the smallest variance factor fails any of the tests of equation (6.9) to (6.11) the data used is deemed to be insufficient to correctly resolve ambiguities.

FARA, like all the rapid ambiguity resolution algorithms discussed in this thesis, is much more effective using dual frequency P code data. Additional steps which incorporate dual frequency P code data through wide-laning and have similar statistical foundations to those steps listed above are also given in Frei and Beutler (1990).

6.1.2 FARA Results

The fundamental steps of the fast ambiguity resolution approach as described by Frei and Beutler (1990) were implemented in a C-language program and tested with the Feb. 12th, 15th and 17th data sets (see Chapter 3 for data set details). Investigations of FARA discussed here differ from those of AFM and LSAST, since the initial coordinate estimation steps could not be separated from the ambiguity resolution procedure. Therefore, instead of showing results starting the ambiguity searching around a "true" point, searching is based around a float solution estimate.

One cannot expect good results using FARA over periods as short as two minutes since a float solution over such a short period would be too weak to provide good coordinate and ambiguity estimates. This is better visualized by referring to Figure 4.1, which shows the change in the relative geometrical dilution of precision (RGDOP) as a function of time. Accordingly, FARA investigations made here are based on 5 minutes of data.

Tests were conducted using two 5 minute data periods on Feb. 12th, 15th and 17th at a 60 s data rate. These tests proved to be generally successful. Similar tests using the same 5 minute data periods at a 15 s data rate were unsuccessful. Results for one of the successful FARA 5 minute solutions are reviewed in detail, followed by an explanation for the lack of success ata a 15 s rate, and a summary of results for Feb. 12th, 15th and 17th.

Results pertaining to the application of FARA using 5 minutes of data at a 60 s data rate (6 epochs) on Feb. 12 from 349999 to 350299 seconds of GPS week are presented in Tables 6.2 to 6.4 and Figures 6.1 and 6.2. In Table 6.2 the ambiguity estimates attained from a float solution and their respective standard deviations are shown. True ambiguities are also shown for comparison purposes. It can be seen that two of the

five ambiguities would be rounded to the incorrect ambiguity if a nearest integer algorithm was used. Equation (6.4), based on the Student t distribution, was applied to define ambiguity ranges. The maximum and minimum values used were rounded to the nearest integer. Solutions using significance levels of 0.1, 0.01 and 0.001, which correspond to Student t statistics of 1.72, 2.82 and 3.79 respectively (for the 22 degrees of freedom applicable here) were attempted. As shown in Table 6.4, the smaller significance levels resulted in larger confidence intervals and a dramatic increase in the number of ambiguity sets to be considered as potential solutions (from 72 for $\alpha = 0.1$ to 1200 for $\alpha = 0.001$).

The ambiguity differences, formulated following equations (6.5) and (6.6) and the respective standard deviations formulated using equation (6.7) are shown in Table 6.3. The number of ambiguity sets under consideration were greatly reduced by applying equation (6.8) to this data. From Table 6.4 it can be seen that a significance level of 0.1 resulted in all ambiguity sets being rejected, whereas a significance level of 0.01 and 0.001 resulted in 9 and 24 ambiguity sets being accepted respectively. This demonstrates the sensitivity of FARA to the chosen significance level α.

Fixed solutions were computed for the 9 and 24 ambiguity sets referred to in Table 6.4. The standard deviations (square root of the variance factor) for each of these solutions is plotted against the distance from the true solution in Figures 6.1 and 6.2 for significance levels of 0.01 and 0.001 respectively.

Table 6.2
Ambiguity Estimates and Standard Deviations
(Feb. 12th, 720 m, 6 satellites, 5 min., 60 s data rate)

Satellite Pairs	Real Ambiguity Estimate , N_j (cycles)	True Ambiguity (cycles)	Standard Deviation, σ_{N_j} (cycles)
2-19	-17,329,426.7	-17,329,426.0	0.6
6-19	-14,178,677.6	-14,178,677.0	0.4
11-19	-11,027,757.7	-11,027,758.0	0.4
16-19	1,575,518.2	1,575,519.0	0.4
18-19	15,754,175.6	15,754,176.0	0.2

Table 6.3
Ambiguity Differences and Their Standard Deviations
(Feb. 12th, 720 m, 6 satellites, 5 min., 60 s data rate)

Satellite Pairs Used in Differencing	Real Ambiguity Difference Estimates, N_i-N_j (cycles)	True Ambiguity Difference (cycles)	Standard Deviation of Difference, $\sigma_{N_{ij}}$ (cycles)
2-19, 6-19	-3,150,749.2	-3,150,749.0	0.2
2-19, 11-19	-6,301,668.1	-6,301,668.0	0.7
2-19, 16-19	-18,904,945.1	-18,904,945.0	0.2
2-19, 18-19	-33,083,601.7	-33,083,601.0	0.4
6-19, 11-19	-3,150,918.9	-3,150,919.0	0.6
6-19, 16-19	-15,754,195.9	-15,754,196.0	0.1
6-19, 18-19	-29,932,852.5	-29,932,852.0	0.3
11-19, 16-19	-12,603,277.0	-12603277.0	0.7
11-19, 18-19	-26,781,933.6	-26,781,933.0	0.4
16-19, 18-19	-14,178,656.6	-14,178,656.0	0.4

Table 6.4
Number of Ambiguity Sets Remaining After Testing Confidence Intervals
(Feb. 12th, 720 m, 6 satellites, 5 min., 60 s data rate)

Criteria For Selecting Ambiguity Sets	**Statistical Parameters**		
	$\alpha = 0.1$ df = 22 t = 1.72	$\alpha = 0.01$ df = 22 t = 2.82	$\alpha = 0.001$ df = 22 t = 3.79
Nj, σ_{N_j} and confidence interval	72	384	1200
$N_i - N_j$, $\sigma_{N_{ij}}$ and confidence interval	0	9	24

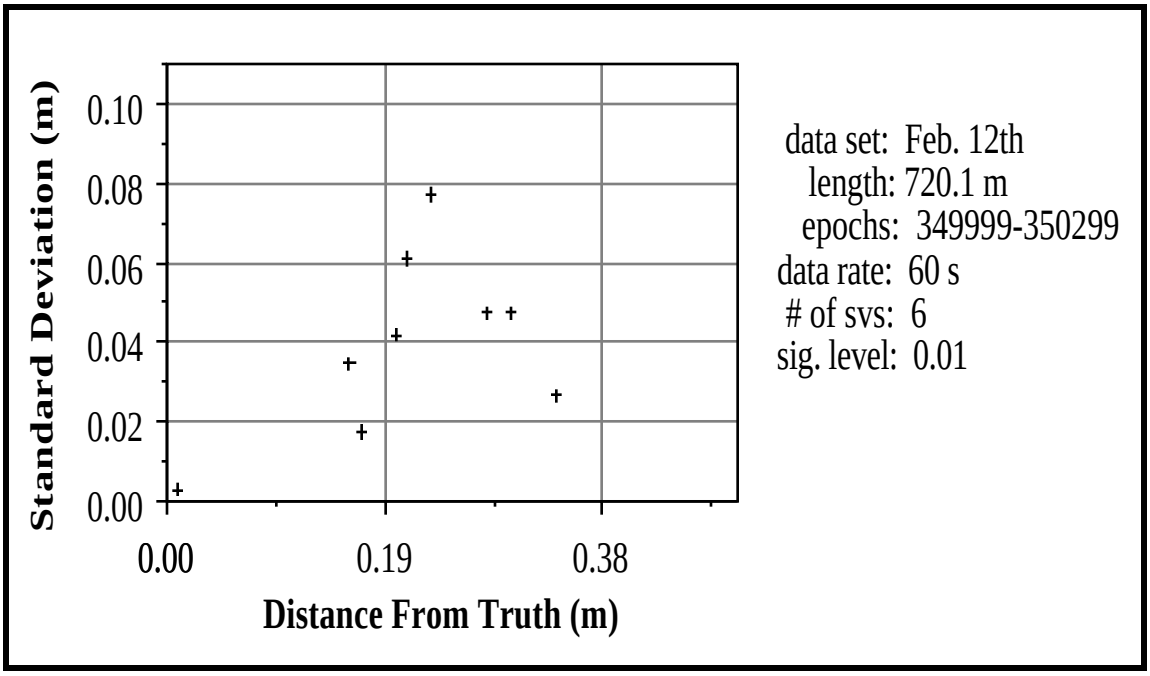

Figure 6.1
FARA Standard Deviations Versus Distance From Truth For α = 0.01

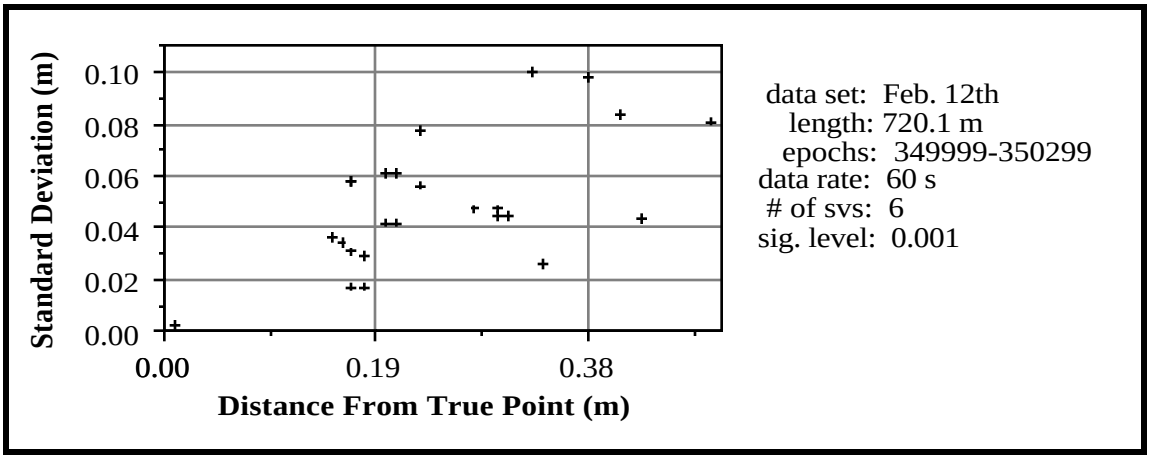

Figure 6.2
FARA Standard Deviations Versus Distance From Truth For α = 0.001

In both Figures 6.1 and 6.2 the smallest variance factor is clearly distinguishable at 1 cm from the truth with a double difference standard deviation of 3 mm, and the second smallest is some 17 cm from the truth with a standard deviation of 17 mm. The Fisher test of equation (6.11) agreed with the hypothesis of the solutions with the smallest and second smallest variance factors being independent, supporting the point nearest the true point as corresponding to the correct set of integer ambiguities. It can be seen from the figures that there was no loss of information or increase in difficulty in distinguishing the correct solution by using a significance level of 0.001 instead of 0.01. In this statistical application, the additional computational burden of using a smaller significance level is negligible compared to the risk of rejecting a good observation, hence the use of a 0.001 significance level is reasonable. This is the value used in examples given by Frei and Beutler (1990).

As previously mentioned, using the same data at a 15 s rate instead of a 60 s rate proved to be unsuccessful. When applying the second confidence interval criteria of equation (6.8) all potential ambiguity sets were rejected from consideration. The explanation for this lies with suspected correlations, likely due to multipath and internal

measuring effects, between the data, which eradicates the underlying statistical assumptions. Due to the statistical testing which underlies FARA, normally distributed uncorrelated observations are vital. Recalling the multipath correlations shown for code observations in Chapter 4 and knowing that similar cyclic multipath behavior characterizes carrier phase observations (Georigiadou and Kleusberg, 1988), one would expect the assumptions of normally distributed uncorrelated observations to be a potential source of problems. It is interesting that Frei and Beutler (1990) use a data interval of 60 s in their data processing examples as opposed to a smaller data interval (e.g. 15 s). The longer data rate avoids overly optimistic covariance information which could result from short term correlations. Long term cyclical fluctuations due to multipath could still pose a problem.

FARA results from Feb. 12th, 15th and 17th are presented in Tables 6.5 to 6.7. Two 5 minute solutions, at a 60 s data interval, were computed for each day. There were 22 degrees of freedom for each solution. The times given in the second column of each table are the times of the first epoch of observation used. For each solution period, two sets of results were computed, one based on $\alpha = 0.01$ ($t = 2.82$) and the second based on $\alpha = 0.001$ ($t = 3.79$). In previous discussions it was stated that it is wise to use $\alpha = 0.001$. However, memory limitations of the program and computer configuration used to test FARA would not support the large number of points to be considered in some cases when $t = 3.79$, but solutions were still possible when $t = 2.82$. (Program optimization could overcome this problem but was not pursued in this research.) Consequently, to produce results for all data sets and allow for comparisons, solutions for both $t = 2.82$ and $t = 3.79$ are presented.

In each table, the number of ambiguity sets remaining after the rejection criteria based on confidence intervals for ambiguities (σ_{N_j} as per equation (6.4)) and ambiguity

differences ($\sigma_{N_{ij}}$ as per equation (6.8)) are given. If the described computer memory limitations were exceeded in testing, "mem." is entered in the table and no further entries are made. The variance factor (scaled by 1,000,000) and the distance from the truth for the corresponding fixed carrier phase solution for the smallest and second smallest variance factors are tabulated. The ratio of the variance factors, as per the Fisher test (equation (6.11)) is also given.

Table 6.5
Feb. 12th FARA Results
(720 m baseline, 6 satellites, 5 min., 60 s rate)

	Time		**#Sets After**		**Smallest**		**2nd Smallest**		
	(sec)	**t**	σ_{N_j}	$\sigma_{N_{ij}}$	**vf***	**Dist.**	**vf***	**Dist.**	**Ratio**
1a	349999	2.82	384	9	6.7	0.01m	302.5	0.17m	45.1
1b	349999	3.79	1200	24	6.7	0.01	302.5	0.17	45.1
2a	350299	2.82	960	40	9.5	0.00	183.6	0.38	19.3
2b	350299	3.79	2520	mem.	…	…	…	…	…

Table 6.6
Feb. 15th FARA Results
(720 m baseline, 6 satellites, 5 min., 60 s rate)

	Time		**#Sets After**		**Smallest**		**2nd Smallest**		
	(sec)	**t**	σ_{N_j}	$\sigma_{N_{ij}}$	**vf***	**Dist.**	**vf***	**Dist.**	**Ratio**
1a	3835	2.82	480	9	199.6	0.48 m	707.9	0.60m	3.5
1b	3835	3.79	800	40	10.6	0.00	199.6	0.48	18.8
2a	4135	2.82	900	19	122.4	0.38	316.6	0.79	2,6
2b	4135	3.79	2700	mem	....	.....	.....	...	...
2b	4135	3.20	900	37	8.6	0.00	122.4	0.38	14.2

Table 6.7
Feb. 17th FARA Results
(4.1 km baseline, 6 satellites, 5 min., 60 s rate)

	Time (sec)	t	#Sets After σ_{Nj}	#Sets After σ_{Nij}	Smallest vf*	Smallest Dist.	2nd Smallest vf*	2nd Smallest Dist.	Ratio
1a	175466	2.82	216	0	---	---	---	---	---
1b	175466	3.79	480	27	12.3	0.04m	188.1	0.51m	15.2
2a	175766	2.82	600	29	24.4	0.04	299.9	0.40	12.2
2b	175766	3.79	3600	mem	…	…	…	…	…

* variance factor, scaled by 1,000,000, in m^2

First examining Table 6.5, for a 720 m baseline, one can see the general success of FARA, with the only shortcoming being memory limitations of the program used (for solution 2b) rather than the algorithm itself. Table 6.7 shows similar success for a 4.1 km baseline. For solution 1 of the 4.1 km baseline, all potential solutions were rejected from consideration using t = 2.82, but the correct solution was found using t = 3.79.

The solutions for Feb. 15th were not as clean as those for Feb. 12th and 17th. For both observation periods on Feb. 15th, when t = 2.82, the correct ambiguity sets were rejected from consideration and points 0.48 cm and 0.38 cm from the true point, for solutions 1a and 2a respectively, had the smallest variance factors. When t = 3.79 the solution for the first observation period was successfully determined and the solution for the second observation period was not possible due to program memory limitations. To ensure a correct solution would be found if the program used had not been limited by memory constraints, a solution with t = 3.2 (solution 2c) was attempted and found to be successful.

Note that for the two cases where the correct solution was not found (i.e., for Feb. 15th, solutions 1a and 2a) the variance factor ratios of 3.5 and 2.6 were very small. In comparison the successful solutions had ratios ranging from 12.2 to 45.1. For the 27 degrees of freedom applicable for the solutions here and $\alpha = 0.01$, the critical value for the Fisher distribution is 2.6. Using this value, all the solutions would pass the Fisher test, including the two false solutions on Feb. 15th when t = 2.82. This suggests the Fisher test as applied here is too lenient.

In summary, FARA has been found to be generally successful at a 60 s data rate using five minutes of six satellite single frequency data over 720 m and 4.1 km baselines. The use of confidence intervals around ambiguity differences effectively eliminates numerous potential ambiguity sets which would have otherwise been considered. The limitation with FARA is its sensitivity to elements which defeat the statistical normality of the data. To be applied routinely, a greater understanding of, and means to cope with, correlations between epochs of GPS observations are required.

6.2 LEAST SQUARES AMBIGUITY SEARCH TECHNIQUE

The least squares ambiguity search technique (LSAST) as described by Hatch (1991a) and Hatch (1991b) was initially designed for kinematic positioning and based on differential corrections to support efficient real-time processing. It is modified here to apply to double differencing. The algorithm for LSAST is presented, followed by results.

6.2.1 LSAST Algorithm

The LSAST can be broken down into three steps; initial coordinates of an unknown point are estimated, sets of ambiguities around the initial point are defined and the least squares ambiguity search algorithm is applied. Initial coordinates of an unknown point may be estimated using a double difference code solution as discussed in Chapter 4 and a volume around this point may be defined by using code solution accuracy estimates. Sets of ambiguities for the primary observations are generated by finding the range of ambiguities which fall within the volume, as described in Section 5.2.2. Here "primary" observations are those double difference observations necessary to solve for a unique position, and "secondary" observations are the remaining redundant double difference observations. The next step forms the basis of the LSAST and so is explained in some detail.

The LSAST algorithm is based on a sequential adjustment, first using the primary observations for an initial solution and then using the secondary observations to update the solution. Equations used by Hatch (1991a) follow the phase expression formulation as given in Krakiwsky (1990) and Adams (1987). These equations are shown below for the parametric case applicable here. The matrices and vectors are as defined in Section 2.3 but have been annotated with the subscript "p" for primary observations, "s" for secondary observations and "c" for the complete set of observations (i.e. primary plus secondary). The correction vector for the solution using the primary observations, $\hat{\delta}_p$, is given as

$$\hat{\delta}_p = \left(A_p^T C_{l_p}^{-1} A_p \right)^{-1} A_p^T C_{l_p}^{-1} w_p. \qquad (6.12)$$

The solution is then updated using the secondary observations, giving the updated correction vector

$$\hat{\delta}_c = \hat{\delta}_p - N_c^{-1} A_s^T C_{l_s}(w_s + A_s\hat{\delta}_p) \ , \qquad (6.13)$$

where

$$N_c = \left(N_p + A_s^T C_{l_s}^{-1} A_s\right) . \qquad (6.14)$$

The LSAST algorithm which applies these equations, with the goal of efficiently resolving integer ambiguities, is shown for a single epoch in Figure 6.3. Explanations of each step are given, followed by a description of how several epochs would be incorporated into this algorithm. It is assumed that one begins with a number of potential ambiguity sets for the primary double difference observations.

At a single epoch, the only variable of equation (6.12) which changes with each ambiguity set is the misclosure vector, w_p, and the only variable portion of equation (6.13) which changes is the innovations vector, y_s, where

$$y_s = (w_s + A_s\hat{\delta}_p) . \qquad (6.15)$$

This is more readily apparent by expanding the general form of the misclosure vector. Rearranging the observation equation (2.9) and neglecting error terms, the misclosure vector is

$$w = \Delta\rho - (\Delta\Phi + \lambda \Delta N). \qquad \text{(in metres)} \qquad (6.16)$$

At a given epoch, the calculated and observed double differences ($\Delta\rho$ and $\Delta\Phi$) will remain unchanged while the double difference ambiguities (ΔN) change with each ambiguity set being tested. For efficiency, the coefficients of w_p and y_s, in the initial update equations ((6.12) and (6.13) respectively) may be precomputed as shown in the first box of Figure 6.3.

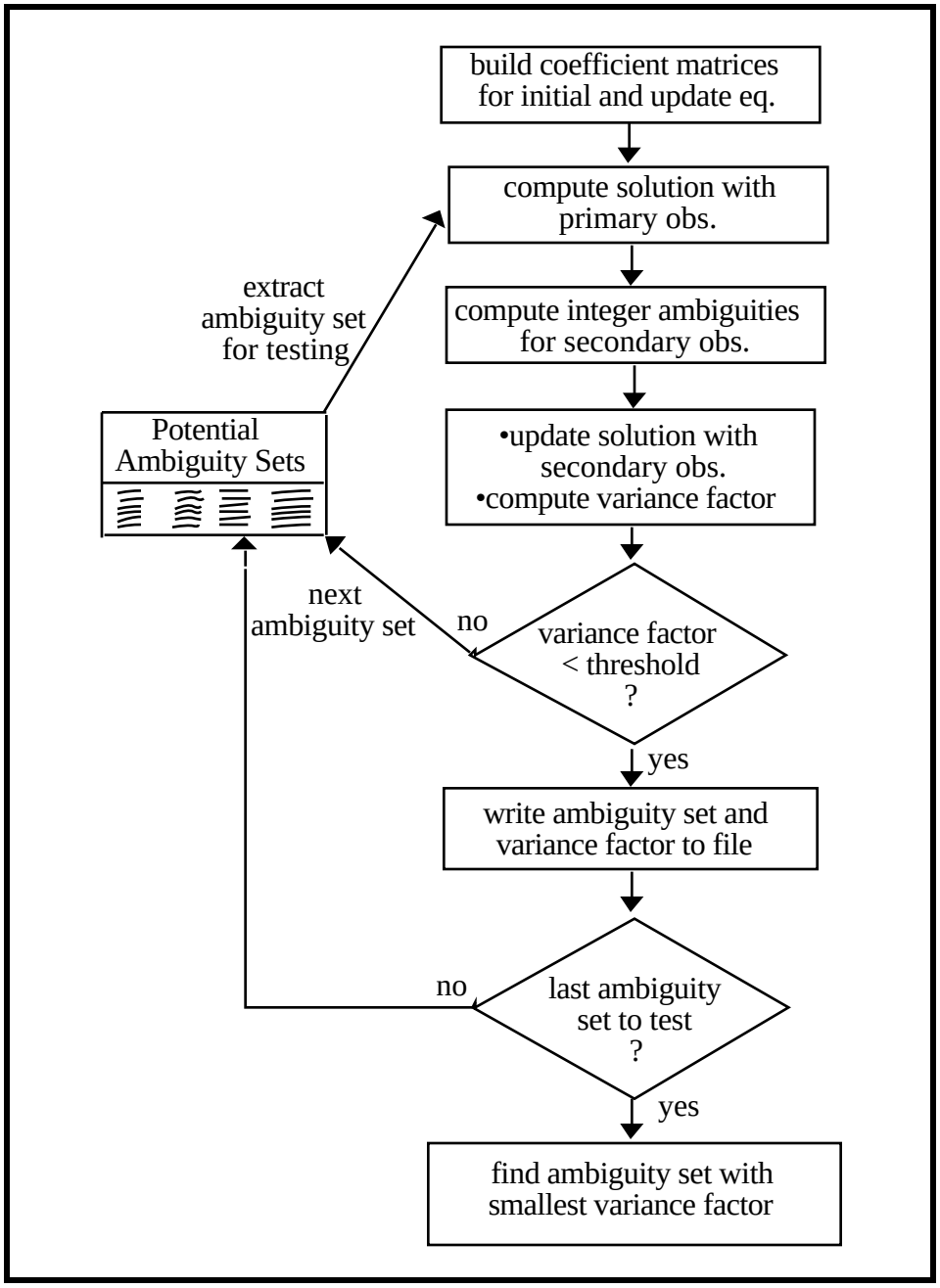

Figure 6.3
Major Elements of LSAST for a Single Epoch

Next, the first ambiguity set to be tested is used to compute a corresponding potential solution using the primary observations following equation (6.12). The ambiguities for each secondary observation are then calculated as

$$\Delta N_S = \text{nint}(\Delta\Phi - \Delta\rho/\lambda) \quad \text{(in cycles)} \tag{6.17}$$

where nint(•) is the nearest integer operator, $\Delta\Phi$ the observed double difference and $\Delta\rho$ the calculated double differences based on the position determined by the unique primary observations solution.

It is important to understand why equation (6.17) is used to derive the integer ambiguities for the secondary satellites. As previously mentioned, the means of choosing the best set of ambiguities is by choosing the one which yields the solution with the smallest variance factor, which also implies the solution with the smallest residuals. When the primary solution is updated by the secondary observations (equation (6.13)), the resulting residuals are the smallest when the innovations vector is the smallest. Choosing ambiguities for secondary satellites using equation (6.17), i.e. choosing the ambiguities which come closest to the primary solution, will result in the smallest innovations vector and hence the smallest residuals. This step eliminates needlessly searching other extraneous potential secondary satellite ambiguities.

Using the computed ambiguities for the secondary satellites, the updated position vector may be computed following equation (6.13). The corresponding residuals, $\hat{v}_c$, for the updated solution, $\hat{\delta}_c$, are computed as

$$\hat{v}_c = w_c + A_c \hat{\delta}_c. \tag{6.18}$$

The variance factor for this single epoch can finally be calculated using the same formulation as used in FARA (equation (6.11)), i.e.:

$$\hat{\sigma}_o^2 = \frac{\hat{v}^T C_l^{-1} \hat{v}}{n-u}. \tag{6.19}$$

Here the number of observations, n, will correspond to the number of double difference observations and the number of unknowns, u, will be three, for the unknown x, y and z coordinates.

As shown in Figure 6.3, the computed variance factor is compared to some prespecified threshold. If it exceeds the threshold, the ambiguity set is rejected from consideration and the next ambiguity set is extracted for testing. If it is within the threshold it is saved. The process is repeated until all potential ambiguity sets have been tested.

Figure 6.3 summarizes the steps for a single epoch. Several epochs are combined by Hatch (1991b) by independently applying the least squares algorithm (as shown in Figure 6.3) at successive epochs and meaning the resulting variance factors. The number of potential ambiguity sets at each successive epoch is reduced through rejections from variance factor threshold testing. Ideally, only one unique ambiguity set will remain after variance factor testing. The success of meaning observations over several epochs is dependent on the data being free of cycle slips.

In the implementation of LSAST described by Hatch (1991b), the square root of the variance factor was first tested against a threshold of 0.009999 L1 wavelengths (about 2 mm). Through testing he found this value to be too pessimistic and so he raised the threshold. It is this testing, to accept or discard potential solutions, which Hatch claims to be one of the best features of the algorithm since only viable solutions are saved and considered at successive epochs.

Some enhancements of LSAST may be implemented. First, the position estimated with the primary satellites can be checked to see if it falls within the prescribed search cube. If it does not, the ambiguity set being considered can be rejected. Second, a Fisher

test to compare resulting variance factors, as used with FARA (equation (6.11)) can be carried out with the smallest and second smallest variance factors. Note that using this test at a single epoch means only two degrees of freedom exist for observations from six satellites (five double differences). Accordingly, the ratio between the smallest and second smallest variance factors would be 19 at a significance level of 0.05, 39 at a significance level of 0.25 and 99 at a significance level of 0.01. If means of variance factors between epochs are taken (as proposed by Hatch) these would still be the appropriate test statistics.

In the following section LSAST results are presented, based on a C-program implementing the algorithm shown in Figure 6.3. In the program, variance factors over consecutive epochs are averaged and points outside the prespecified search cube are rejected.

6.2.2 LSAST Results

The LSAST was applied to the same epochs of observations as the AFM solutions (Tables 5.7 to 5.9) for Feb. 12th, 15th and 17th (see Chapter 3 for data descriptions). The search cube used had 0.5 m edges and was centered around the "true" point. Results are given in Tables 6.8 to 6.10. In each table, the first column gives the solution number, the second column indicates the first epoch of the 2 minutes over which LSAST is applied, the third column shows the PDOP for the four primary satellites and the fourth column gives the number of points of intersection of the primary satellites within the search cube.

Comparing the PDOPs and the number of points in the cube between Tables 6.8, 6.9 and 6.10, the relationship explained by Hatch (1991b) and graphically illustrated in Figure 5.10, is well demonstrated. The comparatively good PDOPS of Feb. 15th resulted

in five to nine points in the cube, whereas the poorer PDOPS of Feb. 12th and 17th had two to four points in the cube. Note, slight variations in the number of points in the cube for solution sets with similar PDOPS are likely a result of noise or errors in the data (particularly multipath) which causes alterations in a given solution depending on the epoch of data used.

In each of the Tables 6.8 to 6.10, variance factors for the ambiguity sets with the smallest and second smallest AF are shown along with their distances from the true point. The variance factors are in units of metres squared, scaled by 1,000,000. They are the product of two variance factors (with 2 degrees of freedom) meaned over two epochs. Since LSAST is based on testing ambiguity sets rather than point coordinates, the precise magnitude of the distance from the truth is not critical, but the relative distance between the ambiguity sets which yield the smallest and second smallest variance factors are significant.

The ninth columns of Tables 6.8 to 6.10 give the ratio between the second smallest and smallest variance factor, which is used in the F test of equation (6.1). For a 95 per cent confidence level (significance level of 0.5), and two degrees of freedom, following equation (6.1), the ratio between the second smallest and smallest LSAST results should be greater than 19. The final column in the tables shows "√" if the ratio is above 19, indicating ambiguities could be resolved, and an "×" if the ratio falls below 19, indicating the ambiguities could not be resolved with statistical certainty.

Table 6.8
Feb. 12th LSAST Results (720 m Baseline, 6 Satellites, 0.5 m Cube)

	Time (sec)	4 sv PDOP	# Points in Cube	Smallest vf*	Smallest Dist.	2nd Smallest vf*	2nd Smallest Dist.	Ratio	> 19?
1	349999	70	3	6	.01 m	590	0.34 m	98	√
2	350119	85	3	12	.01	420	0.30	35	√
3	350239	103	3	80	.01	374	0.33	5	×
4	350359	127	2	80	.01	310	0.29	4	×
5	350479	157	4	12	.01	170	0.28	14	×
6	350599	196	3	6	.01	138	0.27	23	√

* variance factor, scaled by 1,000,000, in m^2

Table 6.9
Feb. 15th LSAST Results (720 m Baseline, 6 Satellites, 0.5 m Cube)

	Time (sec)	4 sv PDOP	# Points in Cube	Smallest vf*	Smallest Dist.	2nd Smallest vf*	2nd Smallest Dist.	Ratio	> 19?
1	3835	10.4	5	36	.01 m	1392	0.24 m	39	√
2	3955	9.8	6	36	.01	899	0.21	25	√
3	4075	9.3	7	22	.01	870	0.21	40	√
4	4195	8.9	9	13	.01	235	0.26	18	×
5	4315	8.5	7	4	.01	208	0.27	52	√

* variance factor, scaled by 1,000,000, in m^2

Table 6.10
Feb. 17th LSAST Results (4.1 km Baseline, 6 Satellites, 0.5 m Cube)

	Time (sec)	4 sv PDOP	# Points in Cube	Smallest vf*	Smallest Dist.	2nd Smallest vf*	2nd Smallest Dist.	Ratio	> 19?
1	175466	35	3	32	0.04 m	2280	0.19 m	71	√
2	175586	41	4	18	0.02	2531	0.12	141	√
3	175706	48	4	39	0.03	2873	0.12	74	√
4	175826	57	4	44	0.03	2734	0.18	62	√
5	175946	68	4	77	0.03	2571	0.18	33	√
6	176066	82	4	199	0.03	849	0.31	4.3	×

* variance factor, scaled by 1,000,000, in m^2

In all the results shown, the ambiguity set with the smallest variance factor is the correct ambiguity set. Nevertheless, using the Fisher statistical test for solution independence, the ratio between the smallest and second smallest variance factor are sometimes too small to trust the solution. Note that in these tests, no variance factor threshold rejection level, as proposed by Hatch (1991a) and shown in Figure 6.3, was used. If one had been used, the acceptance and rejection of solutions shown in the last column of Tables 6.8 to 6.10 would likely be different. In some cases only the ambiguity set with the smallest variance factor would remain, and in other cases no solutions would remain (Abidin, 1991). The decision of what threshold level to use would be dependent on thorough empirical testing. In his presentation of the application of LSAST, Hatch (1991b) reported that he was still exploring ways to determine the acceptability of a solution.

Preliminary findings show no loss of ambiguity resolution abilities when moving from a 720 m baseline to a 4.1 km baseline (these investigations are too limited to make any conclusive statements). Looking at the ratios from the tables, it can be seen that the results from the 4.1 km baseline appear if anything, better than the results of the 720 m baselines.

Results shown in Tables 6.8 to 6.10 can be directly compared with AF results using the double difference plane intersection techniques from Tables 5.7 to 5.9 since they were derived from identical observations. In all cases using LSAST, the ambiguity sets with the smallest variance factors were the correct ambiguity sets. In all cases using AFM, the test points with the largest AF were the correct test points. The differences between the LSAST and AFM results are the judgments as to the goodness of the solutions. From previous discussions concerning each of these ambiguity resolution

techniques, the decisions as to whether the solutions are trustworthy still leaves much room for investigations and improvements.

In general, comparing Tables 6.8 to 6.10 with Tables 5.7 to 5.9, the results seem reasonably compatible. The relation between the two sets of results will become more apparent in the discussion of the relations between AFM and LSAST in the following section.

6.3 COMPARISON OF AMBIGUITY RESOLUTION TECHNIQUES

Three ambiguity resolution techniques that can be used with single frequency data, AFM, FARA and LSAST, have been described, and results using each technique have been presented. As previously mentioned, FARA, LSAST and conventional static integer search techniques all rely on minimizing the variance factor, which is in essence the minimization of the quadratic form of the residuals. From the discussion in Chapter 5, it is known that the AFM maximizes the summation of the cosines of the observed minus calculated double differences. It is shown in Lachapelle et al. (1992) that the fundamental effect of the least squares and AFM techniques are the same. Furthermore, LSAST can be derived from AFM. The relationship between LSAST and AFM is shown in the first section, and the fundamental methodology and characteristics of AFM, FARA and LSAST are reviewed in the second section.

6.3.1 The Relationship Between AFM and LSAST

The equivalence of LSAST and AFM (using double difference plane intersection searches) is shown for a single epoch case. The implementations of AFM and LSAST

are discussed, and a better rapid static algorithm for applying these techniques assuming cycle slip free data is presented.

The development of the relation between LSAST and AFM starts by expanding the AF expression as a Taylor's series (Lachapelle et al., 1992). Rewriting equation (5.5) to consider only the cosine terms gives

$$AF(x,y,z) \quad = \quad \sum_{k=1}^{nepoch} \quad \sum_{j=1}^{nsat-1} \cos\theta, \tag{6.20}$$

$$\text{where} \quad \theta = \Delta \Phi^{kj}_{obs} - \Delta \rho^{kj}_{calc}(x,y,z)\,. \qquad \text{(in radians)} \tag{6.21}$$

The cosine term can be expanded as a Taylor series to give

$$\cos\theta = 1 - \frac{\theta^2}{2!} + \frac{\theta^4}{4!} - \frac{\theta^6}{6!} + \ldots \tag{6.22}$$

Replacing the cosine term in equation (6.20) with the series expansion of equation (6.22), but neglecting higher order elements gives

$$AF(x,y,z) \approx (nepoch \bullet (nsat-1)) - \frac{1}{2} \sum_{k=1}^{nepoch} \sum_{j=1}^{nsat-1} \theta^2\,. \tag{6.23}$$

It can be seen that AF(x,y,z) is maximized when θ^2 is minimized. Assuming

$$\theta^2 \left(\frac{\lambda}{2\pi}\right)^2 = \hat{v}^2, \qquad \text{(in metres)} \tag{6.24}$$

then the sum squares of the residuals (as formulated in the least squares ambiguity search technique) may be derived from the AF as

$$\sum_{k=1}^{nepoch} \quad \sum_{j=1}^{nsat-1} \hat{v}^2 \approx 2\{\, nepoch \bullet (nsat-1) \; - \; AF(x,y,z) \,\} \frac{\lambda^2}{2\pi}\,. \tag{6.25}$$

Now consider the assumption of equation (6.24). The formulation for the adjusted residuals, $\hat{v}$, is given in equation (6.12). In a convergent least squares solution $\hat{\delta}$ approaches zero, and so $\hat{v}$ approaches w. Accordingly, from equation (6.16),

$$\hat{v} \approx w = \Delta\rho - (\Delta\Phi + \lambda \Delta N) \quad \text{(in metres)} \qquad (6.26)$$

at convergence. Note the difference between equations (6.21) and (6.26), namely equation (6.26), used in least squares techniques, includes the double difference ambiguity term ΔN whereas equation (6.21) does not. This is the essence of the difference between the least squares and the AF techniques. In the equivalence expression of (6.24) and resulting derivation of (6.25), only fractional values of $\hat{v}$ are considered and the ambiguity term is neglected. Furthermore, neglecting higher order terms means equation (6.23) is only valid for small angles (i.e. points close to integer cycles) as illustrated in Figure 6.4. Taking these points into consideration, it can still be shown that LSAST and AFM are essentially equivalent when the double difference plane intersection technique is used with AFM (see Section 5.2.2).

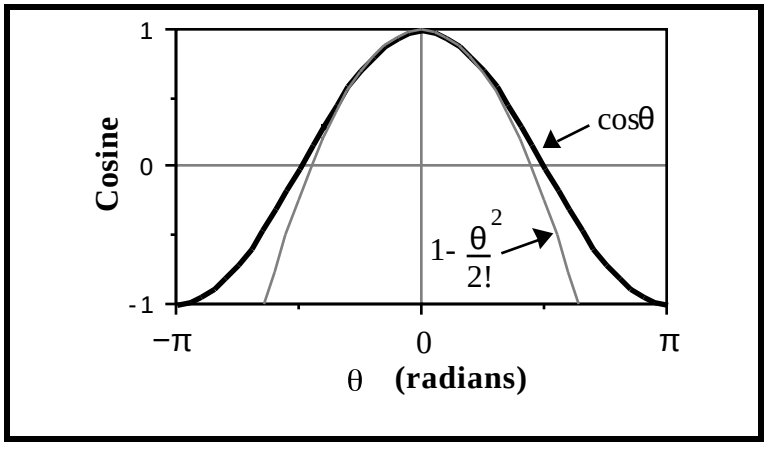

Figure 6.4
Effect of Truncation in Cosine Series Expansion

With AFM, the point of intersection between three double difference planes computed using a trial set of ambiguities at a single epoch will yield $\cos\theta$ terms of 1 since by definition $\theta = \Delta\Phi - \Delta\rho = 0$ for a unique solution. Similarly, following LSAST, by definition the residuals for the primary observations will be zero. For the redundant observations, the AF will measure how well the fractional ambiguities meet the point determined by the primary observations, and all but points with small angles θ will be rejected using the $\cos\theta < 0.7$ rejection criteria. For the redundant (secondary) observations, the LSAST will also measure how well the fractional ambiguities meet the point determined by the primary satellites (the limitation to fractional ambiguities to be considered is a result of equation (6.17)). Hence for AFM using the double difference plane intersection technique, equations (6.24) and (6.25) are valid. They are not valid if AFM using grid searches or mini-grid cube searches are used since the LSAST ambiguity sets will not intersect at the same points as the test grid points.

A minor difference between AFM when using double difference plane intersection searches and LSAST as applied here, is that the latter allows for consideration of the double difference correlations through the use of a weight matrix C_1^{-1} in the formulation of the a posteriori variance factor (equation (6.19)). Hatch (1991a) does not consider these correlations because he deals with uncorrelated single difference observables rather than correlated double difference observables.

There are differences between AFM and LSAST as a result of their described implementations with regards to threshold testing and their basis on test points or test ambiguity sets. Mader (1990) recommends a threshold test of 0.7 for $\cos\theta$ for each independent observation in AFM. Hatch (1991a) advocates testing the variance factor at each epoch against some prespecified threshold in LSAST. The implementations of these thresholds have different effects. For instance, if one observation with a very small

residual was combined with an observation with a large residual, Hatch's algorithm may accept the ambiguity set, whereas if one observation with a cosθ of 0.69 was combined with an observation with a cosθ of 0.99, Mader's algorithm would reject the test point from consideration. An example of this is evident by comparing solution 1 of Table 5.9b, which shows an AFM result, with solution 1 of Table 6.10 which shows a LSAST result for the identical 2 epochs. Using AFM, no test points passed the $\cos\theta < 0.7$ test for all observations. Using LSAST this point would not be rejected if a scaled variance factor threshold of 40 was set (assuming the variance factor at each epoch to be < 40).

Even using the double difference plane intersection technique with AFM can yield different results from LSAST over consecutive epochs due to AFM's basis on test points and LSAST's basis on ambiguity sets. For AFM using the double difference plane intersection technique, Remondi (1991) computes a unique solution with primary observables at a single epoch. At that epoch, test point coordinates are estimated. These coordinates are then used for all subsequent AF computations as it is the x, y and z coordinates being tested. For LSAST, Hatch (1991a) tests sets of ambiguities at successive epochs. At each epoch a sequential fixed solution is used with these ambiguities, first using the primary observables and then using the secondary observables. Consequently, from epoch to epoch, the ambiguity sets being tested remain the same but the position determinations and respective residuals change. The testing of x, y and z coordinates with AFM consequently allows for cycle slips, but the testing of ambiguity sets does not.

The developments for AFM and LSAST have followed procedures used in publications, which are more directed towards kinematic surveys. Modifications to the above algorithms described would make them more suitable for rapid static surveys.

However this does not negate any of the investigations made herein since the underlying concepts of AFM and LSAST are the same in static or kinematic mode.

In static mode, if software was implemented with efficient and effective cycle slip detection algorithms for short observation spans, an improved version of AFM or LSAST could be implemented. In this case, rather than computing a unique solution with the primary observables at one epoch, solutions could be computed using all epochs with the primary observables. This would result in a better position estimate by providing some averaging of short term multipath effects. With AFM, this better solution estimate could then be used with the AF algorithm. However, in the cycle slip free scenario, AFM does not prove to be advantageous over LSAST, so consequently a LSAST algorithm could be applied instead. A sequential LSAST algorithm using primary observables at all epochs, followed by updating by using secondary satellites at all epochs could be implemented.

Up to this point, the relationship between AFM and LSAST has been reviewed and the least squares basis for FARA and LSAST has been shown. A comparison of the three techniques is given in the next section.

6.3.2 Methodology and Characteristics of AFM, FARA and LSAST

The main elements of the ambiguity resolution techniques reviewed in Chapters 5 and 6 are summarized in Table 6.11. Variations of the implementations of each of these techniques is possible, which may result in modifications of the table entries. The differences in the main elements of the ambiguity resolution techniques presented in Table 6.11 result in differences in their characteristics as presented in Table 6.12.

In Section 5.3.1, observation conditions under which AFM should be applied to optimize the chances of success are discussed. These observation conditions apply equally to FARA and LSAST for the same reasons given in Section 5.3.1, hence the first entries in Table 6.12.

Table 6.11
Summary of Ambiguity Resolution Methodologies*

Elements	AFM	FARA	LSAST
initial solution	• code solution	• carrier float solution	• code solution
search domain	• test points	• ambiguity sets	• ambiguity sets
search space	• $k \cdot \sigma_x$, $k \cdot \sigma_y$, $k \cdot \sigma_z$, from code solution	• $k \cdot \sigma_{Nj}$ from carrier float solution	• $k \cdot \sigma_x$, $k \cdot \sigma_y$, $k \cdot \sigma_z$, from code solution
means to reduce potential solutions	• coarse-fine grid • double diff. plane intersection of primary satellites	• Ni - Nj and $k \cdot \sigma_{Nij}$ from carrier float solution	• double diff. plane intersection of primary satellites
thresholds	• cos(obs-calc) < 0.7	• none	• $\hat{\sigma}_o^2$ < threshold
selection criteria	• maximum AF	• minimum $\hat{\sigma}_o^2$	• minimum $\hat{\sigma}_o^2$
acceptance criteria	• only remaining solution • > threshold • size relative to second largest AF which belongs to secondary peak	• compatible with float solution • Fisher test on ratio of smallest and second smallest variance factor	• only remaining solution • Fisher test on ratio of smallest and second smallest variance factor

* k represents a constant

Under the observation periods required for the three techniques, AFM and LSAST are shown to have potential for instantaneous solutions (assuming enough observations are available) whereas for FARA a preference for observation periods of up to five minutes has been indicated. This is due to the weakness of the carrier phase float solutions over the short time periods used in FARA.

Of the three techniques used, AFM is the only method which can tolerate data with cycle slips since it is based on testing points rather than ambiguity sets. Note that AFM cannot tolerate half cycle slips. This should not be a major concern since most receivers are designed to avoid half cycle slips.

For both LSAST and AFM using the double difference plane intersection search technique, primary observables are used to define potential ambiguity sets and potential test points respectively. In Section 5.3.2 the AFM dangers of the best test point being too far from the true point are discussed. It is shown that a point too far from the true point may not be considered as a potential solution, and a false peak may instead be erroneously accepted. It is this problem which gave impetus to the mini-grid cube search technique. It is also recommended that the double difference observations from the four satellites which give the best PDOP be used with AFM. The same arguments for good PDOP apply to LSAST but are not quite as vital as for AFM, since a good point is less apt to be rejected from consideration with LSAST if thresholds are set judiciously.

The last four rows in Table 6.12 characterize the effect of code and carrier multipath on each solution type. The multipath effects have been further categorized by multipath magnitude and periodicity. Such categorization is warranted since multipath with large magnitudes (for instance C/A code multipath of 10 m instead of 20 cm) will have different implications than multipath with large periods but small magnitudes (for instance 60 minute periods instead of 5 s periods).

The effect of carrier multipath on LSAST and AFM are essentially the same. Both have the effect of causing the potential rejection of a good solution if an observation is too corrupted by carrier multipath to have an ambiguity which approaches an integer. For both FARA and LSAST residuals and the resulting variance factors will be larger, the larger the multipath magnitude. Similarly, for AFM, the AF values will be smaller. The longer the periodicity of carrier multipath as compared to the data interval used, the more correlated the observations. As a result covariance matrices for the results will be too optimistic. The variance factor for FARA will also be too optimistic, due to larger degrees of freedom than warranted, considering the correlated nature of the observations. The same would be true of LSAST if observations over several epochs were combined in an adjustment.

Code observations are used in the same manner for LSAST and FARA, so consequently multipath will have the same effects on the code observations. If the magnitude of code multipath is high, the initial search cube will be large, meaning a greater computational burden, and more potential for accepting false solutions. Periodicities in code multipath which exceed the data interval used will result in overly optimistic covariance information. If this overly optimistic covariance information is used to define a search cube, the resulting cube may be too small, resulting in failure of ambiguity resolution.

The natural question which follows investigations and comparisons of ambiguity resolution techniques is, which is the "best"? However, it is more important to understand the behavior of the measurements and techniques than to know which method is the "best", because if a "best" ambiguity resolution technique is used inappropriately, erroneous results are likely.

Table 6.12
Characteristics of Ambiguity Resolution Techniques

	AFM	FARA	LSAST
observation conditions	• satellites > 15^o • baselines < 10 km • the mores satellites the better	• satellites > 15^o • baselines < 10 km • the more satellites the better	• satellites > 15^o • baselines < 10 km • the more satellites the better
observation period (L1 only)	• potential for instantaneous solution	• five minutes preferred	• potential for instantaneous solution
tolerant of cycle slips ?	• yes	• no	• no
small primary obs. PDOP important?	• yes or may omit solution (for double diff. plane intersection)	• not applicable	• yes, but less important than for AFM
effect of carrier multipath (magnitude)	• potential rejection of good solution • smaller AF	• larger residuals and variance factor	• potential rejection of good solution • larger residuals and variance factor
effect of carrier multipath (periodicity)	• not major problem since AFM not subject to statistical testing	• σ_{Nj} and σ_{Nij} too optimistic, true solution potentially omitted • overly optimistic variance factors	• overly optimistic variance factors if adjustment over several epochs
effect of code multipath (magnitude)	• poor initial coordinate estimate, large search cube	• none	• poor initial coordinate estimate, large search cube
effect of code multipath (periodicity)	• σ_x, σ_y, σ_z too optimistic and solution potentially not in search cube	• none	• σ_x, σ_y, σ_z too optimistic and solution potentially not in search cube

Nevertheless, generalizations of the suitability for the above techniques in different situations are possible. (Note these generalizations are all based on the premise of using only L1 carrier phase data with high accuracy C/A code measurements.)

If data which has not been prescreened for cycle slips is used, AFM is the best. Although independent cycle slip detection and correction algorithms are possible, they may be ineffective over very short observation periods (e.g. one minute). If data is cycle slip free, AFM has no advantages over LSAST.

One shortcoming with FARA is its inability to take advantage of high accuracy code measurements. In Section 4.3.2, carrier float solutions over a 5 minute period were shown to have the same level of accuracy as precise C/A code solutions over the same period. For shorter time periods a rapid deterioration in carrier float solutions can be expected. Consequently, for observation periods less than five minutes in length LSAST is more suitable than FARA. Another shortcoming with FARA is its sensitivity to the statistical parameters upon which it is based. Nevertheless, applying FARA over five minutes at a 60 s data interval consistently proved to be successful.

In applications of AFM and LSAST in a search cube around the true point with 0.5 m edges, the true points were found using just two epochs of observations over two minutes, although in many cases there was not enough certainty in the solution to support the answer as being correct. Furthermore, the code solution accuracies found in Chapter 4 were not good enough to support a 0.5 m cube, although use of overly optimistic covariance accuracy estimates might lead one to believe otherwise. With more satellites, one would expect AFM and LSAST to be successful using a larger search cube. Using LSAST in a batch mode over five minutes (but still using a sequential adjustment for primary and secondary satellites), one would expect results consistent with FARA. This would assume cycle slip free data, as does FARA.

The combination of ambiguity resolution techniques proposed in Abidin (1991) holds merit. LSAST can be used with AFM to check for cycle slips. It would be interesting to compute accurate code and float solutions simultaneously, and use the covariance information from the float solution along with a search cube from the code solution in ambiguity resolution.

CHAPTER 7

CONCLUSIONS AND RECOMMENDATIONS

Rapid static GPS holds great promise for precise and efficient surveying. In this thesis, rapid static survey measurements and techniques applicable for single frequency high accuracy C/A code receivers were investigated. Coordinate estimation over rapid static time periods (up to five minutes), based on double difference code measurements, carrier measurements and code-carrier measurements combined, were studied using preanalysis and post-processing techniques. Rapid ambiguity resolution using the ambiguity function method, the fast ambiguity resolution approach and the least squares ambiguity search technique were tested and compared. Conclusions made throughout this thesis are given below, followed by recommendations for further investigations.

7.1 CONCLUSIONS

Conclusions are grouped under those related to multipath effects, reliability preanalysis, and ambiguity resolution techniques. The grouping by multipath effects is appropriate since the magnitude and periodicity of multipath on code and carrier measurements was prevalent in most of the investigations made in this thesis. Note that although receiver measurement accuracies also affect solutions and are intertwined with

multipath, the focus in this thesis has been on multipath, since it is generally larger in magnitude and tends to have longer correlation periods.

1) Multipath Effects

a) Averaging across a full observation period tends to mitigate the influence of the magnitude of multipath and usually results in the best possible solution. However, since multipath can have periods extending over an hour, one cannot expect to eliminate its effects through averaging in rapid static surveys.

b) The magnitude of carrier multipath and measurement noise can affect ambiguity resolution techniques. For example, if threshold levels used to reject points from consideration in AFM are too rigid, observations corrupted by multipath may result in a correct point being unduly rejected from consideration. In a severe case, carrier multipath could prohibit successful ambiguity resolution.

c) The cyclical nature of multipath can result in overly optimistic covariance information for code, carrier or code-carrier combined solutions. This is because GPS adjustment solutions are based on the assumption of observations being uncorrelated between consecutive epochs. The extent to which observations are correlated between consecutive epochs is a function the receiver measurement characteristics, and more significantly, the periodicity of the multipath in a given data set relative to the data interval used.

d) The effect of overly optimistic covariance information, resulting from correlations caused by the cyclical nature of multipath, has implications on the significance of accumulated relative dilution of precisions (RDOPs). Theoretically, the product of the relative dilution of precision (RDOP) and the measurement accuracy (including all errors) gives the achievable solution accuracy. Tests with real data

show this relationship to be valid for instantaneous code solutions (i.e., at one epoch) but invalid for accumulated code solutions (i.e., over several epochs). Furthermore, although RDOPs show ambiguity resolution is theoretically possible using a simple combination of high accuracy C/A code and carrier measurements in an adjustment, solutions with real data show the combination of C/A code and carrier measurements to be inadequate for ambiguity resolution, again mainly due to neglected multipath correlations.

e) The effect of overly optimistic covariance information, resulting from correlations caused by the cyclical nature of multipath, has implications for ambiguity resolution techniques which rely on covariance accuracy estimates. This was demonstrated through FARA's success with five minutes of data at a 60 s data interval and failure over the same period at a 15 s interval. At the 60 s data interval, the covariance information used to decide which ambiguity sets should be considered as potential solutions was more realistic.

2) Reliability Preanalysis (Note, the validity of these reliability preanalysis findings are limited by unaccounted for correlations between consecutive epochs of observations.)

a) GPS baseline adjustments are well controlled, even over the short periods which characterize rapid static surveys, if a sufficient number of observation epochs and satellites are used (e.g., five epochs of observations from six satellites over one minute). The redundancy benefits of combined code and carrier solutions over carrier alone are only significant over very short observation periods (e.g., one minute).

b) For periods of up to five minutes, internal reliability is dependent on the number of observation epochs rather than the period or interval of observations.

c) External reliability increases as the number of epochs of observations increases (since the extra epochs reduce the effect of an observational error).

d) Very accurate code measurements at a high data rate can significantly improve carrier external reliabilities.

3) Ambiguity Resolution Techniques

a) A coarse-fine grid search with AFM is computationally more efficient than a fine grid search, but tests using a coarse grid of $\lambda/4$ showed that often a good solution was overlooked. The cause for the lack of success with the coarse-fine grid technique is attributed to the proximity of AF peaks with the single frequency, six satellite data used for testing.

b) A double difference plane intersection search with AFM is more efficient than a coarse-fine grid search. The dangers of defining AF test points using a single epoch of observations can be mitigated by using mini-grid cubes around the point of double difference plane intersection. This step is effective, but unnecessary in most circumstances.

c) Results showed criteria proposed to decide the trustworthiness of a given AFM solution to be effective, since no false solutions were accepted. If anything, the established criteria was too rigid. The AFM, as applied in this thesis with the double difference plane intersection search, preserves its invariance to cycle slips.

d) A functional relationship between the number of satellites (and geometry) and the search cube size which would allow for successful ambiguity resolution using AFM was shown.

e) Compatible results are achievable with AFM and LSAST, assuming data is cycle-slip free. The close relationship between LSAST and AFM using double difference plane intersection techniques explains the compatibility of results. With the criteria used to judge both AFM and LSAST, no false results were accepted, but several good results were rejected. The development of reasonable thresholds and acceptance criteria for both methods is perhaps the most challenging part of these ambiguity resolution techniques.

f) All the ambiguity resolution techniques reviewed have merits, as does the combination of more than one technique. AFM is best if data has cycle slips. FARA is a reasonable technique for observation periods of five minutes. Otherwise LSAST is the best algorithm to use.

7.2 RECOMMENDATIONS

The investigations made in this thesis are a subset of those needed towards the objective of developing efficient, effective rapid static surveying techniques. Recommendations which follow include further investigations needed based on the findings of this thesis as well as complementary investigations needed, which were not within the scope of this thesis.

1) Recommendations for Further Investigations Based on Findings in This Thesis

a) One of the greatest challenges with rapid static surveying techniques is the judicious decision as to whether a solution is good enough to confirm that ambiguities have been successfully resolved. Investigations in this thesis, have been made with the luxury of knowing the "true" solution. This is not the case

with practical field applications. Applications of statistics is complicated by correlations between epochs of observations. The nature of these correlations as they arise from multipath and other noise are not predictable. Cyclic signatures from multipath may be in the order of 10's of seconds or 10's of minutes. More investigations are required in this area.

b) Means to randomize multipath effects in a static environment are required to be able to take full advantage of observations made at a high data rate in rapid static surveys.

c) Theoretical developments should be made into the relation between satellite geometry and the number of points in a given search cube, with an eye towards better defining situations where ambiguities may or may not be successfully resolved.

d) Investigations using seven and eight satellite data sets are needed to better understand the AFM relationship between the search cube size and the number of satellites and geometry needed to solve for a solution. Tests over larger cube sizes are also needed.

e) Tests using the modifications described in Chapter 6, for cycle slip free data, are worthy of investigation.

f) The ambiguity resolution techniques described in this thesis should be tested with several different receiver types. In particular, FARA should be tested to see if the problems encountered due to overly optimistic covariance information is equally common with other receiver types.

g) Reliability analysis carried out in this thesis was based on a confidence level $(1-\alpha)$ of 99.9% and a power of the test $(1-\beta)$ of 80%. These values, conventionally used for network analysis, have been extended for use with GPS baseline analysis. Investigations should be made to see if these values are appropriate for GPS baseline analysis, or if different values should be adopted.

2) Recommendations for Complementary Investigations

a) The investigations in this thesis have been limited to high accuracy C/A code data with single frequency carrier phase data. Greater success with rapid static surveys could be achieved, unperturbed by the impending threat of P code access denial, if a high accuracy C/A code receiver also had L2 squaring carrier phase data. Currently no such receiver is available.

b) Investigations into rapid static ambiguity resolution techniques using dual frequency P code data are warranted. The multipath correlations investigated in this thesis are apt to also be a point of concern using dual frequency P code data.

c) Investigations into ambiguity resolution over longer baselines are required. In cases where ambiguities cannot be resolved as integers, the benefit of accurate code measurements to the final solution should be examined.

Rapid static GPS is a remarkably efficient tool available for surveyors. Investigations made in this thesis provide insight into the measurements and techniques for rapid static GPS surveys using C/A code and carrier measurements. The challenge of routinely and confidently using rapid static surveys in a production environment, without P code observations, lies ahead.

REFERENCES

Abidin, H.Z. (1991): "New Strategy for 'On the Fly' Ambiguity Resolution." Proceedings of ION GPS'91, Albuquerque, NM., Sept. 10-13, The Institute of Navigation, Washington, D.C., pp. 875-886.

Abidin, H.Z. and D.E. Wells (1990): "Extra Widelaning for 'On the Fly' Ambiguity Resolution: Simulation of Ionospheric Effects." Proceedings of the Second International Symposium on Precise Positioning with the Global Positioning System, Ottawa, Sept. 3-7, The Canadian Institute of Surveying and Mapping, pp. 1217-1232.

Adams, J.R. (1987): " 'Step by Step' Least Squares Estimation." Papers for the CISM Adjustment and Analysis Seminars, The Canadian Institute of Surveying and Mapping, January 1987.

Allison, T. (1991): "Multi-Observable Processing Techniques for Precise Relative Positioning." Proceedings of ION GPS'91, Albuquerque, NM., Sept. 10-13, The Institute of Navigation, Washington, D.C., pp. 715-725.

Baarda, W. (1968): "A Testing Procedure for Use in Geodetic Networks." Netherlands Geodetic Commission, Publications in Geodesy, New Series, Vol. 2, No. 5, Delft, The Netherlands.

Biacs, Z.F. and E.J. Krakiwsky (1990): "Reliability Measures for Precise GPS Surveys." Proceedings of the Second International Symposium on Precise Positioning with the Global Positioning System, Ottawa, Sept. 3-7, The Canadian Institute of Surveying and Mapping, pp. 883-894.

Biacs, Z.F., E.J. Krakiwsky and D. Lapucha (1990): "Reliability Analysis of Phase Observations in GPS Baseline Estimation." *Journal of Surveying Engineering*, Vol. 116, No. 4, pp. 204-224.

Cannon, M.E. (1990): "High-Accuracy GPS Semi-Kinematic Positioning: Modeling and Results." *Navigation*, Vol. 37, No. 1, pp. 53-64.

Cannon, M.E. and G. Lachapelle (1992a): "Analysis of A High Performance C/A Code Receiver in Kinematic Mode." Proceedings of the National Technical Meeting, San Diego, Jan. 27-29, The Institute of Navigation, Washington, D.C., pp. 49-58.

Cannon, M.E. and G. Lapchapelle (1992b): "Development of Rapid and Precise GPS Static Survey Methods." Phase I Contract Report for Geodetic Survey Division, Canada Centre for Surveying, Energy Mines and Resources, Canada, March 1992.

Caspary, W.F. (1988): "Concepts of Network and Deformation Analysis." Monograph 11, School of Surveying, The University of New South Whales, Australia.

Counselman, C.C. and S.A. Gourevitch (1981): "Miniature Interferometer Terminals for Earth Surveying: Ambiguity and Multipath with Global Positioning System." *IEEE Transactions on Geoscience and Remote Sensing*, Vol. GE-19, No. 4, pp. 244-252.

Delikaraoglou, D., N. Beck, D. McArthur, and K. Lochead (1985): "On The Establishment of 3-D Geodetic Control By Interferometry With The TI-4100 GPS Receiver." Proceedings of The First International Symposium on Precise Positioning with the Global Positioning System, April 15-19, Rockville, Md., pp. 645-655.

Erickson, C., G. Lachapelle and B.B. She (1991): "Precise Rapid Surveys Using a Combination of Code and Carrier Measurements." Proceedings of ION GPS'91, Albuquerque, NM., Sept. 10-13, The Institute of Navigation, Washington, D.C., pp. 691-698.

Euler, H., K. Sauermann and M. Becker (1990): "Rapid Ambiguity Fixing in Small Scale Networks." Proceedings of the Second International Symposium on Precise Positioning with the Global Positioning System, Ottawa, Sept. 3-7, The Canadian Institute of Surveying and Mapping, pp. 508-523.

Fenton, P., B. Falkenberg, T. Ford, K. Ng and A.J. Van Dierendonck (1991): "Novatel's GPS Receiver - The High Performance OEM Sensor of the Future." Proceedings of ION GPS'91, Albuquerque, NM., Sept. 10-13, The Institute of Navigation, Washington, D.C., pp. 49-58.

Fö rstner, W. (1979): "On Internal and External Reliability of Photogrammetric Coordinates." Proceedings of ASP-ASCM Convention, Washington, D.C., pp. 294-305.

Frei, E. and G. Beutler (1990): "Rapid Static Positioning Based on the Fast Ambiguity Resolution Approach 'FARA': Theory and First Results." *manuscript geodaetica*, Vol. 15, pp. 325-356.

Georigiadou, Y. and A. Kleusberg (1988): "On Carrier Signal Multipath Effects in Relative GPS Positioning." *manuscript geodaetica*, Vol. 13, No. 3, pp. 172-179.

Gillis, D. and L. Nabe (1988): "Calibration Baselines in Canada." *CISM Journal*, Vol. 42, No. 3, pp. 207-215.

Grü ndig, L. and J. Bahndorf (1984): "Accuracy and Reliability in Geodetic Networks - Program System OPTUN." *Journal of Surveying Engineering*. Vol. 110, No. 2, pp. 133-145.

Hatch, R. (1982): "The Synergism of GPS Code and Carrier Measurements." Proceedings of the Third International Geodetic Symposium on Satellite Doppler Positioning, Las Cruces, NM., February 8-12, DMA/NGS, Washington, D.C., pp. 1213-1232.

Hatch, R. (1991a): "Instantaneous Ambiguity Resolution." Proceedings of IAG International Symposium 107 on Kinematic Systems in Geodesy, Surveying and Remote Sensing, Sept. 10-13, 1990, Springer Verlag, New York, pp. 299-308.

Hatch, R. (1991b): "Ambiguity Resolution While Moving - Experimental Results." Proceedings of ION GPS'91, Albuquerque, NM., Sept. 10-13, The Institute of Navigation, Washington, D.C., pp. 707-713.

Henson, D., E.A. Collier and K.R. Schneider (1985): "Geodetic Applications of the Texas Instrument TI 4100 GPS Navigator." Proceedings of The First International Symposium on Precise Positioning with the Global Positioning System. April 15-19, Rockville, Md., pp. 191-200.

Hé roux, P. (1992): Personal Communication, March 1992.

Krakiwsky, E.J. (1990): *The Method of Least Squares: A Synthesis of Advances*. Lecture Notes 42, Department of Surveying Engineering, The University of New Brunswick (1975). Reprinted as Pub. 10003 of the Department of Surveying Engineering, The University of Calgary. Retyped August 1990.

Lachapelle, G., M. Casey, R.M. Eaton, A. Kleusberg, J. Tranquilla and D. Wells (1987): "GPS Marine Kinematic Positioning Accuracy and Reliability." *The Canadian Surveyor*, Vol. 41, No. 2, pp. 143-172.

Lachapelle, G., W. Falkenberg, D. Neufeldt and P. Kielland (1989): "Marine DGPS Using Code and Carrier in A Multipath Environment." Proceedings of ION GPS-89, The Institute of Navigation, Washington, D.C., pp. 343-347.

Lachapelle, G. (1991): "GPS Observables and Error Sources For Kinematic Positioning." Proceedings of IAG International Symposium 107 on Kinematic Systems in Geodesy, Surveying and Remote Sensing, Sept. 10-13, 1990, Springer Verlag, New York, pp. 17-26.

Lachapelle, G., M.E. Cannon, C. Erickson and B. Falkenberg (1992): "High Precision C/A Code Technology For Rapid Static DGPS Surveys." Proceedings of the 6th International Symposium on Satellite Positioning, Columbus, Ohio. (in press)

Leick, A. (1990): *GPS Satellite Surveying*. John Wiley & Sons, New York.

Lichten, S.M and W.I. Bertiger (1989): "Demonstration of Sub-Meter GPS Orbit Determination and 1.5 Parts in 10^8 Three-Dimensional Baseline Accuracy." *Bulletin Geodesique*, Vol. 63, pp. 167-189.

Lu, G. (1990): "Reliability Preanalysis in GPS Surveys." Final Report for Shell Contract: Phase II. Department of Surveying Engineering, The University of Calgary.

Lu, G., B. Townsend and G. Lachapelle (1990): "ANARDOP: A Program for the Pre-Analysis of the Relative Dilution of Precision." Proceedings of the Second International Symposium on Precise Positioning with the Global Positioning System, Ottawa, Sept. 3-7, The Canadian Institute of Surveying and Mapping, pp. 921-934.

Lu, G. (1991): "Quality Control for Differential Kinematic GPS Positioning." MSc Thesis. Pub. 20042 of the Department of Surveying Engineering, The University of Calgary.

MacKenzie, A.P. (1985): "Design and Assessment of Horizontal Survey Networks." MSc Thesis. Pub. 20011 of the Department of Surveying Engineering, The University of Calgary.

Mader, G.L. (1990): "Ambiguity Function Techniques for GPS Phase Initialization and Kinematic Solutions." Proceedings of the Second International Symposium on Precise Positioning with the Global Positioning System, Ottawa, Sept. 3-7, The Canadian Institute of Surveying and Mapping, pp. 1233-1247.

McNeff, J.G. (1991): "GPS Signal Policy." Proceedings of ION GPS'91, Albuquerque, NM., Sept. 10-13, The Institute of Navigation, Washington, D.C., pp. 33-37.

Mikhail, E.M. (1976): *Observations and Least Squares*. Harper & Row, New York.

Novatel Communications Ltd. (1991): "GPSCard™ Model 1001 Technical Specifications." Calgary, Alberta.

Remondi, B.(1984): "Using the Global Positioning System (GPS) Phase Observable for Relative Geodesy: Modeling, Processing, and Results." Ph.D. Dissertation, Center for Space Research, The University of Texas at Austin, Austin.

Remondi, B. (1985): "Performing Centimeter Accuracy Relative Surveys in Seconds Using GPS Carrier Phase." Proceedings of the First International Symposium on Precise Positioning with the Global Positioning System, Rockville Maryland, April 15-19, pp. 789-797.

Remondi, B. (1990): "Pseudo-Kinematic GPS Results Using the Ambiguity Function Method." NOAA Technical Memorandum NOS NGS-52, Rockville, MD..

Remondi, B. (1991): "Kinematic GPS Results Without Static Initialization." NOAA Technical Memorandum NOS NGS-52, Rockville, MD..

Talbot, N. (1991): "Sequential Phase Ambiguity Resolution for Real-Time Static Differential GPS Positioning." *manuscript geodaetica*, Vol. 16, pp. 274-282.

Tranquilla, J.M. and J.P. Carr (1990): "GPS Multipath Field Observations at Land and Water Sites." *Navigation*, Vol. 37, No. 4, pp. 393-414.

Van der Marel, H. and A.J.M. Kösters (1989): "Statistical Testing and Quality Analysis in 3-D Networks (part II) Applications to GPS." Proceedings of IAG International Symposium 102 on the Global Positioning System: An Overview, Edinburgh, Aug. 7-8, Springer Verlag, New York, pp. 290-297.

Van der Marel, H.(1990): "Statistical Testing and Quality Analysis of GPS Networks." Proceedings of the Second International Symposium on Precise Positioning with the Global Positioning System, Ottawa, Sept. 3-7, The Canadian Institute of Surveying and Mapping, pp. 935-949.

Van Dierendonck, A.J., P. Fenton and T. Ford (1992): "Theory and Performance of Narrow Correlator Spacing in a GPS Receiver." Proceedings of the National Technical Meeting U.S. Institute of Navigation, San Diego, Jan. 27-29, pp. 115-124.

Vanicek, P. and E.J. Krakiwsky (1982): *Geodesy: The Concepts*. North-Holland, New York.

Wells, D.E., N. Beck, D. Delikaraoglou, A. Kleusberg, E.J. Krakiwsky, G. Lachapelle, R.B. Langley, M. Nakiboglu, K.P. Schwarz, J.M. Tranquilla, P. Vanicek (1986): *Guide to GPS Positioning.* Canadian GPS Associates, Fredericton, N.B..

Wü bbena, G. (1989): "The GPS Adjustment Software Package - GEONAP - Concepts and Models." Proceedings of the 5th International Geodetic Symposium on Satellite Positioning", New Mexico State University, Las Cruces, N.M., March 13-17, Vol. 1, pp. 452-461.